NTNU – Trondheim
Norwegian University of
Science and Technology

Experimental and modeling study of subsea releases of oil and gas.

Oil behavior and effects in a cold or Arctic marine environment as a function of release conditions, oil chemistry and dispersant injection.

Dorien Anna Engelbertha
Dunnebier

Environmental Toxicology and Chemistry
Submission date: May 2015
Supervisor: Øyvind Mikkelsen, IKJ
Co-supervisor: Per Johan Brandvik, SINTEF

Norwegian University of Science and Technology
Department of Chemistry

Experimental and modeling study of subsea releases of oil and gas.

Oil behavior and effects in a cold or Arctic marine environment as a function of release conditions, oil chemistry and dispersant injection.

Dorien Anna Engelbertha
Dunnebier

Environmental Chemistry and Toxicology
Submission date: May 2015
Supervisors: Per Johan Brandvik, SINTEF and NTNU
Øyvind Mikkelsen, NTNU

Norwegian University of Science and Technology
Department of Chemistry

Abstract

With oil exploration going into deeper waters and more extreme environments, more detailed knowledge is needed about the fate of oil in case of a release.

This thesis focuses on initial droplet formation, secondary breakup and fate of oil in a subsurface release and the effect of subsurface injection of dispersants.

The objectives were to study initial droplet formation, the effectiveness of different surfactant blends when injected in warm oil, secondary droplet breakup and to model hypothetical oil releases in the Barents Sea.

The effectiveness of tested surfactant combinations increased when the temperature of Troll B oil increased. However, a decrease was observed when the commercially available dispersant Corexit 9500A was injected in Kobbe oil at increasing temperatures. This observed change in behavior and effectivity could be related to surfactant and/or oil chemistry.

The secondary breakup mechanism tip-streaming, where small droplets shed of the parent droplet due to deformation after surfactant treatment, has been studied and observed to be finished within 10 minutes after the release at different dispersant-to-oil ratios. After one hour in very turbulent conditions, the droplets were stable and spherical in shape.

Simulations with the OSCAR model have shown how a reduction in droplet size due to dispersant injection can change the environmental fate of the released oil.

Further research could be of interest to see whether the change in dispersant effectiveness is a result of oil or surfactant chemistry and to study tip-streaming at higher oil temperatures.

Acknowledgements

My supervisors are adjunct professor and senior scientist dr. Per Johan Brandvik at Environmental Technology, SINTEF Materials and Chemistry and professor Øyvind Mikkelsen at the Analytical Chemistry group at the Department of Chemistry, NTNU. I am very grateful for all the opportunities I received to learn and improve my knowledge on oil spill chemistry and would like to thank them for the good supervision and discussions.

I also would like to thank all the people at SINTEF Materials and Chemistry, Environmental Technology for their help, and in specific senior engineer Daniel Krause, research scientist dr. Emlyn Davies and senior engineer Frode Leirvik at SINTEF Materials and Chemistry, for their scientific and technical support. And of course the kanonball team and the Friday-swim-in-the-fjord-club for all the fun!

Last but definitely not least I would like to thank my family and friends for always supporting me, wherever I go.

Trondheim, May 21st, 2015

_____

Dorien Anna Engelbertha Dunnebier

Table of contents

Nomenclature

Latin letter	Explanation	Unit
°API	Density	-
a	Constant of proportionality	-
A	Empirical factor	-
b	Interpolation of plume radius to time	-
B	Empirical coefficient	-
c	Constant of proportionality	-
C_A	Convex hull	-
D	Orifice diameter	m
d_0	Diameter	m
d_{95}	95% maximum droplet diameter	m
D_c	Equivalent circular diameter	m
d_i	Characteristic diameter	m
d_i	Droplet diameter	m
d_j	Droplet diameter	m
d_{max}	Maximum stable droplet diameter	m
D_{min}	Minimum droplet diameter	m
D_{sp}	Spheroidal diameter	m
f_A	Weigth fraction surfactant A	-
Fr	Froude number	-
g’	Reduced gravity	m/s^2
g_{dj}	Breakage frequency d_j	s^{-1}
$HLB_{a/b}$	HLB value of A or B	-
ki	Parameter in Rosin-Rammler	-
L_{maj}	Major axis	-
L_{min}	Minor axis	-
n	Gas void fraction at nozzle exit	-
N	Gas void fraction	-
N	Number of droplets per m^3	-
Oh	Ohnesorge number	-
P_s	Pixel size	m
Re	Reynolds number	-
t	time	s
U	Exit velocity	m/s
U_n	Velocity, corrected for void fraction	m/s
U_{oil}	Velocity of oil at outlet	m/s
Vi	Viscosity number	-
V_i	Cumulative volume fraction	-
$W_{b,n}$	Rise velocity droplet	m/s
W_e	Entrainment velocity	m/s
We	Weber number	-
We*	Modified Weber number	-
W_s	Net separation velocity	m/s
X’/D	Relative breakup length	-

Greek letter	Explanation	Unit
α	Spreading parameter	-
β_0	Constant	-
$\beta_{1/2/3}$	Regression coefficients	-
$\beta_{(di, dj)}$	Breakage probability density function for creation of d_i due to breakage of d_j.	-
δ	Cohesive energy density	$MPa^{1/2}$
ε	Dissipation rate	M^2/s^3
μ	Dynamic viscosity of jet fluid	Pa s
μ_0	Exit velocity	m/s
π	Number of pi	-
ρ	Density	Kg/m^3
ρ_{oil}	Density of oil	Kg/m^3
ρ_{water}	Density of water	Kg/m^3
σ	Oil-water interfacial tension	N/m

Abbreviations

Abbreviation	Explanation
BOP	Blowout preventer
CDOG	Comprehensive Deepwater Oil and Gas
DOR	Dispersant-to-oil ratio
DREAM	Dose-related risk and assessment model
ERMS	Environmental Risk Modelling System
GoMRI	Gulf of Mexico Research Initiative
GOR	Gas-to-oil ratio
HLB	Hydrophile-lipophile balance
IFT	Interfacial tension
LISST	Laser In-Situ Scattering Transmissometry
MEMW	Marine Environmental Modelling Workbench
MVD	Median volume diameter
OSCAR	Oil Spill Contingency and Response
ParTrack	Particle tracking for drilling discharges
SIT	Simulated insertion tool

List of figures

List of tables

1. Introduction

The United States Geological Survey estimated in 2008 that approximately 90 billion barrels of oil, 44 billion barrels of natural gas liquids and 1,669 trillion cubic feet of natural gas lie in undiscovered Arctic fields, and estimated is that ca 84 % of these reserves are offshore(USGS, 2008).

It is therefore not surprising that many countries and companies show interest in the Arctic. However, the conditions in this region are extreme with freezing cold, hard wind and sea-ice in many places throughout the year. Combined with constant darkness in winter, responding to a blow-out with the traditional methods can be challenging. Hence, it is necessary that techniques are improved for oil spill response to surface spills or subsurface blowouts, the latter being the focus in this thesis.

In 2010, the world faced one of the largest oil spills in history. During the Macondo blowout in the Gulf of Mexico, roughly five million barrels of oil leaked into the ocean, calling for an emergency response. Besides mechanical recovery and in-situ burning, dispersants were used both on the surface and subsea, and this was the first time subsea application of dispersants was performed on a big scale (Juhaz, 2011).

More knowledge is required about the behavior of dispersants in a subsea application. The objective of this project was therefor to model subsea releases of oil in the arctic and study the effectiveness of the respond method. To do so and obtain input, sub-objectives were to test the dispersion of an Arctic crude oil under various conditions to obtain more knowledge about the fate after released into the water and response. A second objective was to use experimental design to study the behavior of surfactants, which are an important part of the dispersants, under various temperatures to see how the behavior and effectivity would change with increasing temperature.

This thesis discusses the results of these experimental and simulation studies towards the subsurface application of dispersants.

In the next chapter, the theory behind oil spills, droplet formation and droplet break up will be explained as well as the composition of crude oils and their fate after release and the subsurface oil spill response will be described. The third chapter contains details about the oils and dispersants that have been used, and the methods used, namely: the MiniTower, the Inverted Cone and the simulation program OSCAR. These theoretical chapters are followed by the results and discussion. This part is split into three parts after the three different methods. Finally, in the last chapter, the conclusions from this work will be defined and explained.

2. Theory

In this chapter, the theory behind subsurface releases of oil is explained, together with oil spill modelling, oil and surfactant chemistry.

2.1 Subsurface blowout

Oil in water can have a natural or an anthropogenic cause. An example of a natural cause is the seepage of oil out of the a reservoir on the bottom of the sea and although such releases can continue for very long periods of time, they are usually in low quantities and therefor of small risk.

An anthropogenic release can be accidental or intentional, an example of the latter being operational discharges. In an accidental oil release, a separation is made between surface releases e.g. a grounded ship, and releases under water, so called subsurface releases, e.g. leaking pipelines or a well blowout (Wang and Stout, 2007).

A well blowout can have several causes like unexpected pressure changes, blow-out preventer (BOP) failures, fracture at the casing shoe, etc. A blowout does not always have to cause large releases of oil, but as has been experienced with the Macondo blowout, it can have a large environmental impact (Holand, 1997).

Within subsurface releases, again a distinction is made, between shallow water and deep water releases.

2.1.1 Deep water / shallow water

There is no exact definition of deep water and different organizations use different depths but here a water depth of more than 300 meters is considered deep. Down at the seafloor, pressures are much higher and temperatures much lower than in the upper water column or on the seafloor in more shallow waters. These differences in conditions may result in different blowout behavior when occurring in deep water or in shallow water.

Spills in shallow water and spills in deep water differ from each other in several ways. In deep water, the gas shows non-ideal gas behavior, the possibility for gas dissolving and due to the high pressure a strong compression of the gas with possibility to hydrate formation (Zheng et al., 2003). This can cause the buoyancy to reduce and the plume becomes sensitive to ambient density stratifications and crossflows.

This as opposed to blow outs in shallow to moderate water where expanding gas generates a large buoyancy and thus carrying the entrained water plume together with the dispersed oil and gas bubbles to the surface. On the surface, there is an outward flow from the entrained water creating a thin oil slick.

During a deep water blowout, the gas and oil will separate from the plume and rise individually. The larger droplets will rise more rapidly and surface close to the point of blow out and can form a tick oil slick on the surface. The smaller droplets have a longer rising time

and can surface far away from the source, where they will form a thin surface slick. The advantage of the latter is that they are more likely to undergo natural dispersion and go back into the water column (Johansen et al., 2013).

2.1.3 Oil spill modeling

Over the years, many models for oil spill modelling both surface and subsurface have been developed. In 1980 Fanneløp and Sjøen developed the first blowout models (Fanneløp and Sjøen, 1980). However these models were only developed for subsurface blowouts in shallow to moderate water. As explained earlier, the oil plume as a result from a deepwater blowout behaves much different from a plume in shallow to moderate water. Among the differences is the possible dissolving of gas and gas hydrate formation. Topham was in 1984 the first one to include hydrate formation in a subsurface blowout model for deep water conditions (Johansen, 2003). In 2000 Johansen and in 2001 Yapa et al. published about the development of new deepwater blowout models. It is not possible to discuss all oil models here but excellent reviews of models up to the year 1999 have been written by Reed et al. (1999) and Yapa and Zheng (1997). The models by Johansen and Yapa et al. will be described into more detail in the next section.

2.1.3.1 CDOG

In 1997 Yapa and Zheng described a model developed for subsurface blowouts in shallow water and the subsequent model testing in 1998 (Yapa and Zheng, 1997, Zheng and Yapa, 1998). This Lagrangian model takes ambient current and (un)stratified environments into account. In 1999 an improvement of the 1997 model was published (Yapa et al., 1999), followed by a new improvement in 2001. Yapa et al. (2001) published a paper describing a modified version of that model, including hydrate formation and decomposition, which made it more suitable for deepwater blowouts. In 2002, two more papers were published regarding this model about the model formulation (part I by Zheng et al., 2003) and about the testing of the model and comparison with field experiments (part II by Chen and Yapa, 2003) followed. This model is called CDOG and is a Lagrangian model that includes the hydrodynamics of the jet and plume, the phase changes and thermodynamics of gas and the impact of the latter on the former. To be able to compute ambient density stratification, ambient temperature and salinity variations are included just like ambient velocity variations to calculate entrainment, jet/plume hydrodynamics and oil and gas in the far-field part.

2.1.3.2 Deepblow

DeepBlow is a model for deeper oil fields and a continuation of the SINTEF BLOW model which was developed for depths up to 350 m. Earlier in the theory part of this thesis is explained how deep water blowouts differ from blowouts in shallow to moderate water. Johansen (1997) performed a literature study towards deep water blowout and concluded that the eularian BLOW model was not sufficient anymore and thus the model was modified to the lagrangian DeepBLOW. Modifications and inclusions were:

- Effects of cross-currents

- non-ideal gas behavior
- dissolution of gas in sea water
- formation and subsequent disintegration of hydrates

(Johansen, 2000).

2.1.3.3 GoMRI

After the Deepwater Horizon Spill in 2010, BP offered 500 million US dollars for 10 years of independent research towards oil spills, the impact and response. This project is called the Gulf of Mexico Research Initiative (GoMRI). As stated on the website:

'The ultimate goal of the GoMRI will be to improve society's ability to understand, respond to and mitigate the impacts of petroleum pollution and related stressors of the marine and coastal ecosystems, with an emphasis on conditions found in the Gulf of Mexico. Knowledge accrued will be applied to restoration and to improving the long0term environmental health of the Gulf of Mexico.' (www.gulfresearchinitiative.org)

One of the projects funded by this research initiative is the development of a new subsurface blowout model called VDROP-J (Zhao et al., 2014a).

2.3.1.4 VDROP

The VDROP model is recently developed by Zhao et al. (2014b) and is based on the following population balance equation:

$$\frac{\delta n(d_i,t)}{\delta t} = \sum_{j=i+1}^{n} \beta(d_i,d_j)g(d_j)n(d_j,t) - g(d_i)n(d_i,t) + \sum_{j=1}^{n}\sum_{k=1}^{n} \Gamma(d_j,d_k)n(d_j,t)n(d_k,t) - n(d_i,t)\sum_{j=1}^{n}\Gamma(d_i,d_j)n(d_j,t)$$

Equation 1

The first sum describes the droplet breakup and the second part sum describes the droplet coalescence. Both are again divided. In the first sum, droplet breakup, the first term describes the creation of droplets d_i as a result of the break-up of d_j droplets. The second term describes the breakup of d_i droplets into smaller ones. The second sum, droplet coalescence with rate $\Gamma(d_k, d_j)$ in m^3/s, is split between the formation of d_i as d_k and d_j coalesce in the first term and the coalescence of di with other droplets resulting in new, larger droplets, in the second term.

N is the number of droplets per m^3, d_i (m) is the droplet diameter at a given time t (s). $\beta(d_i, d_j)$ describes the dimensionless breakage probability density function for the creation of di, due to the breakage of droplets with diameter d_j .The breakage frequency of d_j droplets is described by $g(d_j)$ with unit s^{-1}.

The model can be used to predict the droplet size distribution in turbulent regimes taking oil viscosity and the oil-water interfacial tension into account. The model has been validated against several laboratory experiments (Zhao et al., 2014b).

2.3.1.5 VDROP-J

Modifications have been made to the VDROP model to predict the droplet size distribution from the Deepwater Horizon blowout.

This special type of the original model has been validated using two datasets: one from Brandvik et al. (2013), who performed oil experiments in the so-called TowerBasin. This is a basin which is 6 m high and 3 m in diameter, containing 42 m^3 of filtered seawater, and is used to study droplet size distributions of both dispersed and non-dispersed oil. The second experiments used to validate the model were the DeepSpill field experiments from 2000 (Johansen et al., 2003). Two combinations were released in those experiments: seawater and LNG and diesel and LNG. The modelling results of VDROP-J matched with the experiments with a R^2>0.99 (Zhao et al., 2014a).

2.3.1.6 OSCAR

The above described models, are all plume models. SINTEF has developed a model which can be used for overall oil spill simulation. OSCAR is a collection of models and databases related to oil spill contingency and response (OSCAR) and part of the Marine Environmental Modelling Workbench (MEMW). MEMW consists of three numerical models, all developed by SINTEF:

- DREAM: Dose-related Risk and Effects Assessment Model
- ParTrack: Particle tracking for drilling discharges
- OSCAR: Oil Spill Contingency And Response

The third one, OSCAR, is also the model used in this thesis. It can be used to quantify the consequence of an oil spill and the response effectiveness by computing the fate of the oil and can also be used for contingency planning and risk analysis (SINTEF Marine Modelling Group, 2014).
Originally it consisted of three components: The Fates model: which is a 3D model used to simulate oil and chemical spills, SINTEF's Oil Weathering Model (OWM): a model and database for the weathering of oils, and Oil Spill Combat: a model developed by SINTEF to analyze oil spill emergency response strategies, as can be seen in figure 1 (Reed et al., 1995a, Aamo et al., 1993, Daling et al., 1990, 1991, all as referred to in Reed et al., 1995b).

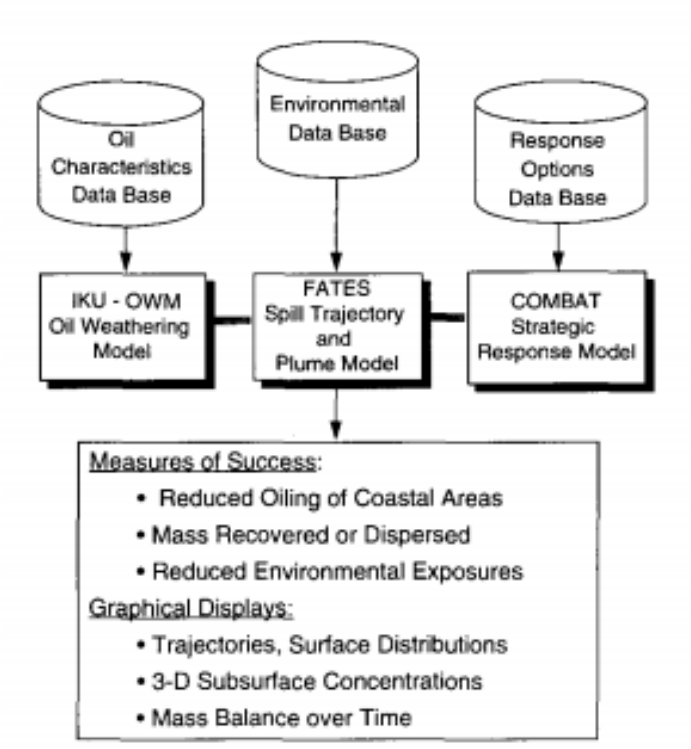

Figure 1: representation of the components of the OSCAR model (Reed et al., 1995b).

In modelling, two often used representations of fluid flow are Eulerian and Lagrangian. Eularian consideres elements in a fixed space and Lagrangian uses elements moving with the fluid. (Durst, 2008). OSCAR uses particles that are either strictly Lagrangian, like the plankton or dissolved substances. These are transported together with the surrounding water. The other type of particles are pseudo-Langrangian, i.e. droplets in the water column. They are not only transported with the surrounding water but vertical rising or settling velocity caused by the turbulent water. The total plume is pictured as cylindrical elements that do not interfere with each other but do change over time due to entrainment and rising. Every element has its own characteristics like location, radius, mass, length, average velocity and more (Johansen, 2000).
In addition to the motion, all particles have a stochastic or probabilistic component resulting in two simulations never being exactly the same, even though the scenarios are equal (SINTEF Marine Modeling Group, 2014).

Over the years, OSCAR has been upgraded and updated to nowadays version as part of MEMW 6.6.1, one of these inclusions is Plume3D.

2.3.1.7 Plume3D

Plume3D is a multiphase plume model developed from the above described DeepBlow model as part of an Environmental Risk Management System (ERMS) project. A few modifications were made as new constituents, mineral particles and dissolved chemicals were included in this model compared to DeepBlow. For example, droplets or bubbles separating from the plume will no longer influence the plume behavior so do not have to be

included in the near-field part of the model. Instead the separated droplets are now modeled in the far-field part.

Figure 2 shows how the net separation velocity for droplets or buoyant bubbles can be calculated. $W_{b,n}$ is the rise velocity, W_e is the entrainment velocity and W_s is the net separation velocity normal to the trajectory of the plume. The retention time of the bubble or droplet is reduced by the addition of the axial component of the rise velocity to the axial plume velocity (Johansen and Durgut, 2006).

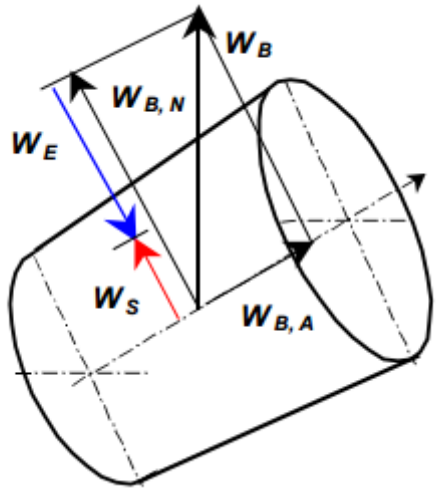

Figure 2: Representation of net separation velocity on oil droplet (Johansen and Durgut, 2006).

2.3.1.8 Advection in near-field and far-field

Particles inside the plume have a position *x, y, z* at a given time t, which is a result of time interpolation of the plume coordinate *X,Y,Z (k).* As the plume has experiences radial expansion, a spherical random displacement of length *R=b(t)*, where b is the interpolation of the plume radius to time t is added.

After separation, the advection rule changes. It is now determined by the superimposition of the particle's rising on the local ambient current velocities *u, v, w*.

The computation of the particle separation from the plume is done using probabilistic calculations at each time step and for each size class of each constituent. Exact details on these calculations are described in Johansen and Durgut, 2006.

2.3.1.9 Plume termination

Over time, it is possible that the plume phase is terminated, this can happen in several ways:

- The plume surfaces and for the far field particles now a radial spreading velocity is superimposed on the common far-field advection rule.
- The plume is trapped and the for the computing, the common far-field rules apply.
- The plume touches the seafloor and just as for the surfacing plumes, a radial spreading velocity is superimposed (Johansen and Durgut, 2006).

1.4.3 Modified weber number

In order to better understand and be able to predict the droplet break-up and droplet size distributions during blowouts, SINTEF build a new facility called TowerBasin to study the distributions on a larger scale (Brandvik et al., 2013, Johansen et al., 2013). The original Weber number showed no longer a good representation for the droplet size distribution and these experiments lead to a new, modified Weber number, which in turn led to a new and modified algorithm for determining droplet size distributions and modelling. Peter Johan Bergh Lindersen tested this new algorithm during the writing of his master thesis, using both a modelling and a laboratory study. Among the results was that the new algorithm results in larger droplets in the distribution and when up scaled, a larger median volume diameter than the maximum stable droplet size. This new algorithm is dependent on the viscosity, which is different for every oil, and is therefore an important part in predicting the efforts needed in blowout cases (Bergh Lindersen, 2013).

2.1.4 Initial droplet formation and secondary break up

A schematic image of the processes in the initial plume are presented in figure 3.

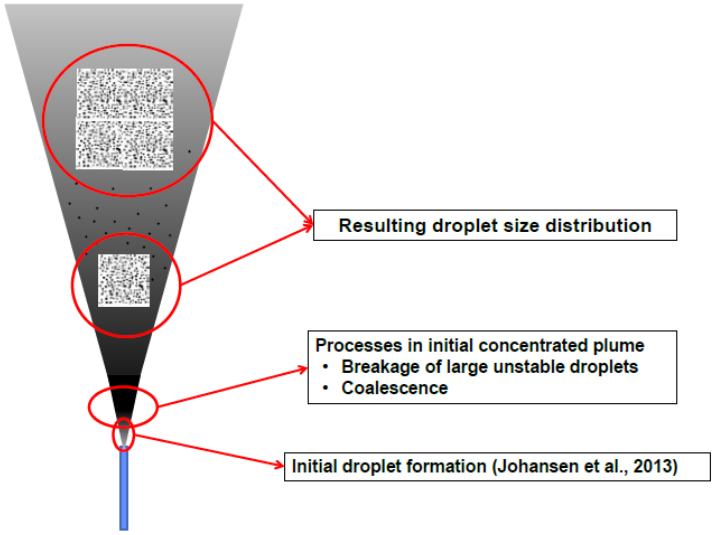

figure 3: Initial droplet formation and the processes in the initial concentrated plume (Davies et al., 2015).

There are different mechanisms that can be responsible for the breakup of oil droplets after release and these depend on both the conditions at the nozzle and the properties of the oil. Possible mechanisms:

- Buoyant forces outrange interfacial forces, causing pendant droplets.
- Axial or transverse instabilities of the jet.
- Atomization, this causes droplets forming almost immediately after exiting the jet and forming a wide range of droplet sizes.

The secondary breakup of droplets has been studied intensively by, among others, Masutani and Adams (2000), and Johansen et al. (2003, 2013).

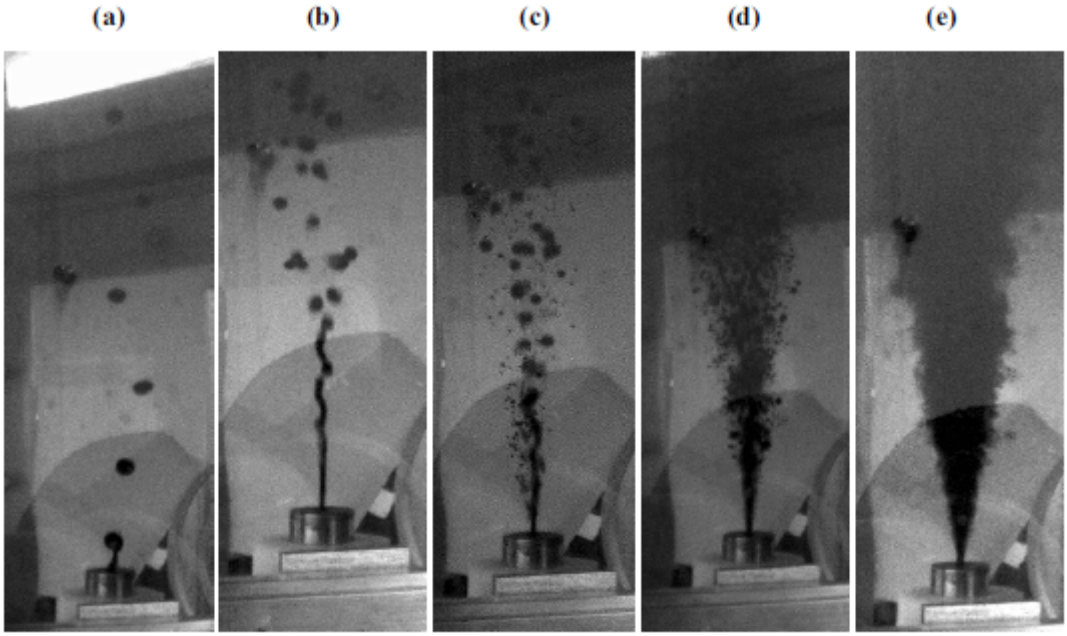

Figure 4: Observed modes of breakup of an oil jet in water, Genesis crude oil, 2 mm diameter orifice and 18.1 °C tap water (Masutani and Adams, 2000)

Figure 4 shows the resulting plumes of the oil in water experiments by Masutani and Adams (2000). The first two images show jet breakup at low velocity, where Reyleigh instability dominates, resulting in droplets larger than the orifice. With increasing jet velocity, the jet breakup moves away from the nozzle and a sinuous mode called Type I is observed. Two instability mechanisms operate in parallel at higher velocities: the jet surface becomes unstable and breaks up into fine droplets close to the nozzle, yet the core continues as a fluid filament breaking up more downstream in larger droplets. Type II instability is observed in c in the figure. As the velocity increases, near-atomization is observed: the breakup of the jet core filament moves closer to the nozzle and droplets become smaller as can be seen in d. Atomization can be seen in e, a fine droplet cloud.

After studying the breakup of liquid jets in water Masutani and Adams concluded that a Reynolds (Re) vs. Ohnesorge (Oh) diagram could describe the breakup regime of an oil jet in water. Figure 5 shows the Re vs. Oh diagram and equations 2 and 3 the Reynolds and Ohnesorge number.

Reynolds number

$$Re = \frac{-\rho UD}{\mu}$$

Equation 2

Ohnesorge number:

$$Oh = \frac{\mu}{(\rho\sigma D)^{1/2}}$$

Equation 3

U is the exit velocity, D the orifice diameter, σ the oil-water interfacial tension, ρ is the density and μ the dynamic viscosity of the jet fluid.

The linear relationship between the Ohnesorge number and the Reynolds number:

$$Oh = cRe^{-1}$$

Equation 4

c is a constant of proportionality.

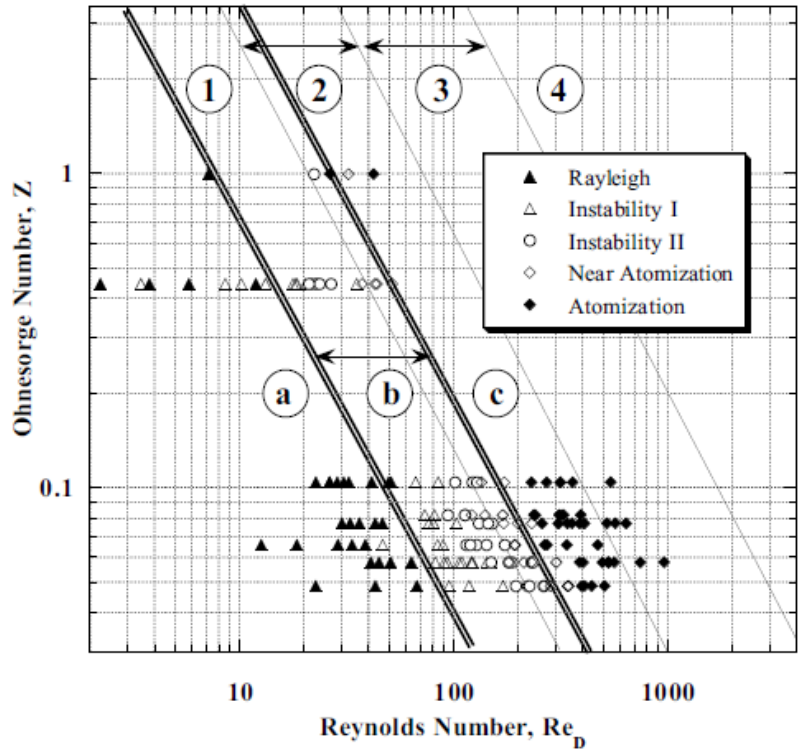

Figure 5: Reynolds vs Ohnesorge diagram. The datapoints are results from the oil in water study. The double lines represent the boundaries between breakup regimes. a= Rayleigh, b= type I and II and c= atomization. The solid lines are boundaries from previous studies of liquid jets into gas. 1=Rayleigh, 2 and 3 are first and second wind-induced breakup and 4=atomization (Masutani and Adams, 2000).

Between the laminar and transitional breakup regimes and between the transitional and turbulent breakup regimes, there is a linear relationship which can be described by the above Ohnesorge equation. Between transitional and turbulent or atomization breakup there is a boundary, which results in a constant Weber number.

The Weber number:

$$We = \frac{U^2 D\rho}{\sigma}$$

Equation 5

The Ohnesorge number is related to the Weber number. Combining that with the above equation, the following relationship is found:

$$We = c^2$$

Equation 6

The Ohnesorge number can also be written as a combination of the Reynolds number and the Weber number:

$$Oh = \frac{We^{1/2}}{Re}$$

Equation 7

The rise velocity depends on the physical properties of oil, but for oil droplets in the range of 5-10 mm the maximum rise velocity is about 12-15 cm/s. Figure 6 shows the plume and rising of different sizes of droplets.

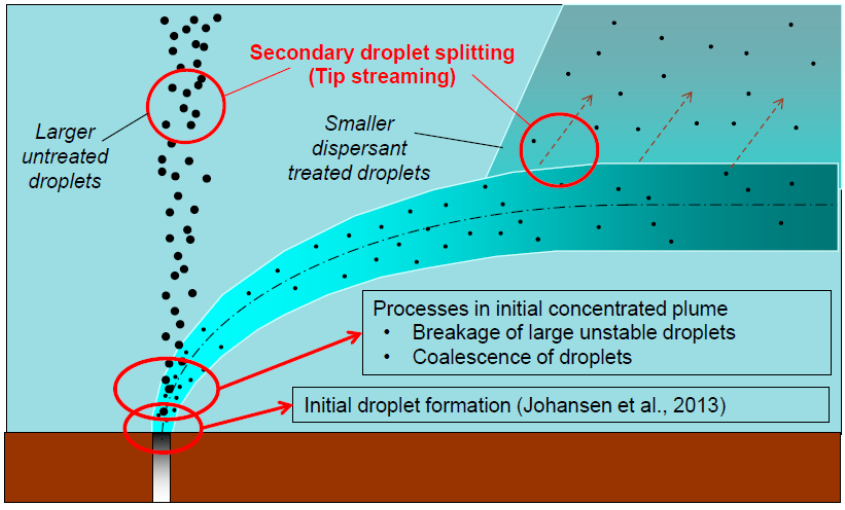

Figure 6: Representation of the processes in the plume such as secondary droplet breakup (Davies et al., 2015).

This velocity also depends on the initial droplet formation in a turbulent jet, which depends on the exit conditions at the source like exit velocity μ_0 and the diameter d_0. These exit conditions determine the droplet size and the maximum oil droplet sizes is related to the Weber number as has been suggested by Karabelas (1978), who noted that although the weber number has originally been defined for turbulent pipe flow, it can also be used for an oil jet in water.

The relationship between the Weber number and the 95% droplet size d_{95}

$$d_{95} = c d_0 We^{-0.6}$$

Equation 8

c is an empirical coefficient (Karabelas, 1978).

(Johansen 2003, 2013)

2.1.5 Weber number scaling law

Hinze (1955) described the maximum stable droplet size prediction in stationary turbulence by equation 9.

$$d_{max} = a \left(\frac{\sigma}{\rho}\right)^{3/5} \varepsilon^{-2/5}$$

Equation 9

a is a constant of proportionality, ρ is the density of the continuous phase (water) and ε is the dissipation rate.

However, in a turbulent jet, with atomization conditions, it was found that the dissipation rate ε decreases when the droplets rise away from the nozzle. As the droplet is not completely broken up yet, it reaches a region with a lower ε value.

Martines-Bazán and Montañés (2002) used this d_{max} equation as a basis and when including the relative downstream distance X/D and equaling the dissipation rate ε to U^3/D, the following equation can be used for calculating the d_{max}:

$$\frac{d_{max}}{D} = A We^{-3/5}$$

Equation 10

A is an empirical factor that depends on the relative break up length X'/D.

To better describe the droplet size distributions when upscaling droplet size distributions to real scale cases, Johansen et al. 2013 performed several experiments in the TowerBasin, testing both dispersed and non-dispersed oil. Based on the results of the experiments, a modified Weber number was developed:

$$We^* = \frac{We}{[1 + B \cdot Vi(\frac{d_{50}}{D})^{\frac{1}{3}}]}$$

Equation 11

Vi is the viscosity number and B is an empirical coefficient.

The median volume diameter (MVD) can now be expressed as:

$$\frac{d_{50}}{D} = A \cdot (We^*)^{-3/5}$$

Equation 12

The above equations, only count for releases with a single fluid like oil. When oil and gas are combined, a correction for the void fraction was introduced:

$$U_n = \frac{U_{oil}}{(1-n)^{1/2}}$$

Equation 13

U_{oil} is the oil only outlet velocity and n is the nozzle exit gas void fraction.

When there is a large volume of oil released, a correction for the buoyancy is needed:

$$U_c = U_n(1 + Fr^{-1})$$

Equation 14

$$Fr = \frac{U_n}{(g'D)^{1/2}}$$

Equation 15

And

$$g' = g\frac{\rho_w - \rho_{oil}(1-n)}{\rho_w}$$

Equation 16

When these equations are taken into account, the resulting We* number is:

$$We^* = \frac{\rho U_c^2 D}{\sigma}$$

Equation 17

(Lefebvre, 1989, Johansen et al., 2013,).

2.1.6 Droplet size distribution functions

There are several functions possible to describe the droplet size distribution using the characteristic size for the droplet size distribution estimation. Two regularly used distribution functions are the log-normal and the Rosin-Rammler distribution functions.

The log-normal distribution is a function of $x = \ln(d)$, mean value is $m =< x >$ and a standard deviation σ. The median volume diameter is the mean value: $m = \ln(d_{50})$

The Rosin-Rammler distribution is a two-parameter distribution function, using characteristic diameter d_i, cumulative volume fraction V_i and spreading parameter α.

$$V(d) = 1 - \exp\left[-k_i\left(\frac{d}{d_i}\right)^{\alpha}\right.$$

Equation 18

$$k_i = -\ln(1 - V_i)$$

Equation 19

(Bergh Lindersen, 2013, Lefebvre, 1989, Johansen et al., 2013).

2.1.7 Tip-streaming

One special cause of droplet break-up that is studied in this thesis, is tip-streaming. Described by ,among others, Taylor in 1934, tips-streaming is an often observed result of treating oil with surfactants in a shear flow and a mechanism of droplet breakup. The idea behind a surfactant is to reduce the surface tension of the oil, or any other fluid. The chemistry behind surfactants is explained later in this chapter. In a shear flow, the surfactant can enhance droplet break up in different manners. The droplet can fracture which results in several droplets with similar size or it can show tip streaming. In the latter, the droplet is no longer spherical but more sigmoidal (De Bruijn) or umbrella like (this study, see figure 7) with small droplets dripping of the parent droplet (De Bruijn, 1993).

Figure 7: tip-streaming of a Kobbe oil droplet treated with Corexit 9500A DOR 1:100 (Dunnebier, 2015).

Figure 8 shows how a spherical droplet becomes deformed and can eventually show tip streaming. The reason for the deformation or non-spherical shape is that in a flow, the surfactant on a droplet is swept sideward, to the poles of the droplet. The concentrations on the sidepoles is now much larger than the initial mixture concentration (Eggleton et al., 2001).

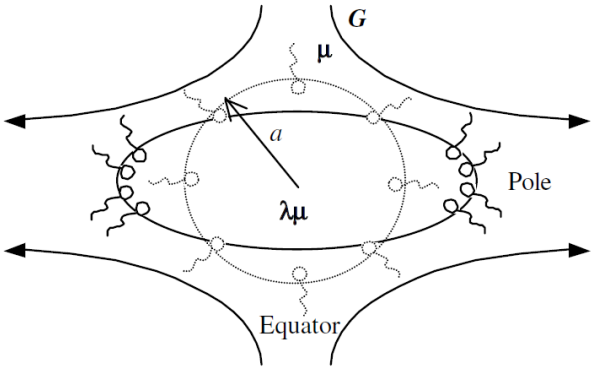

Figure 8: schematic figure of a droplet in a uniaxial flow (Eggleton et al., 2001)

Gopalan and Katz (2010) studied the turbulent break up of dispersed crude oil, showing the formation of microthreads behind 300-1400 µm droplets. This thread formation can be caused by surfactant accumulation (Anna and Mayer, 2006), shearing by coflowing liquid (Suryo and Basaran, 2006) or electrohydrodynamic forcing (Collins et al., 2008)(Gopalan and Katz, 2010). The authors showed that when a crude oil droplet is mixed with dispersant, a long, micron sized thread of oil can be observed trailing behind the droplets. The threads would eventually breakup, presumably due to a reduction of the surfactant concentration.

2.2 Oil chemistry

2.2.1 Chemical composition

There are two main groups of components in crude oil: hydrocarbons and hetero-atomic organics. The former consists of paraffins, naphthenes and aromatics and the latter of resins and asphaltenes.

Hydrocarbons:

Paraffins: n-alkanes and iso-alkanes. An important subgroup are the paraffins with more than 20 carbon atoms called waxes. These waxes can precipitate at low temperatures.

Naphthenes: cycloalkanes with one or more saturated rings and optionally one or more paraffinic side chains.

Aromatics: unsaturated cyclic hydrocarbons, can be mono- or poly-aromatic.

Heteroatomic organics: molecules that do not only contain hydrocarbons, but can also contain oxygen, nitrogen, sulphur and trace metals.

Resins: bigger molecules weighing in the range of 700 to 1000. They often have a polar part and surface active properties.

Asphaltenes: this is the group of the biggest molecules consisting of condensed polycyclic aromatic compounds with a molecular weight in the range of 1000 to 10 000.

Figure 9 shows the general composition combinations of crude oils. The arrow in the middle shows the general change in composition due to biodegradation.

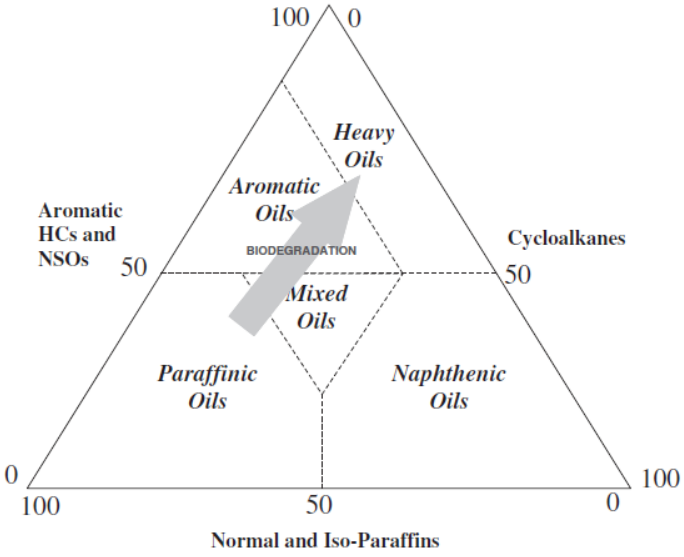

Figure 9: General composition of crude oils. The arrows show the change in composition due to biodegradation. (Wang and Stout, 2007 after Tissot and Welte (1984)).

2.2.2 Physical properties of crude oil differ with chemical composition. The four most important properties for marine oil releases are explained here. The latter three are so-called rheological properties: the flow properties of a fluid (Rønningsen, 2012).

Density: the density is calculated by the mass of a substance divided by the volume of the substance. For crude oil this is approximately between 0.78 and 0.95 g/ml at 15.5 °C. Oils with a higher amount of low molecular weight components generally have a lower density where the opposite counts for oils with higher weight components like asphaltenes and aromatics. Within oil chemistry, another type of density is commonly used, called API gravity.

$$^{\circ} API = \frac{141.5}{Specific\ gravity} - 131.5$$

Equation 20

Where the specific gravity is the same as the also used term relative density. It is the specific gravity of the oil relative to that of water at 15.6 °C. If the API gravity is below 10 °API, the oil will sink in water where those above 10 °API float. As a measure of classification, if an oil has a API gravity of 31.1 °API or more, it is considered a light oil, between 22.3 and 31.1 °API a medium oil and below 22.3 °API a heavy oil.

Viscosity: The resistance of the oil against flowing is expressed as viscosity with unit being pascal-second: Pa·s, where pascal is 1 N/m^2. Viscosity decreases with increasing temperature and is usually measured at summer and winter temperatures i.e. 5 °C and 13 °C. The viscosity usually increases with water uptake, making emulsions more viscous than the oil.

Pour point: The pour point is defined as the temperature where the oil ceases to flow under standardized laboratory conditions. Especially the wax content is important when looking at the pour point. The pour point increases with increasing wax content, which in turn increases during weathering as the lighter components evaporate. This can become a problem for response since a high pour point can limit the effectiveness of a dispersant.

Flash point: also called flame point, is the lowest temperature at which gas is generated by heating of the oil, and the oil can be ignited. Just like the other properties, it depends on the chemical composition and in this case especially on the low molecular weight components. With time and evaporation, the flash points will increase since the lighter components disappear. The flash point is also used as an indicator for the explosion risk. An often used rule of thumb says that when the flash point of the oil is close to or lower than the sea temperature, there will be a hazard for fire and explosions and that moving into the slick might be dangerous (Sørheim and Moldestad, 2008, Wang and Stout, 2010, Schobert, 2013).

There are more oil properties, such as sulfur content, but those are less of interest for this thesis and will therefore not be discussed.

2.2.4 Weathering of crude oil at the sea surface

When released into the water, several biological, chemical and physical processes will change the oil characteristics. The most important of these weathering processes are shown in figure 10 and the timeframe for the processes is shown in figure 11. These processes are influenced not only by the oil composition and properties but also by the weather conditions and the properties of the seawater.

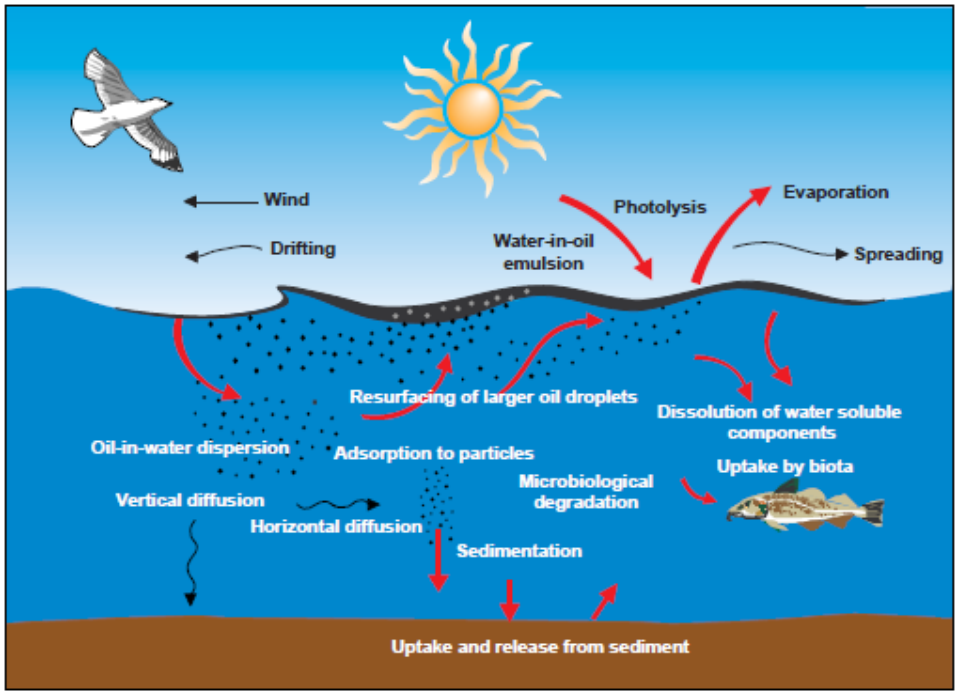

Figure 10: Weathering processes on oil at the seasurface (Sørheim and Øverli Moldestad, 2008)

Spreading: as can be seen in figure 11 evaporation and spreading are the most important weathering processes in the first few hours after the release. When the oil slick spreads out over the water surface the slick becomes thinner but larger in surface. This causes an increase in evaporation and dissolution since more oil becomes exposed. After a certain amount of time, the oil's spreading rate decreases because the viscosity and density increase.

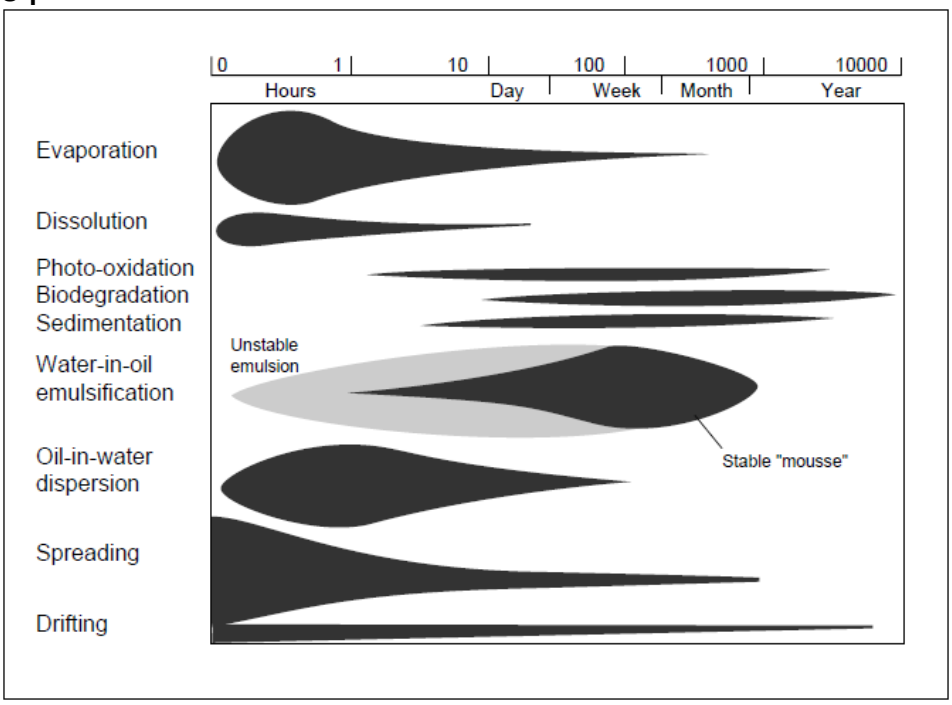

Figure 11: Weathering processes relative to time (Sørheim and Øverli Moldestad, 2008)

Drifting: Just like for spreading, wind and currents can cause drifting of the oil slick.

Evaporation: As more oil becomes exposed, the lighter and more volatile components will evaporate. The rate of evaporation is driven by the vapor pressure of the components in the oil, together with other factors like wind speed and temperature of both water and air. Compounds up to approximately 12 carbons, with a boiling point below 200 °C are generally evaporated within 24 hours. Therefore, products like gasoline can be already completely evaporated within a few days, if the conditions are right. Just like spreading, evaporation changes the oils properties. With the loss of the light components, viscosity and pour points will increase as the heavier components now make up the larger part of the total components.

Photo-oxidation: When exposed to solar ultraviolet radiation, photo-oxygenation reactions involving free radicals can lead to several polar compounds that are water-soluble. On the other hand, the heavier compounds can form even larger molecules and become insoluble. Only photo-oxidation and biodegradation can remove petroleum compounds from the sea surface. During the day the rate will be higher due to higher intensity of the ultraviolet radiation than during the night.

Emulsification: Emulsification is the process of forming a water-in-oil mixture thanks to breaking waves. This increases the viscosity which hinders other weathering processes. Forming an emulsion is dependent, besides the weather conditions, on the chemical properties of the oil. Even though an emulsion is no longer considered a well-mixed phase it does not mean it is completely stable. The water droplets can fuse or break up.

Dispersion: Dispersion is the breaking up of oil droplets into smaller droplets and mix into the water column. A difference is made between natural dispersion, which needs breaking

waves to break and mix the droplets, and chemical dispersion, which uses surfactants to break up the droplets and enhance the natural dispersion. Droplet break-up because of waves give droplets with typically a diameter between 1 and 1000 µm. When the viscosity of the oil increases due to weathering, the natural dispersion will decrease. Chemical dispersion results in droplets in a much smaller range: between 5 and 50 µm. This is when surfactants are sprayed on the oil slick on the sea surface. It is also possible to disperse the oil subsurface by injecting dispersants into the oil plume above the well. The advantage of dispersion is that it increases the biodegradation rate as the oil becomes more available (Sørheim and Moldestad, 2008, Wang and Stout, 2010).

2.3 Surfactant and dispersant chemistry

Dispersants are chemical mixtures used for, among many other things, the treatment of spilled oil. They consist of both surfactants and solvents, the latter to improve the impregnation of the surfactant on the two-phase interface. Surfactants are surface active agents, which are found in food, cosmetic products, detergents and oil spill dispersants. With both a lipophilic and a hydrophilic part, the surfactant can align between two phases like water and the oil and lower the interfacial tension. When sprayed over an oil slick, the lowering of the interfacial tension facilitates the oil to break up and mix into the water column (Sørheim and Moldestad, 2008, Myer, 2005).

The lipophilic/hydrophobic part of the surfactant is usually a hydrocarbon chain of varying length, like fatty acids, and the possibility for oxygenated or fluorinated groups. The hydrophilic part is the part that adds water solubility to the molecule thanks to ionic or highly polar groups. Not all surfactants are pure mixtures. Many mixtures contain the surfactant with different isomers and chain lengths where its name tells the average value of the hydrocarbon chain length.

Surfactants are often classified based on the hydrophilic group:

a. Anionic, a negative charged hydrophilic group like carboxylic acid ($RCOO^- M^+$)
b. Cationic, a positive charged hydrophilic group like ammonium halides ($R_4N^+ X^-$)
c. Nonionic, the hydrophilic group is highly polar but neutral like polyoxyethylene (R-OCH_2CHO-)
d. Amphoteric and zwitterionic, the hydrophilic group can contain a negative or/and a positive charge.

Surfactants can act between a different variety of phases such as solid/liquid, gas/liquid and liquid/liquid. In this thesis only the latter is of interest and will therefore be the only one considered in this thesis(Myer, 2005).

2.3.2 Hydrophile-lipophile balance

The hydrophile-lipophile balance (HLB) is a method to describe the relationship between the properties of the surfactant and its composition.

Different HLB formulas have been developed for different types of surfactants. A more overall formula, based on the contribution of molecular groups of the surfactants was needed and developed. The outcome is usually in a scale from 0 to 20 with the hydrophilic surfactants on the high end and the lipophilic surfactants, which are poorly soluble in water at the low end of this scale.

$$HLB = 7 + \Sigma(hydrophilic\ group\ numbers) - \Sigma(hydrophobic\ group\ numbers)$$

Equation 21

The hydrophilic and hydrophobic group numbers are for example 2.1 for a –COOH group and -0.475 for –CH-, -CH_2- and –CH_3 groups. All numbers can be found in literature.

A separate formula was developed for calculating the HLB of a mixture. This because in mixtures there can be interactions among the different surfactants and it is possible that a single surfactant with a certain HLB number, results in a much less stable emulsion than a mixture of surfactants with the same HLB value.

$$HLB_{mix} = f_A \times HLB_A + (1 - f_A) \times HLB_B$$

Equation 22

In this equation, HLB_A and HLB_B are the HLB values of the components and f_A is the weight fraction of surfactant A in the mixture.

The HLB system has as an advantage that it is simple and easy to use. However, it is also limited since it only takes the surfactant properties into account when calculating the performance.

A second way can be to look at the degree of hydration of the surfactant in relation to the HLB, this is called the Hildebrand solubility parameter or cohesive energy density (δ) (Myer, 2005).

$$\delta\ (MPa^{1/2}) = \frac{243}{54 - HLB} + 12.3$$

Equation 23

2.3.3 Interfacial tension

When to (partly) immiscible phases meet a tension is created at the interface which is called the interfacial tension. This tension is dependent on the two phases; the more different they are from each other, the greater the tension will be. The minimum amount of work which is needed to create this interface is called the interfacial free energy. At the interface, the molecules located there will have a much higher potential energy than the molecules in the bulk.

The surfactant, with its hydrophilic and hydrophobic parts, can move between the two phases and lower the interfacial tension by reducing the unfavorable interactions. This is shown in figure 12. In an oil spill, the application of surfactants, the resulting lowering of interfacial tension and break up of droplets has as a result that the oil now becomes more accessible for hydrocarbon-degrading bacteria and less will wash ashore on the beaches. When using an aircraft, large areas can be treated in a relatively short time which is also an advantage since the emulsification is held back in that way. This compared to mechanical recovery, where ships need time to be called and travel (Myer, 2005, Sørheim and Moldestad, 2008, Rosen and Kunjappu, 2012).

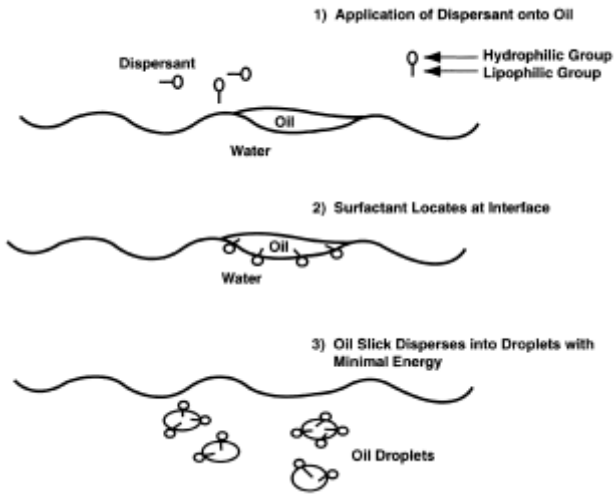

Figure 12: Schematic representation of how dispersants work. The surfactants in the dispersant diffuse in the oil-water interface and lower the interfacial tension. (Lessard and DeMarco, 2000)

A disadvantage is that different oils have different compositions and will therefor react different to a dispersant. Commercial available dispersants are made in such a way that they are applicable on a large range of oils (Lessard and DeMarco, 2000).

2.3.4 Surfactants at higher temperatures

Until 2010 dispersants as an emergency response were used on the surface of the sea. The Macondo oil spill was the first time subsurface injection of dispersants was used as an emergency respond on a larger scale (Juhaz, 2011). It is not surprising therefor that most dispersants are developed for surface application, where temperatures range from Arctic to tropic. However, when oil is released from the well, it can be much warmer. It is therefore important to gain knowledge about the effectivity of surfactants and dispersants when injected into hot oil. Such studies have been done at SINTEF in the past years. Brandvik et al. (2014) performed a study towards the different aspects of subsurface oil releases and dispersant injection techniques. Both cold (15 °C) and warm (51 °C) Oseberg oil was injected with dispersant at different dispersant to oil ratios (DORs) in a tank called the TowerBasin. This TowerBasin is 6 m high and 3 m in diameter and can hold 40 m^3 of filtered seawater. The results of the experiments were not entirely as expected. For all three DORs, 1:100, 1:50 and 1:25, the droplet size distribution was larger for warm treated oil then for the cold dispersed oil. The researchers give three possible explanations: 1) there might be a cooling effect from the dispersant since it is injected cold into warm oil. However, the DOR is low so the volume of cold dispersant is low compared to the volume of warm oil and therefore a cooling effect, if present, should be minimal. 2) when oil is warmed up, the viscosity decreases. The viscosity of the dispersant has not changed, and the difference in viscosity between the two has now increased. It is possible that this increased difference causes a less efficient mixing. But since the oil is less viscous and due to its much bigger volume compared to the dispersant volume, the dispersant should warm up, get a decrease in viscosity and the mixing should be better than with cold oil. 3) The critical micelle concentrations and the

interfacial tension for the oil/water phase could be different at higher temperatures than at lower. It has been observed earlier that the critical micelle concentration at higher temperature could be decreasing. It is possible that some groups of surfactants are more sensitive to temperature than others. In that case the ratio of the surfactants could change and reduce the effectiveness. These results are interesting and in this thesis, a deeper insight will be provided in the possible effect of temperature on surfactants (Brandvik et al., 2014).

2.3.5 Biodegradability

Although this thesis focuses on the chemistry and physics of dispersants, it is important to also gain knowledge about the biological aspects like biodegradation and toxicity.

The biodegradability of dispersants depends on the nature of the surfactants in the mixture. More linear hydrophobic chains are more easily biodegraded where more branches cause a reduction in biodegradability. Oxyethylene groups slow down the degradation process when the number of oxyethylene groups increases. A distinction is made between primary and secondary ethoxylates, the latter degrading slower than the former (Rosen and Kunjappu, 2012).

Quite a number of studies have been performed towards the biodegradation of Corexit 9500A, a commercial available dispersant, and towards the combination of C9500A and oil spilled during the Deep Water Horizon blowout in 2010.

Campo et al. (2013), conducted a study towards the degradation of dioctyl sulfosuccinate (DOSS), a component of Corexit 9500, with and without oil. At a temperature of 25 °C, DOSS was found to have high biodegradation rates both in presence and in absence of oil, with a removal of >99% by day 8 with oil and day 14 without oil. Interesting is that the scientists enriched the cultures on only oil, whereas in other studies the bacteria were enriched on a mixture of oil and dispersant. However, at 5 °C, the biodegradation rates were much lower. The results were more varying with 98% depletion for 1 replicate at day 35 and 2 at day 42 in the absence of oil. On suggestion by the scientists to explain this was that the cryo culture needs time to acclimate to synthesize enzymes that allow the bacteria to take up and degrade the DOSS. In the presence of oil an average of 61% removal was obtained but with a decline (Campo et al., 2013).

2.3.6 Toxicity

This thesis focusses on the dispersant use and effectivity. The use of dispersants however, remains a controversial topic, even after several decades of use. In Norway and the United Kingdom dispersants are allowed as an oil spill emergency response. In the Netherlands it was, until recently, not allowed and in Iceland and Spain the use of dispersants is only allowed as a Last Response Option (EMSA, 2014).

In the next paragraph, a small summary is given of some toxicity study, both towards only dispersant and to dispersant-oil mixtures. Because of different experimental setups,

endpoints and data treatment, the studies in this small summary cannot be compared to each other but are meant to give an overview.

Almeda et al. studied the toxic effects of crude oil, dispersant and treated oil using Louisiana light sweet crude and Corexit 9500A on marine micro zooplankton. Their conclusion is that crude oil dispersed with Corexit 9500A is more toxic than non-treated oil to the micro zooplankton organisms tested in this study (Almeda et al., 2014).

Fuller et al. tested three macro organisms and one bacterial species. By using bioassays, the researchers determined the toxicity of oil, dispersant and treated oil and studied different exposure regimes and the effects of weathering on the toxicity. One of the conclusions of their study was that oil alone is so much more toxic than dispersant that the toxicity of the latter would be negligible (Fuller et al., 2004).

Acute toxicity tests on three arctic species under open-water and ice-free conditions were done by Gardiner et al. (2013). An outcome of their research was that Corexit 9500A was not a contribution to the negative effects observed in the toxicity tests although it did increase the hydrocarbon concentration in the water column. A second important result was that the tested dispersant does not change the toxicity mechanism of the dispersed oil.

3. Materials and methods

In this chapter the experimental part of the thesis will be explained. Basic oil and surfactant chemistry and the ones used for this thesis are first described. This is followed by detailing the experimental design methodology. The last part specifies the technical details of the MiniTower, Inverted Cone and OSCAR systems.

3.1 Oils

For this project, two different crude oils are used: Troll B and Kobbe.

Kobbe is an Arctic oil and one of the formations, together with Realgrunnen, at the Goliat field located in the Norwegian part of the Barents sea. The field licensees are Eni Norge and Statoil where the former is the operator. Both reservoirs are at about 400 m below the sea surface and lie at 1800 m depth. Figure 13 shows the location of the Goliat field. The blue horizontal line in a represents the arctic circle (www.petroleumskartet.no).

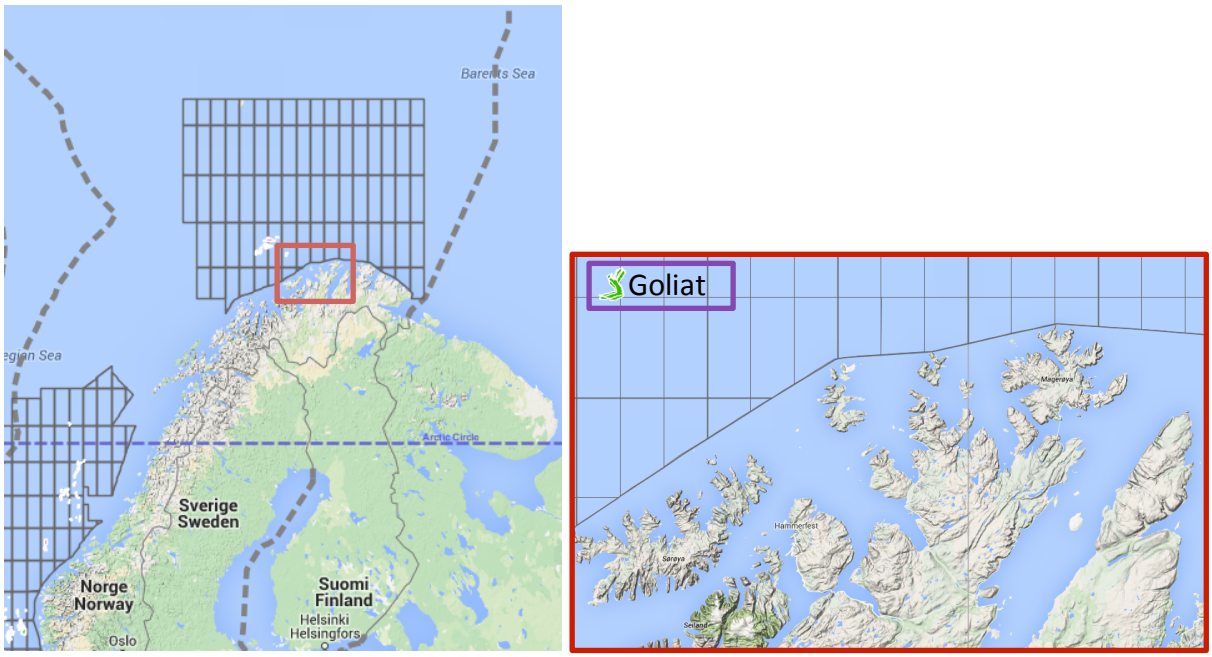

Figure 13: Location of the Goliat field in the Barents Sea (www.petroleumskartet.no).

Although the area is located in the European Arctic, it is not as cold and harsh as similar latitudes in the Canadian or Siberian Arctic. This is due to global thermohaline circulation pattern, which brings warm water to the Norwegian sea as can be seen in figure 14 (www.nasa.org).

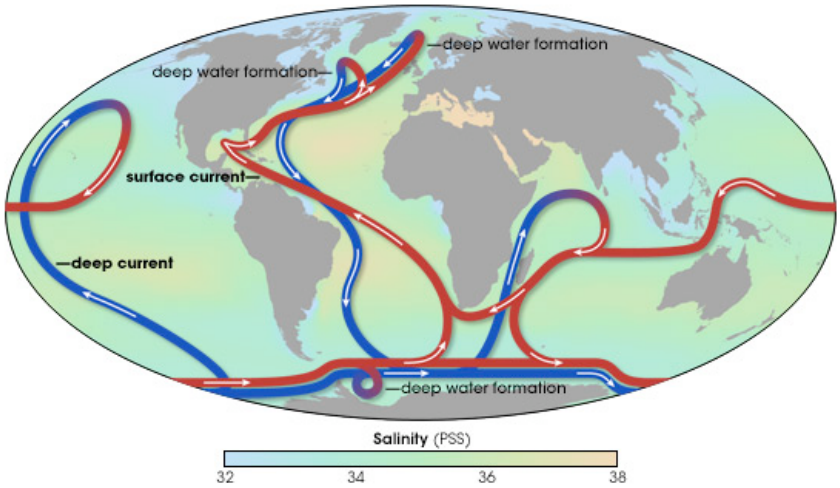

Figure 14: The thermohaline effect over the globe (www.nasa.org).

Kobbe has been used for the inverted cone experiments and for the later MiniTower experiments.

Unfortunately, not a large volume of the Kobbe oil was available for this project. Therefore the experimental design experiments, which is a different part of this thesis to study the behavior of surfactants under varying conditions, has been performed with Troll B.

Just like Kobbe, Troll B is a crude oil but it is not an Arctic one. The Troll field is located in the North Sea northwest of Bergen, as can be seen in figure 15.

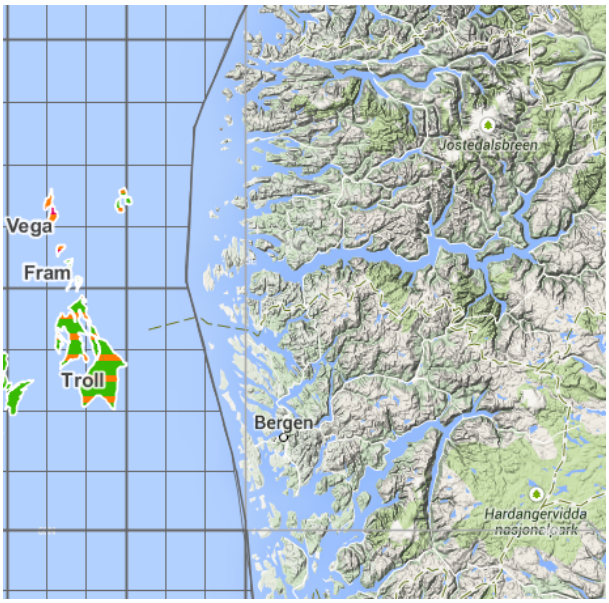

Figure 15: Location of the Troll field in the North Sea (www.petroleumskartet.no).

In table 1 the properties of the two oils are shown. For Kobbe the 2009-0284 batch was used but the property and weathering study was done earlier on a different batch. For Troll the 2013-0409 batch was used but property and weathering study is from batch 2005-0722.

Table 1: Properties of Troll B and Kobbe oil (Andreassen and Rist Sørheim, 2013) for the Troll properties and (Sørheim and Øverli Moldestad, 2008) for the Kobbe properties.

	Troll B	Kobbe
SINTEF-ID	2005-0722 (13 °C)	2006-1061 (5 °C)
Type	Naphtenic oil	Light oil
Pour point (°C)	-39	-39
Viscosity (mPa·s)	27	22
Density (g/ml)	0.893	0.797
Asphaltene content (%)	0.09	0.03
Wax content (%)	1.3	3.4
IFT (mN/m)	-	17

Troll B and Kobbe oil can be compared using table 1 and the diagram in figure 16 where several oils are arranged according to their chemistry. Kobbe is located high in the paraffinic area whereas Troll lies on the naphthenic side.

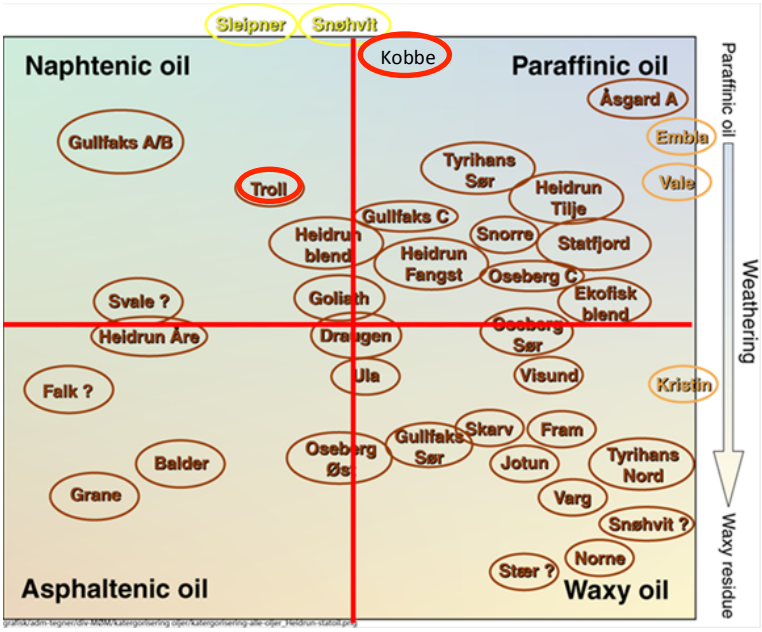

Figure 16: Diagram with different oils according to their properties (Sørheim and Øverli Moldestad, 2008).

3.2 Studied surfactants

The surfactants used in this study are presented in figure 17.

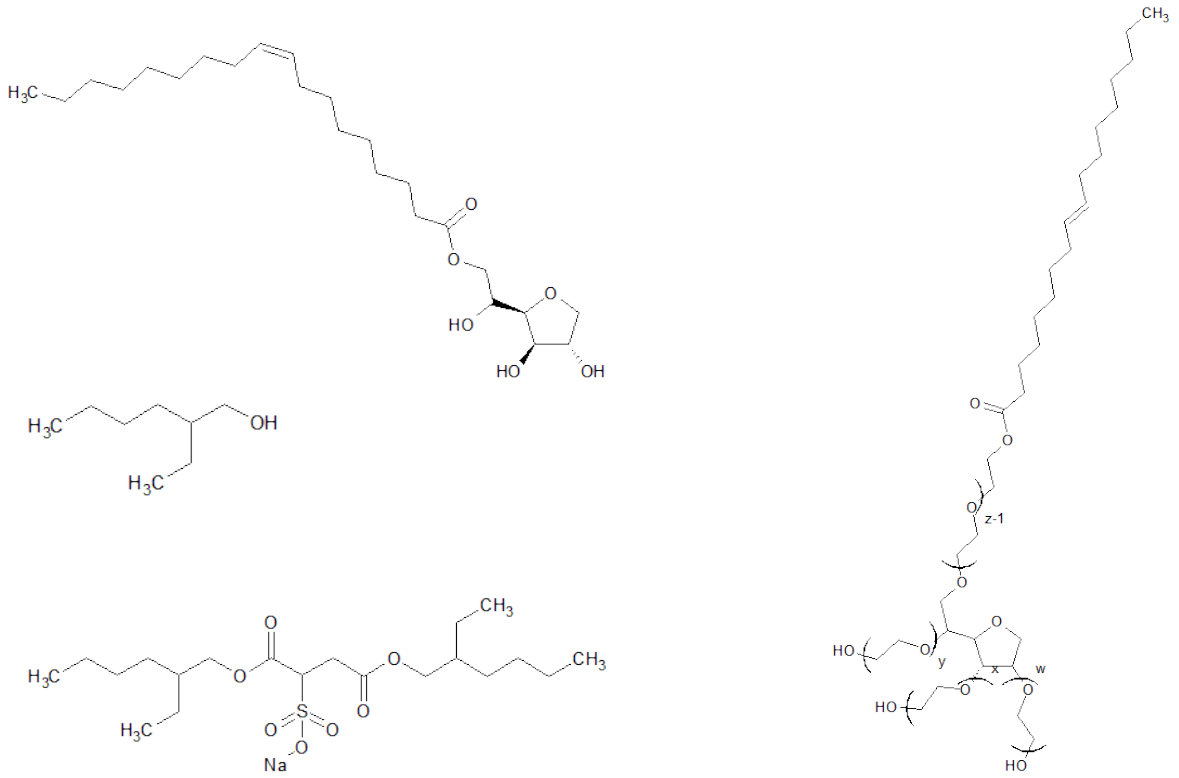

Figure 17: Molecular structures of Span 80 (top left), iso-octanol (middle left), DOSS (bottom left) and Tween 80 (right).

Surfactants can be very viscous or waxy. Using only a mixture of surfactants is often not be sufficient for injection or spraying, therefor a solvent is added. In this study that was a mixture of 2-ethylhexylacetate (figure 18) and de-aromatized paraffin in the ratio 1:2.

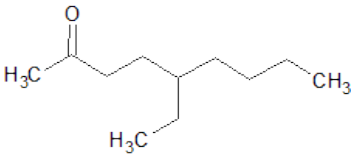

Figure 18: Molecular structure of 2-ethylhexylacetate.

3.2.2 Corexit 9500A

Corexit 9500A is a commercially available dispersant and one of the dispersants used during the Macondo blowout in 2010 in the Gulf of Mexico. During the blowout, the US EPA requested a list of ingredients from Nalco, the producer of Corexit. Corexit 9500 is a mixture of several surfactants:

- 1,2-propanediol
- Butanedioc acid, 2-sulfo, 1,4-bis(2-ethylhexyl) ester, sodium salt (1:1)

- Sorbitan, mono(9z)-9-octadecenoate (Span 80)
- Sorbitan, mono-(9z)-9-octadecanoate, ply(oxy-1,2-ethanediyl) derivatives (Polysorbate 80)
- Sorbitan, tri-(9z)-9-octadecenoate, poly(oxy-1,2-ethanediyl) derivatives (Tween 85)
- Distillates (petroleum), hydrotreated light

(www.nalcoesllc.com)

3.3.3 Dispersant-to-Oil Ratio

Dispersant effectivity is tested in several volumetric DORs. DOR is the abbreviation for Dispersant-to-Oil-Ratio. A common test range is from DOR 1:1000 to 1:50, but in this thesis a smaller range was used. In the initial experiments, three ratios were used: 1:500, 1:250 and 1:100. For the Inverted Cone work DORs of 1:100 and 1:50 were tested. The reason for these low dosages is that subsurface injection of dispersants requires lower dosages than surface application of dispersants.

3.4 Experimental design

Instead of independent experiments, for this project a different approach was made: the experimental design using response surfaces.

3.4.1 Experimental design

Described in , inter alia, The Arrangement of Field Experiments by Ronald A. Fisher in 1926, experimental design is a practical method using a multivariate approach. This method takes interactions and dependency into account. The whole set of experiments are completely thought out before hand and statistics is performed to calculate a response equation. One of the major advantages of experimental design over one-variable-at-a-time experiments is that interactions between the variables are also taken into account in the experimental design method giving more knowledge over a bigger picture. It gives information not only for the points that have been experimental performed, but also about points in between (Leardi, 2009).

3.4.2 Response surface methodology

Box and Wilsons were one of the first to describe the response surface methodology in 1951 as a result of a mixture problem they had to solve for the company they were working for (Box and Wilson, 1951).

As the name says response surface methodology (RSM) uses a surface to describe the response of several experiments.

The response is the measured outcome and the dependent variable. Factors are the input in the experiments, the levels change and as a result, influence the response. Since the response depends on the factors, an algorithm can be written which describes this interaction. The next step is a representation of this algorithm in a surface design (Khuri and Cornell 1987).

For this thesis, three-component mixtures were studied. The two main designs in three-component mixtures are the simplex-lattice and the simplex-centroid design.

3.4.2.1 Simplex lattice

A simplex lattice is a one-dimensional triangle, since there are three components in the simplex, where every corner represents a component. Ten experimental points are uniformly distributed over the triangle, as can be seen in figure 19. The associated algorithm or polynomial has to be of a low degree to decrease the number of coefficients which will otherwise complicate the equation (Scheffé, 1958).

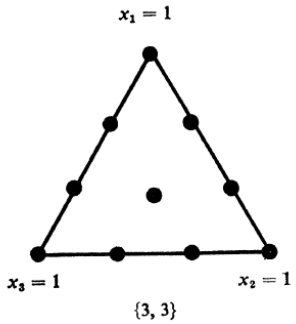

Figure 19: A simplex lattice with 10 experimental points (Scheffé, 1958)

3.4.2.2 Simplex centroid

The simplex-centroid has been described by Scheffé in 1963. A simplex-centroid differs from a simple-lattice in the way that a simplex-lattice has 9 points on the boundaries and only one point in the triangle where a simplex centroid has 4 interior points and 6 points on the boundaries.

3.4.2.3 Special simplex centroid

In 1998 Brandvik and Brandvik and Daling published three acompanying articles about the use of response surface methods for the optimization of oil spill dispersants (Brandvik 1998, Brandvik and Daling, 1998a,b).

In the case for this thesis a slightly different simplex-centroid has been used, similar as the type Brandvik used (Brandvik, 1998). All points now lie within the triangle since the interest is in mixtures and less in 100% one compound compositions. The chosen type gives more information about the inner surface of the triangle (Cornell, 1990). In table 2 the levels of the components in the different mixtures can be read.

Table 2: The levels of components for the three experimental points in the simplex centroid used in this thesis.

Sample	X1 in %	X2 in %	X3 in %
1	80.0	10.0	10.0
2	10.0	80.0	10.0
3	10.0	10.0	80.0
4	45.0	45.0	10.0
5	10.0	45.0	45.0
6	45.0	10.0	45.0
7	56.7	21.6	21.6

8	21.6	56.7	21.6
9	21.6	21.6	56.7
10	33.3	33.3	33.3

3.4.3 polynomials

The resulting response surface can be described with several different algorithms, varying from basic to more complex (Khuri and Cornell, 1987).

Linear:

$$y = \beta_1 1 x_1 + \beta_2 x_2 + \beta_3 x_3$$

Equation 24

Quadratic:

$$y = \beta_1 1 x_1 + \beta_2 x_2 + \beta_3 x_3 + \beta_{12} x_1 x_2 + \beta_{13} x_1 x_3 + \beta_{23} x_2 x_3$$

Equation 25

Special cubic:

$$y = \beta_1 x_1 + \beta_2 x_2 + \beta_3 x_3 + \beta_{12} x_1 x_2 + \beta_{13} x_1 x_3 + \beta_{23} x_2 x_3 + \beta_{123} x_1 x_2 x_3$$

Equation 26

Special quartic:

$$y = \beta_0 + \beta_1 x_1 + \beta_2 x_2 + \beta_3 x_3 + \beta_{12} x_1 x_2 + \beta_{13} x_1 x_3 + \beta_{23} x_2 x_3 + \beta_{1123} x_1^2 x_2 x_3 + \beta_{1223} x_1 x_2^2 x_3 + \beta_{1233} x_1 x_2 x_3^2$$

Equation 27 (Brandvik, 1998).

In the last one, equation 27, the constant β_0 was introduced to increase the interpretability of the coefficients by representing a centering of the model (Cornell 1990)(Brandvik, 1998). In this work, a special quartic without the constant will also be considered and tested.

3.4.5 Multivariance linear regression

To estimate the regression coefficients β_x multivariance linear regression was performed on the experimental obtained outcomes or efficiencies. The above mentioned algorithms were tested using Microsoft Excel regression function, which also tests for lack of fit at the same time.

The laser instrument, later explained in this chapter, measures 20 frames per second and from a chosen amount of seconds, in which the conditions are stable, the data is averaged and standard deviation is calculated.

When following the response surface methodology, the optimum combination of the three components can be found by performing a steepest ascent method (Box et al., 1978)(Brandvik, 1998).

This complete method is mainly meant for optimization of combinations. The goal in this thesis while using this method was to see how there will be a shift over a temperature range in the most effective combination of several surfactants. Therefor the method was not followed exactly but more used as a guideline.

The resulting algorithms were programmed in a Matlab script, which uses the ternplot function to create the response surface. The optimum, or maximum, were calculated together with the resulting optimal combination of the three components.

In the initial phase, three triangles and the associated algorithms were tested. After, one triangle was used to perform heat experiments. The exact set-up of those experiments will be explained later in this chapter together with the technicalities of the MiniTower.

3.5 Preparation of surfactant mixtures

The surfactant mixtures were prepared in a laboratory under normal laboratory conditions. Per triangle, ten different combinations of three different surfactants were mixed. The ratios can be seen in table 3. After pipetting, the blends were stirred overnight on a magnetic stirring plate to ensure proper mixing. The flasks were stored under normal conditions if not immediately used.

Table 3: Levels of components used for the mixing of the surfactant blends.

Sample	X1 in %	X2 in %	X3 in %
1	80.0	10.0	10.0
2	10.0	80.0	10.0
3	10.0	10.0	80.0
4	45.0	45.0	10.0
5	10.0	45.0	45.0
6	45.0	10.0	45.0
7	56.7	21.6	21.6
8	21.6	56.7	21.6
9	21.6	21.6	56.7
10	33.3	33.3	33.3

For the first two triangles, a solution of 60% DOSS and 40% ethanol was used, since no pure DOSS was available. This was corrected by using enough of the solution to reach the desired amount of surfactant and less solvent.

Table 4: The surfactant mixtures used in the initial study.

Triangle	X1	X2	X3
1	Span 80	Tween 80	60% DOSS
2	Tween 85	Iso-octanol	60% DOSS
3	Tween 85	Span 80	DOSS

3.6 SINTEF MiniTower

In this chapter, the technical details and experimental set-up of the MiniTower are described.

3.6.1 Experimental set-up

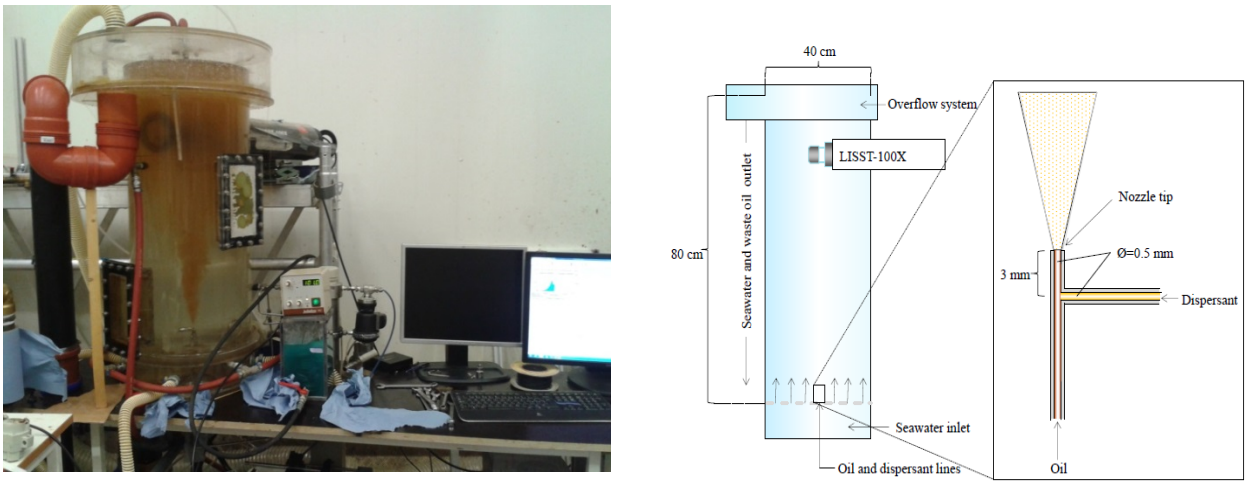

Figure 20: Set-up of the MiniTower (Dunnebier, 2015). On the right a schematic image of the MiniTower (Leirvik, SINTEF, 2013 as in Berg Lindersen, 2013).

Figure 20 shows the experimental set-up for the MiniTower. The diameter of the tower is 40 cm, and for the overflow compartment 60 cm. The whole set-up is 80 cm high with an approximately volume of 80 l. The box filled with blue liquid is the temperature bath, which can hold 2 l of antifreeze/water mixture. The laser can be seen on the right of the tower. The LISST is connected to the computer for real-time results. Filtered, natural seawater enters the MiniTower from the bottom.

3.6.2 Laser In-Situ Scattering and Transmissometry (LISST)

Droplet sizes were measured using the LISST-100X Particle Size Analyzer from Sequoia Scientific inc. LISST is the abbreviation of Laser In-Situ Scattering and Transmissometry and as the name says, it uses laser diffraction to measure droplet sizes with a droplet size distribution as result. The advantage of laser diffraction is that the composition of the particles does not matter since it does not measure a single particle but a group of particles since the scattering of the laser light is observed at multiple small forward angles.

Sequoia Scientific Inc. has several LISSTs but for this thesis only LISST-100X type C was used. This type contains a detector which contains 32 rings logarithmically increasing from 5 µm to 500 µm. A 1cm diameter path reduction model is added to decrease the volume measured and allow higher concentrations (Sequoia Scientific Inc., 2012). The LISST used in this project has an upper limit of 500 µm. As Davies et al. (2012) pointed out, there are some uncertainties in the LISST-100X but for this project, the instrument is suitable.

The LISST-100X records 20 frames per second and within the chosen timeframe, a number of measurements, where the recordings are stable, will be taken and averaged.

3.6.3 Simulated insertion tool (SIT)

The dispersant is injected into the oil 3 mm before the oil is released into the seawater, using a simulated insertion tool (SIT). Both the nozzle and the SIT have a diameter of 0.5 mm.

3.6.4 Temperature

The temperature of the oil is measured approximately 10 cm before the nozzle, the dispersant is always at room temperature. Seawater temperature is measured on top of the MiniTower, in the overflow compartment.

The oil can be brought to a chosen temperature by using an oil heater. This is an extra, longer line which is twisted around a heater in a water bath. To be able to reach higher temperatures, an anti-freeze/water mixture was used in the bath instead of water.

The initial experiments were carried out at three different volumetric dispersant-to-oil-ratios (DORs), namely: 1:500, 1:250 and 1:100. For the temperature experiments, a DOR of 1:100 was chosen.

The oil was continuously heated from approximately 16 °C to 90 °C in 9 minutes. Two releases were alternated: non-treated and dispersant injection. The results of the two releases were compared to each other and effectivity could be calculated using equation:

$$Effectivity = \frac{d_{50,non-treated} - d_{50,treated}}{d_{50,non-treated}} * 100\%$$

Equation 28

3.7 SINTEF Inverted Cone

3.7.1 Experimental set-up

The Inverted Cone is a system developed by SINTEF Materials and Chemistry, Environmental Technology based on the watertunnel facility developed by the University of Hawaii (Davies et al., 2015) to track single oil and treated oil droplets. It allows to study the behavior of an oil droplet in an uniaxial flow, follow the change in equivalent circular diameter (ECD) and observe the tip-streaming phenomena, all for a longer period of time after the initial formation.

The equivalent circular diameter (ECD, or D_c) can be calculated by using equation 29. The assumption is made that the z-dimension of the particle and the area covered by the convex hull (C_A), are directly proportional to each other.

$$D_c = 2\sqrt{\frac{C_A}{\pi}}$$

Equation 29

The spheroidal diameter

$$D_{sp} = 2\sqrt[3]{(0.5L_{maj})^2 0.5L_{min}}$$

Equation 30

$$v = \frac{4}{3}\pi\left(\frac{C_A}{\pi}\right)^{1.5} = \frac{2}{3}\pi(0.5L_{maj})^2 L_{min}$$

Equation 31

The main idea is to get the rising velocity of the released droplets in approximate equilibrium with a downward current. The downward waterflow is gravity-driven and water is drained at the bottom of the set-up (figure 21), there is no re-circulation of water. It is possible to tune the velocity so the droplets stay in the imaging section under stable observation conditions.

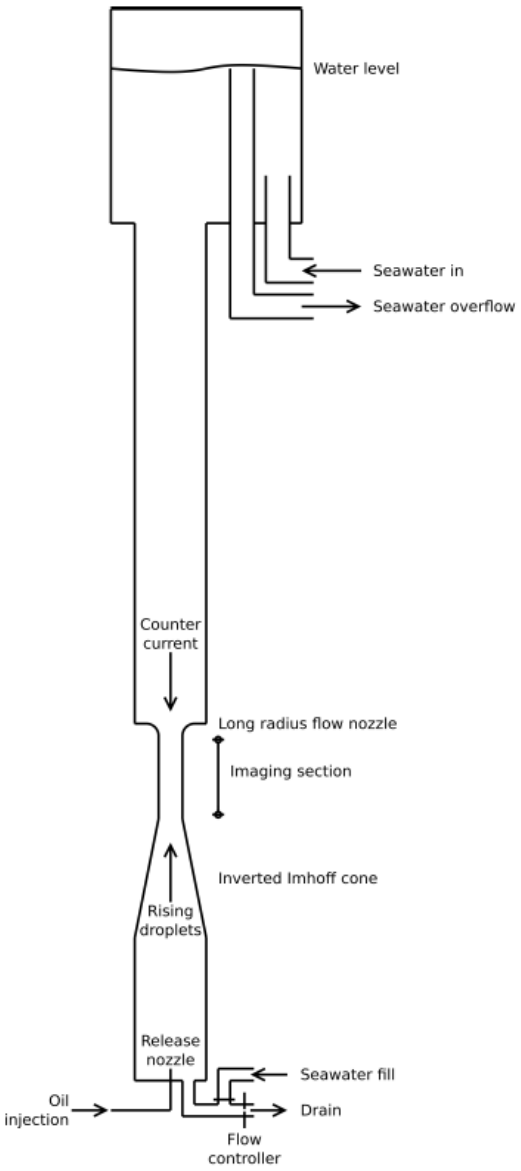

Figure 21: The Inverted Cone set-up shown schematically (Davies et al., 2015)

This imaging section (figure 22) consists of the small 25 mm diameter cylinder which is encapsulated by a container filled with water to reduce optical distortion caused by the curved cylinder surface. The camera is focused on this box and has an imaging section of 35 m high and 25 mm wide. The standard acquisition rate is 7 Hz but if necessary it can be up to 15 Hz.

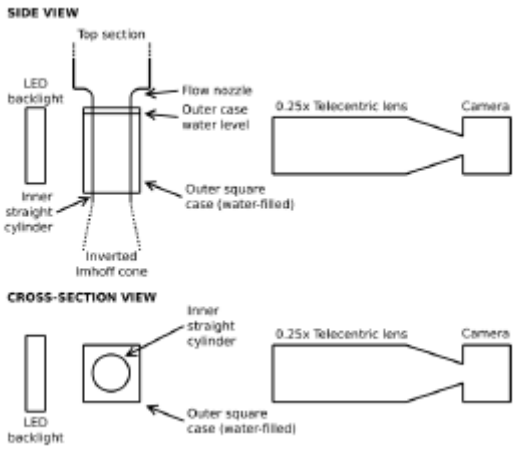

Figure 22: The camera set-up used for the Inverted Cone experiments (Davies et al., 2015).

The minimum droplet size that can be tracked and recorded was 56 µm. This is determined by using equation 32 and as the pixel size is 14 µm for the camera, the minimum droplet size was 56 µm. While recording, a clean background is used for correction in order to reduce noise.

$$D_{min} = 2\sqrt{\frac{12P_s^2}{\pi}}$$

Equation 32

A second cone was added to be able to better regulate the concentration of droplets in the imaging section, see figure 23. Vertical velocity profile of the downward flowing counter current. The velocities shown are approximated from the cone areas and are relative to the velocity in the imaging section.

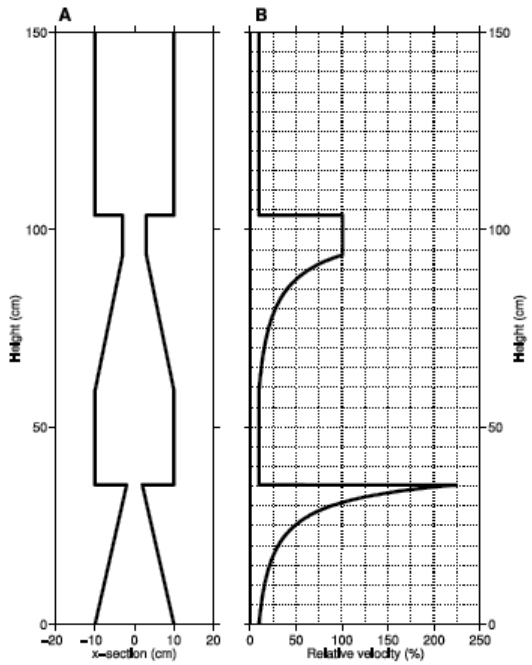

Figure 23: the two inverted Imhoff cones (left) and the velocity relative to the imaging section (right)(Davies et al., 2015).

For more details on the Inverted Cone method, see Davies et al., 2015.

3.7.2 Injection

To ensure that the oil and dispersant injected in the Inverted Cone are properly mixed, a chosen amount of oil and dispersant can be injected and discarded prior to the experimental injection. After the injection into the set-up, the oil will rise through the first cone, into the second cone. It is possible to let only a few droplets rise to the second cone and keep the rest in the first one. This is to lower the droplet concentration and make it easier to track a single droplet.

3.7.3 Montages

Besides tracking a single droplet there is also the possibility to make montages. In order to do so, the pcv is set to zero for the whole time. All droplets will rise freely and from the images and a specific MATLAB script, a montage can be created. A second montage can then be made by keeping all the droplets in the first cone for a longer period of time under turbulent conditions. After the set time, the droplets will be set free and recorded by camera.

3.7.4 Data processing

Several MATLAB scripts, developed by Dr. Emlyn Davies for SINTEF, are used to analyze the Inverted Cone data. The details of the scripts will not be further explained in this thesis.

3.8 OSCAR settings

Simulations of hypothetical oil spills were performed using the Oil Spill Contingency and Response (OSCAR) model, version v6.6.1, developed by SINTEF and earlier explained in chapter 2. These simulations are purely hypothetical without a real incident or specific field operator in mind. In this part, the settings used for these simulations are listed.

Geographical settings

- 71° 18’ N, 22° 15’ E (Barents sea)
- Release on the seafloor: ±356 m depth

Well settings

- Diameter: 0.217 m
- Oil: Kobbe

Blowout settings

- Oil rate: 1500 and 4500 m^3/day
- Gas-to-Oil-Ratio (GOR): 46
- Oil-water $IFT_{non\text{-}treated}$: 0.017 N/m
- Oil-water $IFT_{treated}$: 0.00017 N/m

Other settings

- Simulation time: same as release time: 3 hours and 10 days
- Starting date: January 2nd, 2010
- Starting time: 00:00
- Air temperature: -2 °C
- Liquid/solid particles: 25000
- Dissolved particles: 25000
- Gas particles: 1000
- Output interval: 1 minute for the 3 hour simulations and 1 hour for the 10 day simulations
- Time step: same as output interval

4. Results and discussion

This chapter presents the results of the three different studies: the MiniTower experiments towards surfactant behavior at elevated temperatures, the Inverted Cone experiments to study tip-streaming and in the last part, the simulation study performed with OSCAR.

4.1 MiniTower study of surfactants

In this sub-chapter, the results of the MiniTower experiments will be presented and discussed. The experiments in the MiniTower give information about the initial droplet formation and droplet size distribution of the released (treated) oil and the effect of temperature on the treatment of crude oil with dispersants. The experimental details can be found in chapter 3.6. First, the results of the initial optimization experiments are presented, followed by the results of the temperature experiments.

4.1.1 Initial study

The initial droplet formation and droplet size distribution were studied in the MiniTower. Figure 24 shows two plumes, on the left side a non-treated plume of Troll oil and on the right side a plume of Troll oil where a surfactant blend has been injected in.

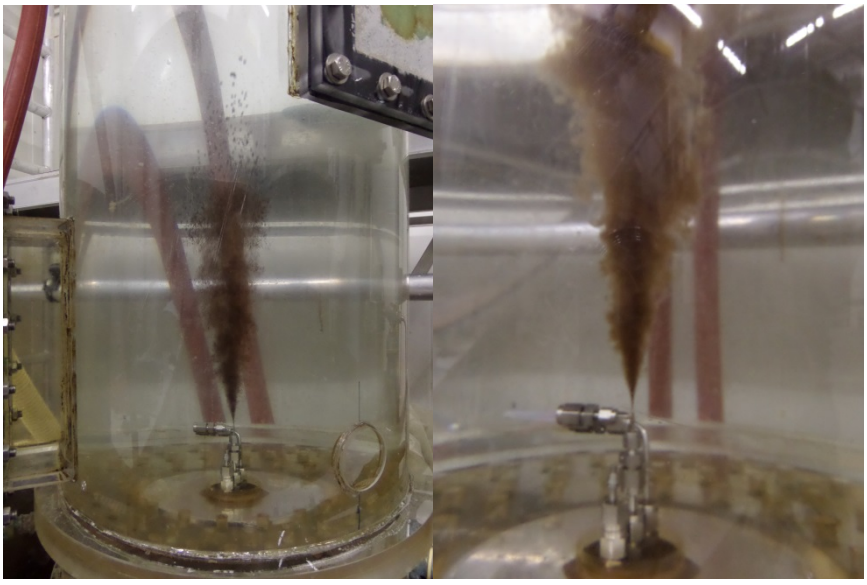

Figure 24: Photos of non-treated and treated Troll oil in the MiniTower (Dunnebier, 2015).

In figure 25 the results of one of the experiments is shown. The four lines represent oil alone (red), DOR 1:500 (green), 1:250 (purple) and 1:100 (blue). A shift in the median volume diameter is observed. The median volume diameter (MVD) for non-dispersed oil is 274 µm, whereas the MVD for the oil dispersed at a DOR of 1:100 is 182 µm. The upward slope after 390 µm is probably caused by a very limited number of large droplets. The LISST has an upper limit of 500 µm and all droplets above this limit are recorded as large droplets. In the relative volume distribution only a few droplets will therefor seem as high percentage of large droplets. Not all figures will be shown here; three triangles of each ten experiments

give 30 results, which is too much to show and discuss here, the combined graphs are therefore presented in appendix A.

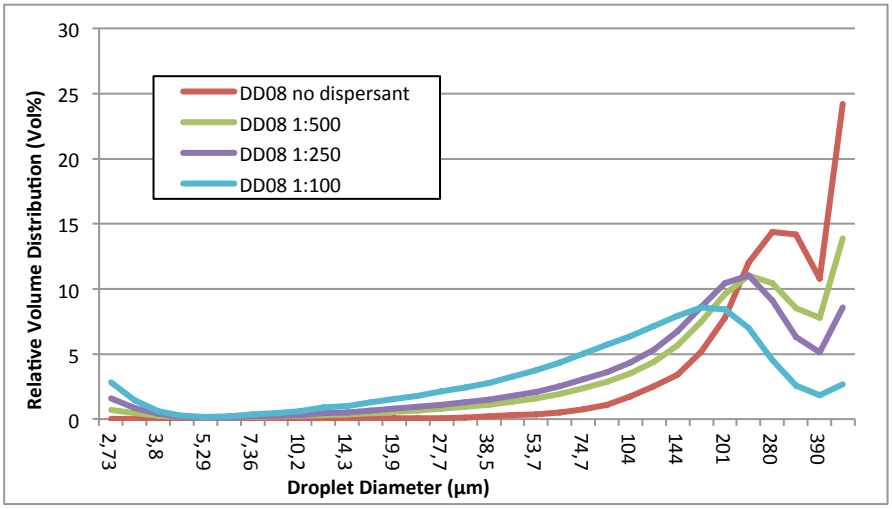

Figure 25: Relative volume distribution vs droplet diameter for dispersant injection of Troll with surfactant mixture DD08. The different lines represent different DORs.

To show how different compositions give different MVDs, volume distributions have been calculated and per triangle non-treated and DOR 1:100 are presented in the following figures. The other figures, DORs 1:500 and 1:250, can be found in appendix A.

In the first three, the non-treated oil volume distributions of all three triangles are shown. It is important to compare these to each other to see if the set-up gives similar results every time.

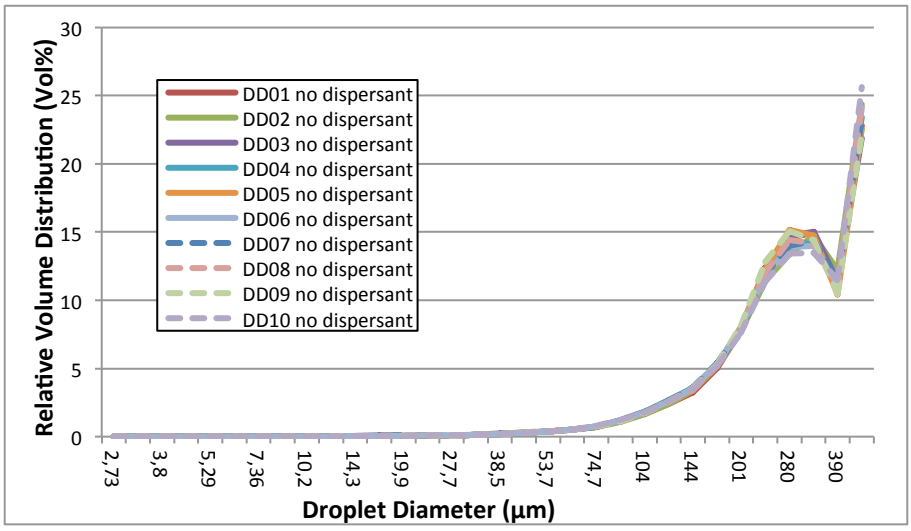

Figure 26: Relative volume distribution vs droplet diameter for non-treated Troll oil in the first experimental triangle.

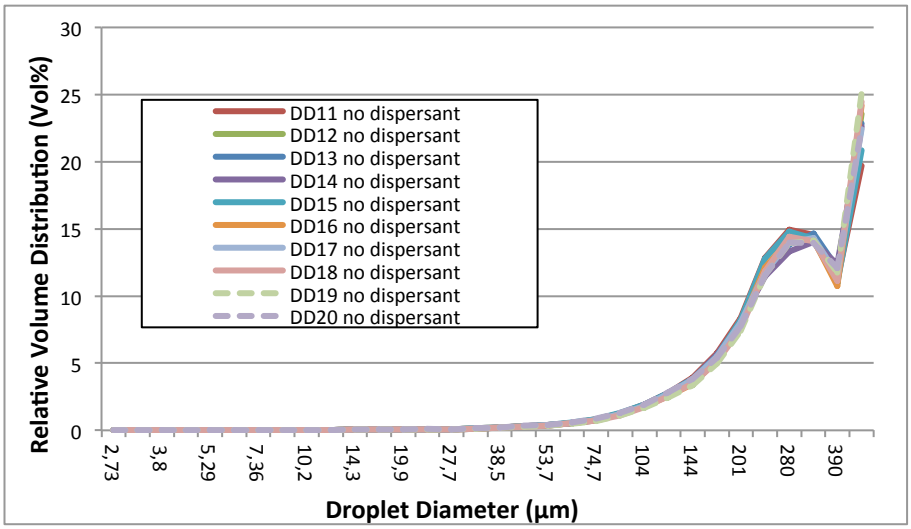

Figure 27: Relative volume distribution vs droplet diameter for non-treated Troll oil in the second experimental triangle.

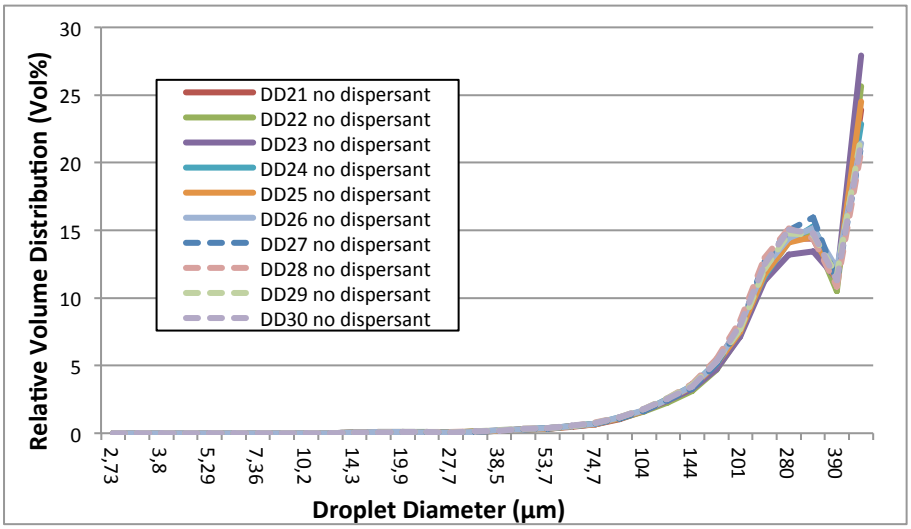

Figure 28: Relative volume distribution vs droplet diameter for non-treated Troll oil in the third experimental triangle.

The following three graphs, 27, 28 and 29, show the relative volume distributions for all surfactant combinations tested at DORs of 1:100. It can be seen that some combinations have a greater shift and more effect then others, for example DD03 and DD05. The upward slope below 5 µm are a result of the lower limit of the LISST being 5 µm. Surfactant droplets mixed in the water can be recorded as very small droplets and added to the relative volume distribution.

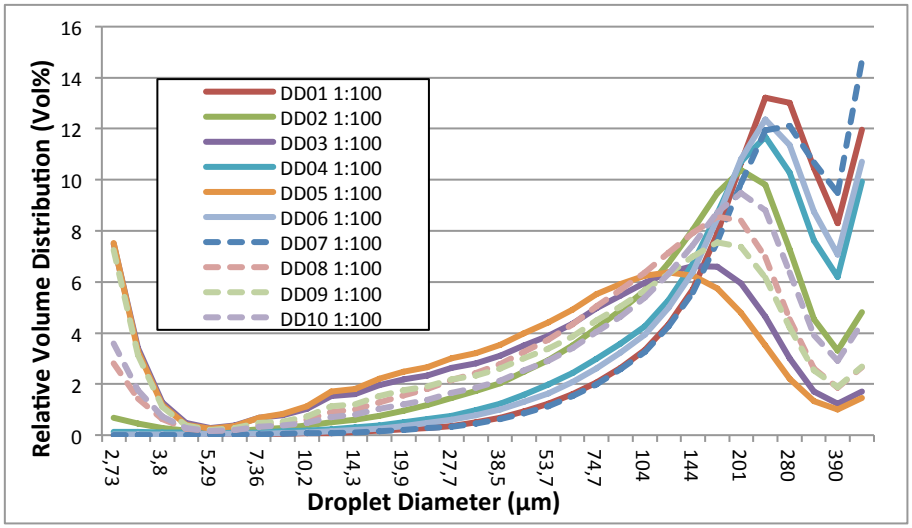

Figure 30: Relative volume distribution vs droplet diameter for Troll oil treated with DOR 1:100 surfactant mixtures of the first experimental triangle.

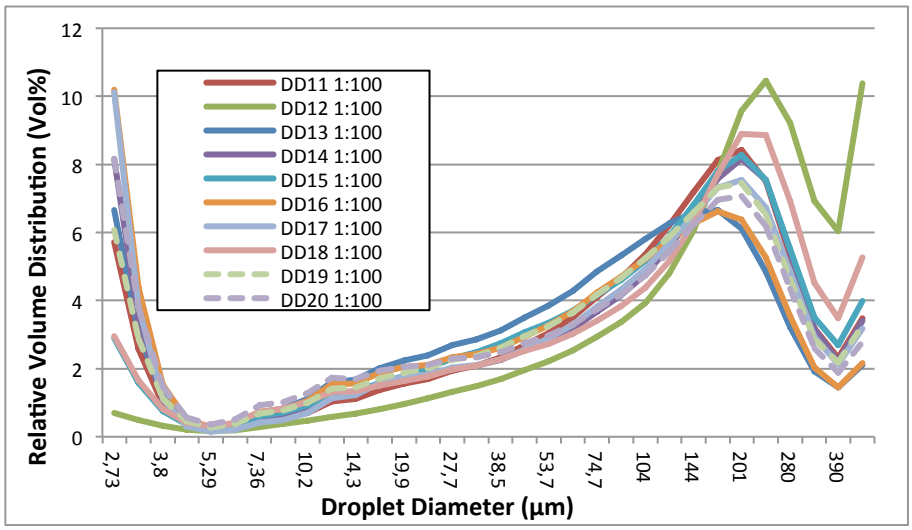

Figure 29: Relative volume distribution vs droplet diameter for Troll oil treated with DOR 1:100 surfactant mixtures of the second experimental triangle.

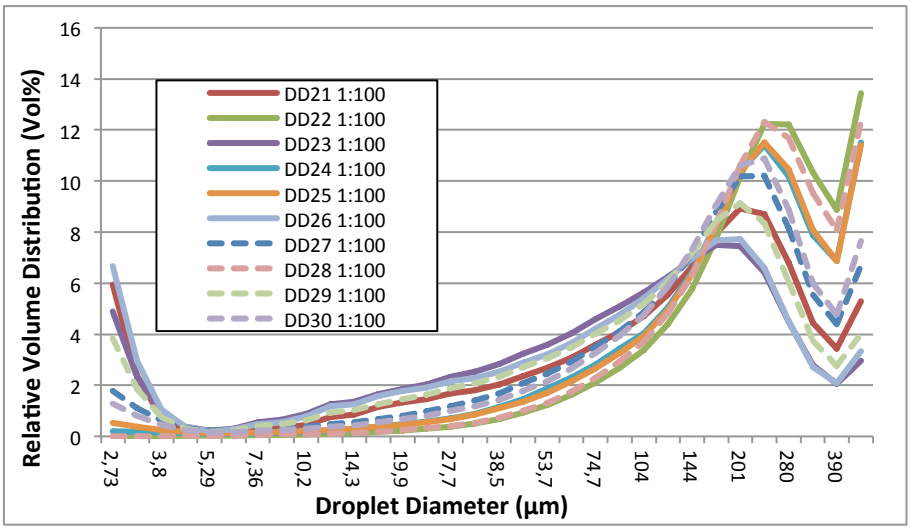

Figure 31: Relative volume distribution vs droplet diameter for Troll oil treated with DOR 1:100 surfactant mixtures of the third experimental triangle.

4.1.2 Temperature effect

The next step was to study the effect of higher temperatures on surfactant effectiveness. Laboratory studies are often performed at room temperatures, however, when oil comes out of the well, it can have a much higher temperature. Therefor higher temperatures are studied in this thesis. The surfactant combination of the third triangle, Tween 85, Span 80 and DOSS, was tested at a DOR of 1:100. Temperature range was from room temperature (17 °C) to approximately 90 °C. The box in which the oil heater was placed, is made out of polycarbonate, which has a glass transition temperature of 147 °C. As a boiling liquid, a mixture of concentrated anti-freeze and water 70:30 was used. For safety reasons, the maximum temperature limit was 120° C, which was reached after 9 minutes. As the oil needs time to warm up, the maximum temperature that could be obtained for the oil was therefore around 90 °C.

As mentioned earlier, this work focused on studying the effect of temperature on surfactants rather than finding the optimum combination. One could study each surfactant or commercial dispersant separately but by studying combinations, the effect on three different surfactants can be studied in an easier and quicker way. The next 9 figures present the results of these experiments with the MVD plotted against the temperature.

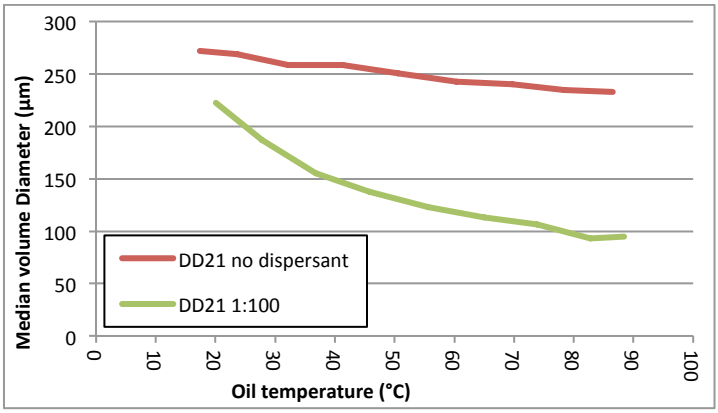

Figure 32: MVD vs. temperature for Troll oil treated with DD21 at DOR 1:100.

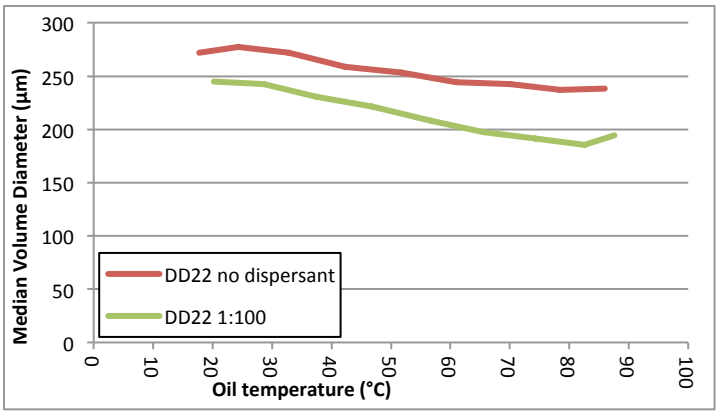

Figure 33: MVD vs. temperature for Troll oil treated with DD22 at DOR 1:100.

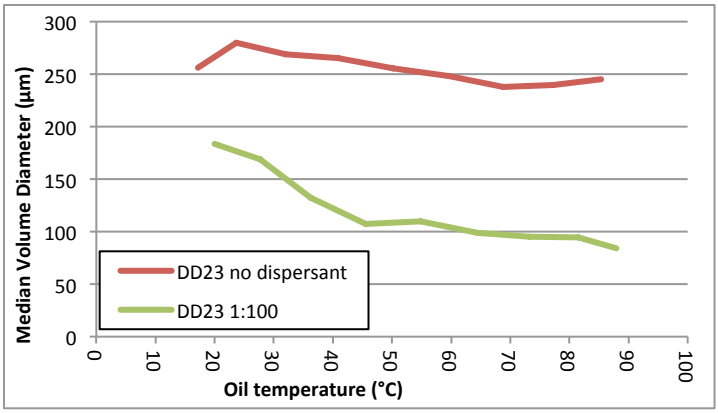

Figure 34: MVD vs. temperature for Troll oil treated with DD23 at DOR 1:100.

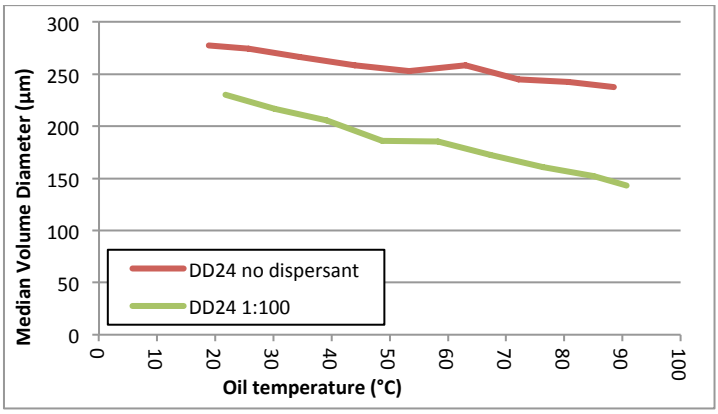

Figure 35: MVD vs. temperature for Troll oil treated with DD24 at DOR 1:100.

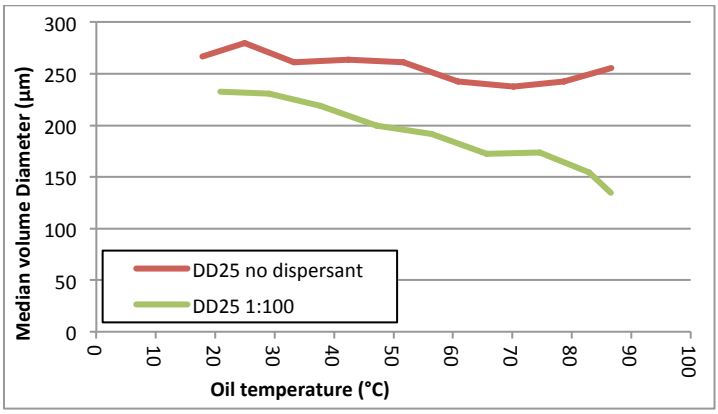

Figure 36: MVD vs. temperature for Troll oil treated with DD25 at DOR 1:100.

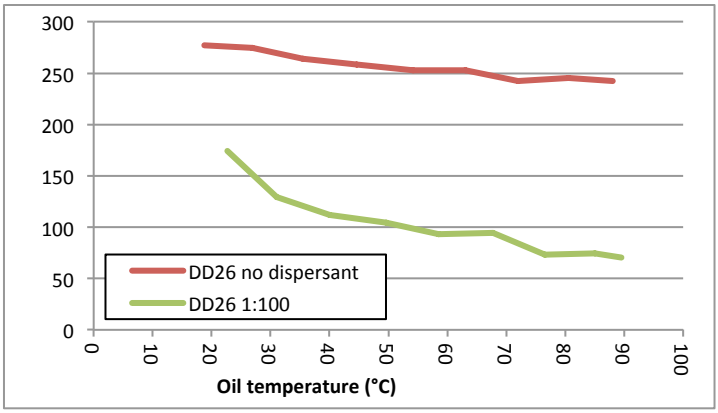

Figure 37: MVD vs. temperature for Troll oil treated with DD26 at DOR 1:100

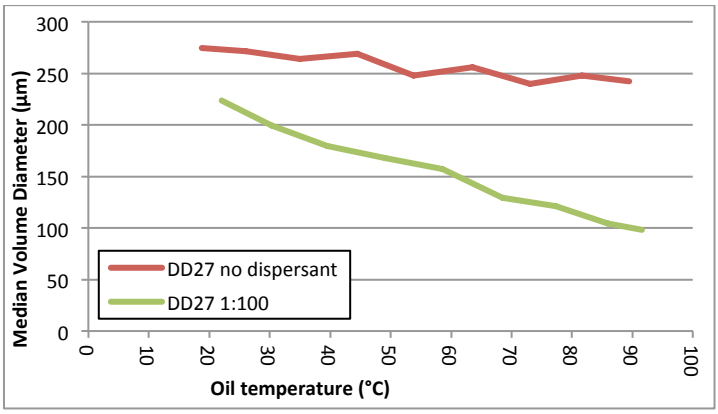

Figure 38: MVD vs. temperature for Troll oil treated with DD27 at DOR 1:100.

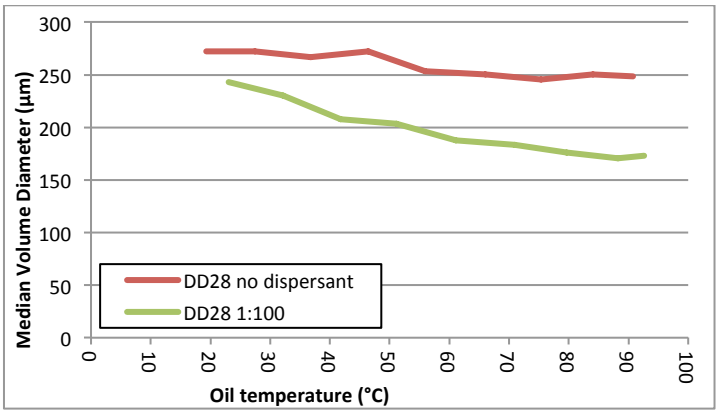

Figure 39: MVD vs. temperature for Troll oil treated with DD28 at DOR 1:100.

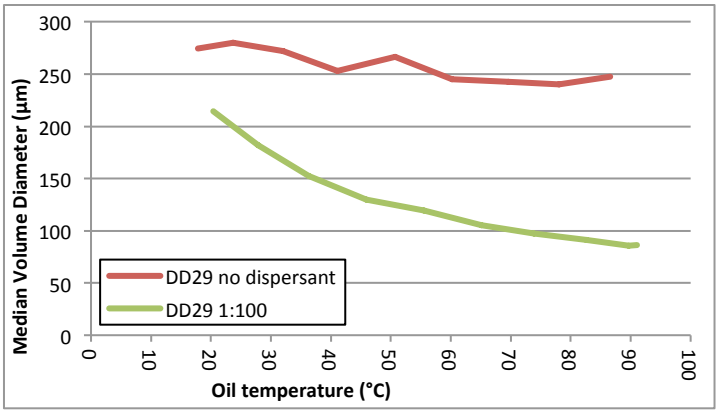

Figure 40: MVD vs. temperature for Troll oil treated with DD29 at DOR 1:100.

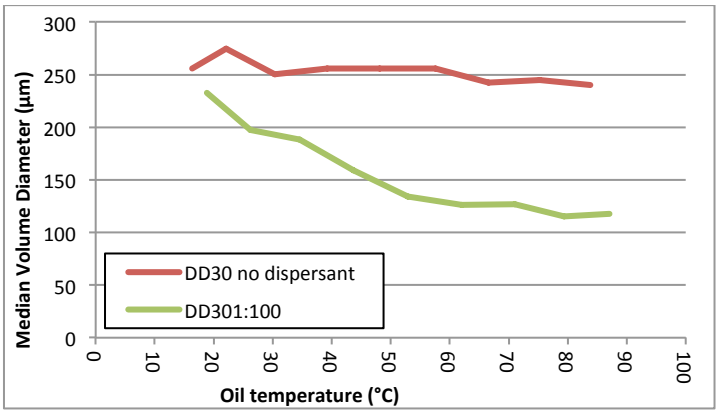

Figure 41: MVD vs. temperature for Troll oil treated with DD30 at DOR 1:100.

In five of the experiments (DD 22, 23, 25, 29 and 30) a lower MVD for the first non-dispersed timeslot than the second was observed. The first MVD was also lower than previously observed in the initial experiments. This has been observed more often and the reason is that in the very initial phase of the experiment the conditions are slightly different from the rest of the experiment due to water and oil mixing. This produces small droplets which rise more slowly and can cause a lower MVD in the first part of the experiment.

In addition to the own surfactant mixtures, also Corexit 9500A was tested. Corexit 9500A is a commercially available dispersant used in many oil spills and tests. The results are presented in figure 42.

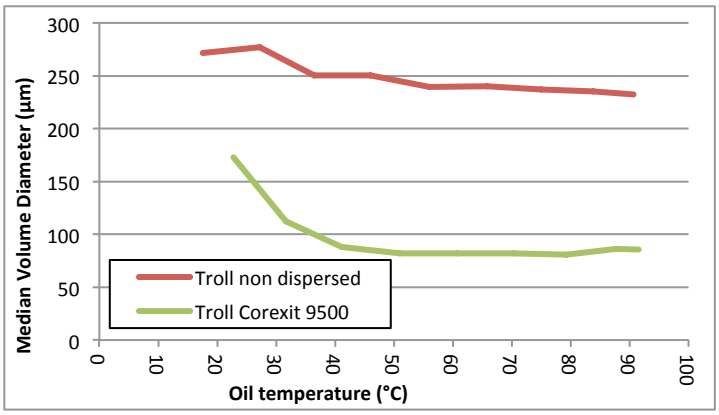

Figure 42: MVD vs. temperature for Troll oil treated with Corexit9500A at DOR 1:100.

Just like the previous graphs, this figure shows a clear decrease in MVD when the temperature increases. The non-dispersed oil had a MVD of 277 µm at T1, decreasing to a MVD of 232 µm at T9. The oil injected with Corexit 9500A, decreased from 173 µm at T1 to 86 µm at T9. However, for Corexit, the effectivity becomes quite constant at temperatures of 50 °C and higher.

For all mixtures, the result was that the warmer the oil, the better the dispersing and the smaller the average droplet diameter was. The expectation was that the MVD would decrease with an increase of temperature. However, the observed results are in contradiction with the results of earlier experiments performed by Brandvik et al. (2014). in the Tower Basin. In those experiments, the authors found the opposite results: the dispersants became less effective at higher temperatures.

In the former work by Brandvik et al. (2014), the following suggestions were given for their results:

- The cold injected dispersant cools the warm oil, and thereby reducing the effect of lower viscosity, warm oil.
- Less efficient mixing is obtained because the viscosity difference between the warm oil and cold dispersant has increased.

- The micelle transitions for the surfactants in the oil and the resulting IFT could change at elevated oil temperatures.

The results from the experimental work presented in this thesis show the opposite. One possible reason is that there is a larger cooling effect in the MiniTower compared to the Tower Basin. The flow in the MiniTower is quite small, 100 ml/min, which gives a small plume. Therefore the cooling effect of the cold seawater could be bigger than in experiments in the Tower Basin. However, there is still a downward slope visible in all graphs meaning that even if there would be a bigger cooling effect, with warmer oil the size distribution still shows smaller droplets.

The temperature experiments for this thesis have been performed in a continuous oil flow, 30 seconds of oil alone and 30 seconds of treated oil alternating. Thus, the effectivity of the treated oil is calculated compared to the previous 30 seconds of non-treated oil. The temperature difference between these two fractions is around 5 °C. Temperature is measured just before the dispersant is injected in the oil and the mixture is blown out of the nozzle. Because the dispersant is injected before the oil is released into the seawater, just a cooling effect would not be likely as the only reason for these interesting results and the downward slope proves that there is an efficient mixing.

The question is whether this different behavior is a result of oil chemistry or surfactant chemistry. Brandvik et al. (2014) studied a different oil than was used for this thesis. Where here Troll B oil is used, Brandvik et al. used Oseberg and only at two different temperatures (15-51 °C) where this project used a constant increasing oil temperature. It is possible that the opposite results may have to do with the oil chemistry, as Troll B and Oseberg are quite different from each other. Salager et al. (2000) studied the partitioning of ethoxylated octylphenol surfactants and the influence of temperature. A change in behavior of the partitioning between the oil-water system was observed as the properties changed as a function of temperature.

As mentioned above, the results of the temperature experiments were surprising. To see if these results are a result of oil chemistry or surfactant chemistry one more experiment was performed with Kobbe and Corexit 9500A. The results can be seen in figure 43.

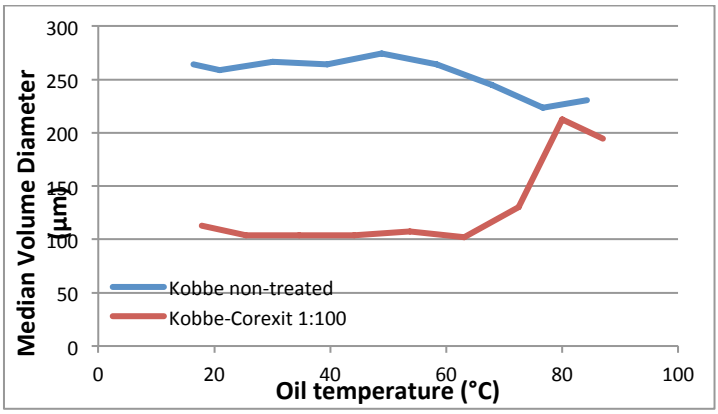

Figure 43: MVD vs. temperature for Kobbe oil treated with Corexit9500A at DOR 1:100.

The Kobbe oil reacts completely different from the Troll oil to dispersion. Up until approximately 60 °C, the MVD is relatively stable between 104 and 113 µm. But, between a temperature of 63 °C and 80 °C, the effectivity suddenly decreases and the MVD for the dispersed oil rises with a slope of 6.5 µm/°C. This is the opposite of what has been observed with the Troll B oil so far, but these results are in accordance to what has been previously observed by SINTEF in the Tower Basin. (Brandvik et al., 2014)

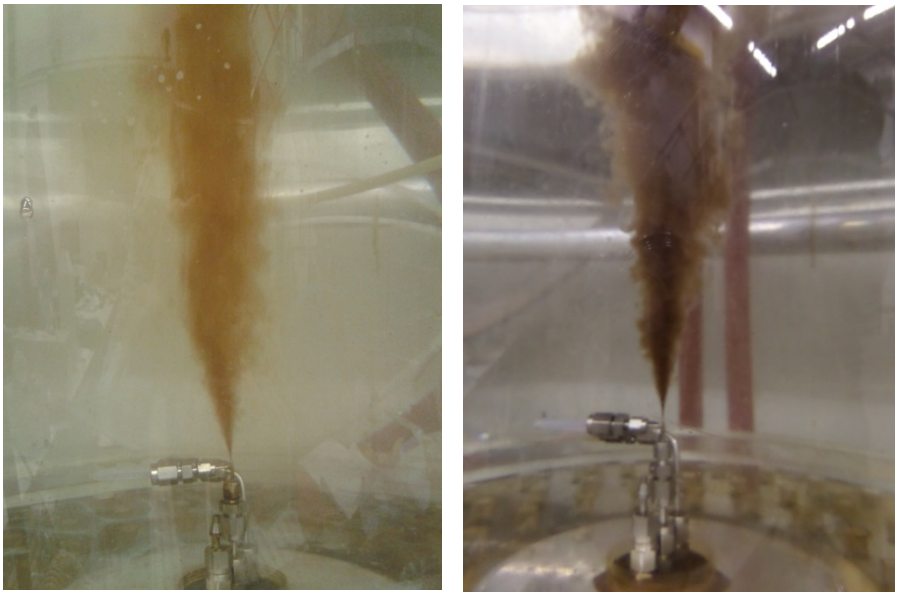

Figure 44: Left: treated Kobbe oil and right: treated Troll oil in the MiniTower (Dunnebier, 2015).

It is important to mention that the Troll B and the Kobbe oil have different properties. Troll B is a more naphthenic oil whereas Kobbe is a light oil. The latter has more lighter components which could influence the effectivity of the surfactants. In figure 44 the two oils can be seen when dispersed in the MiniTower. On the right is the Troll B oil and on the left the Kobbe oil. Kobbe is much lighter of color than Troll B. Due to the limited amount of Kobbe oil available for this project, it was unfortunately not possible to perform more experiments. This would be recommended, also with other oils to see whether this change in MVD with increase in temperature is an effect of the dispersant chemistry or of the oil chemistry.

4.1.3 Response surfaces

To study the results closer, the same aforementioned multivariate linear regression was performed, using the special quartic equation without β_0 (equation 33) and response surfaces were created. The results are shown in figure 45.

$$y = \beta_1 x_1 + \beta_2 x_2 + \beta_3 x_3 + \beta_{12} x_1 x_2 + \beta_{13} x_1 x_3 + \beta_{23} x_2 x_3 + \beta_{1123} x_1^2 x_2 x_3 + \beta_{1223} x_1 x_2^2 x_3 + \beta_{1233} x_1 x_2 x_3^2$$

Equation 33

The coefficients were calculated using the regression function in Microsoft Excel. The coefficients were filled in in the equation and response surfaces were created using MATLAB.

An increase in the y_{max} can be seen when following the figures from T1 to T9. There are some small white parts in some of the response surfaces, which most probably can be attributed to the calculation density, which is 1, and therefor values between 0 and 1% are not represented.

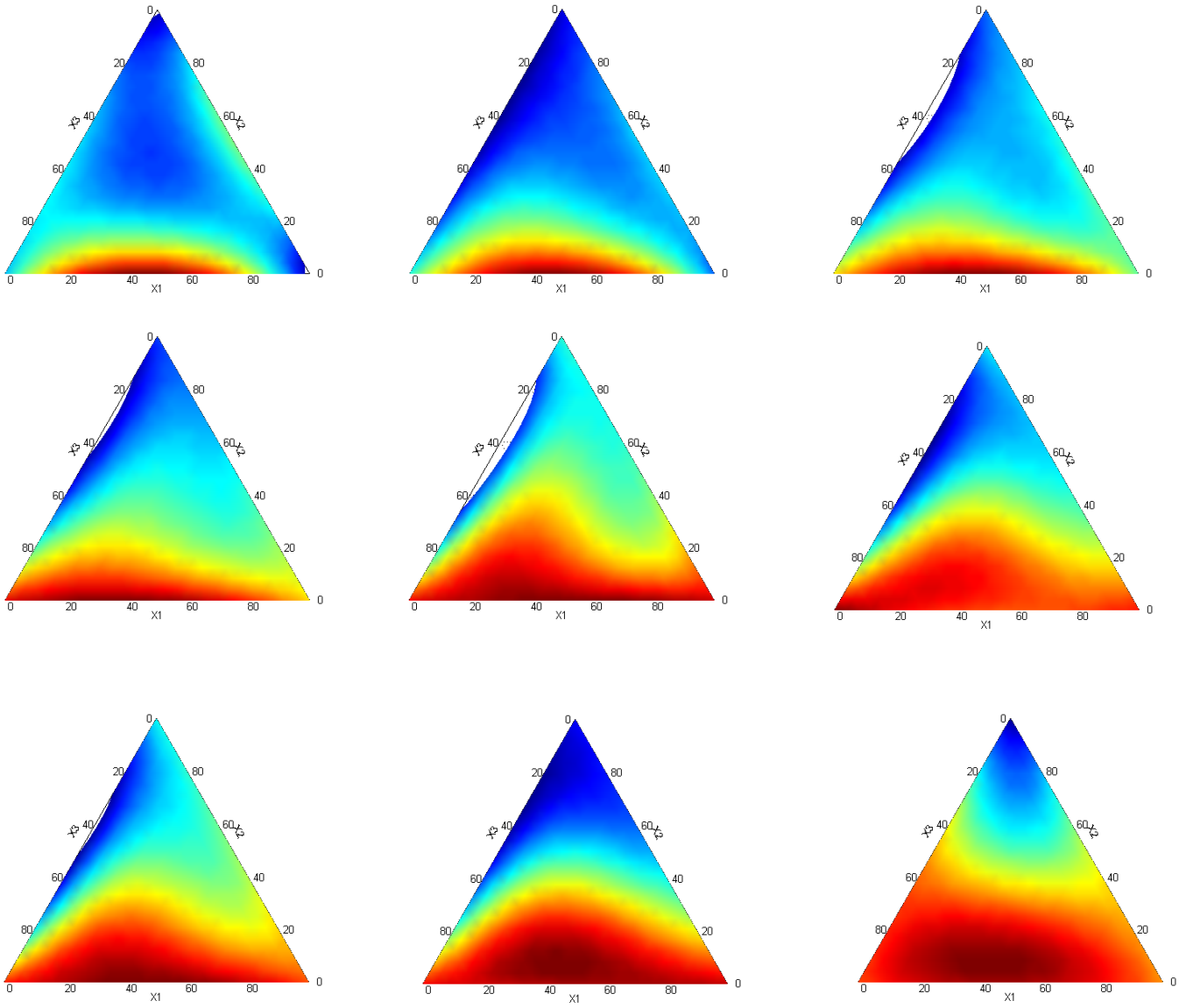

Figure 45: The 9 response surfaces resulting from the temperature experiments. Upper left is at temperature slot T1, the lower left surface is from temperature slot T9. Blue represents very low values of ymax, whereas red represents high values of ymax.

Using the response surface, the maximum response and the associated combination of surfactants was calculated. Those numbers are summarized in table 5.

Table 5: This table shows the ymax and optimum combinations of the three surfactant for the 9 different temperature slots.

Temperature frame	$T_{average}$ °C	y_{max} %	Tween 85 %	Span 80 %	DOSS %
T1	20	65	45	0	55
T2	27	76	46	0	54
T3	36	89	45	0	55
T4	45	81	36	0	64
T5	54	74	54	0	46
T6	64	72	0	0	100
T7	73	78	47	0	53
T8	82	70	40	8	52
T9	88	72	39	7	54

An interesting observation is the shift in optimum composition. First, the maximum response does increase but not extreme, from 65 % at T1, to 72 % at T9. As can be seen in the graphs above, the MVD of the dispersed oil decreases, but the MVD of oil alone does so too. The gap becomes larger, which leads to a higher effectivity for some of the combinations. The highest y_{max} is reached in the third temperature frame where the maximum effectivity is 89 % with a combination of 45% Tween 85 and 55% DOSS. After, when the temperature keeps increasing, the y_{max} fluctuates but decreases.

The optimum use of Tween 85, Span 80 and DOSS (x1, x2 and x3)does change. Where Span 80 did not play an important role at room temperature, at 90 °C it does, going from 0% to 7%. The optimum concentration of Tween 85 decreases from 45% at room temperature to 39% in the last temperature frame, which has an average temperature of 88 °C.

One possibility is that ethoxylated surfactants, like Tweens, become less effective due to the higher temperatures. As shown by Salager et al. (2000) the temperature does change the behavior of ethoxylated surfactants. The results obtained for this thesis, show that Tween 85 plays a much smaller role at higher temperatures.

When looking at table 5, T6 shows quite different predicted values than the other temperature frames. The surfaces are the results of an interpolation between the experimental points and extrapolation between the experimental points and the triangle borders. The estimated optimum combination of the three surfactants at the sixth temperature frame is outside the experimental points and a result of extrapolation, whereas the y_{max} of the other temperature frames fall within the experimental triangle.

4.2 Inverted Cone

This sub-chapter presents the results of the Inverted Cone experiments. In the Inverted Cone it is possible to study secondary droplet breakup, the process after the initial droplet formation, on a close up level, this provides more knowledge about the fate of droplets after initial droplet formation. The theory behind secondary droplet breakup is described in chapter 2.1.7 and the experimental method is explained in chapter 3.7. The sub-chapter is split into two parts: first the results of the tracking experiments are described and the limitations of this method, followed by the results of the experiments that lead to the montages.

4.2.1 Tracking

The objective of this part of the thesis was to study the maximum stable droplet size for Kobbe oil treated with Corexit 9500A. Experiments have been performed for two different DORs, 1:100 and 1:50, and for non-treated oil. A droplet is considered stable when it has stopped tip-streaming and remains spherical with a constant ECD (equivalent circular diameter) over a longer period of time.

In figure 46 this is shown for non-treated oil. The ECD of the droplet is approximately 2000 µm and remains stable for more than 30 minutes, until the droplet was released from the observation cell. The variation in diameter, ± 200 µm, observed in the graph, is a result of experimental uncertainties and the droplet moving around in the small cylinder and sometimes staying close to the sides. Even though a box filled with water has been placed around the cylinder to make up for the visual distortion, MATLAB still sometimes records a smaller diameter due to this visual distortion. A second reason for this variation, is that the cylinder is very difficult to get absolutely clean, therefor the images can be a bit blurry sometimes, which causes MATLAB to record a different diameter than it actually is. However, as can be seen in the graph, both these effects are very small.

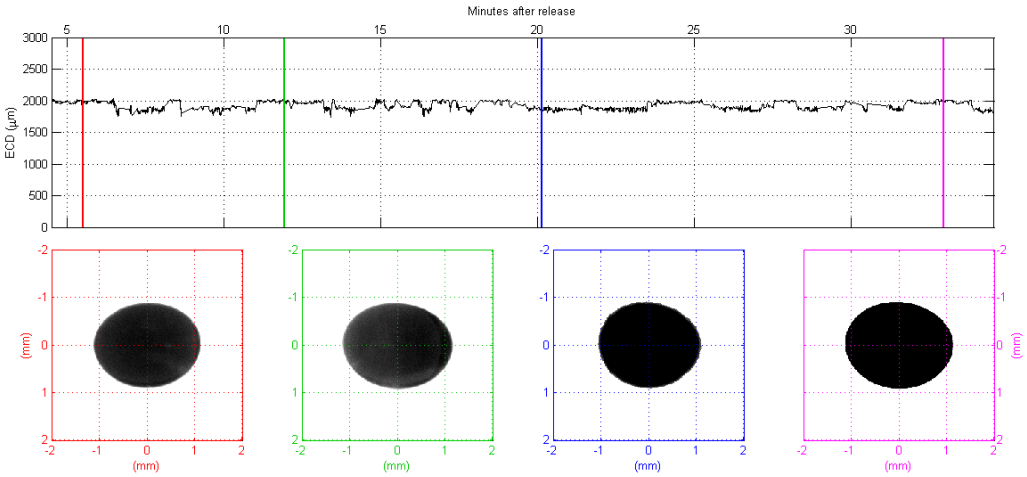

Figure 46: The resulting graph and images of tracking a non-treated Kobbe oil droplet in the Inverted Cone. The graph shows the change in ECD.

The next figure, 47, shows the droplet ECD vs time for a DOR of 1:100. The droplet is tip streaming as can be seen in the first two images of the figure and in the decrease in ECD in the graph. The phenomena tip streaming is explained in chapter 2. At approximately 6.5 min, the droplet has stopped tip streaming but is not completely spherical yet, as can be seen in the third, blue image. In the last, pink image the droplet is nearly spherical and stable in ECD as can be seen in the graph. Unfortunately, the droplet was lost shortly after.

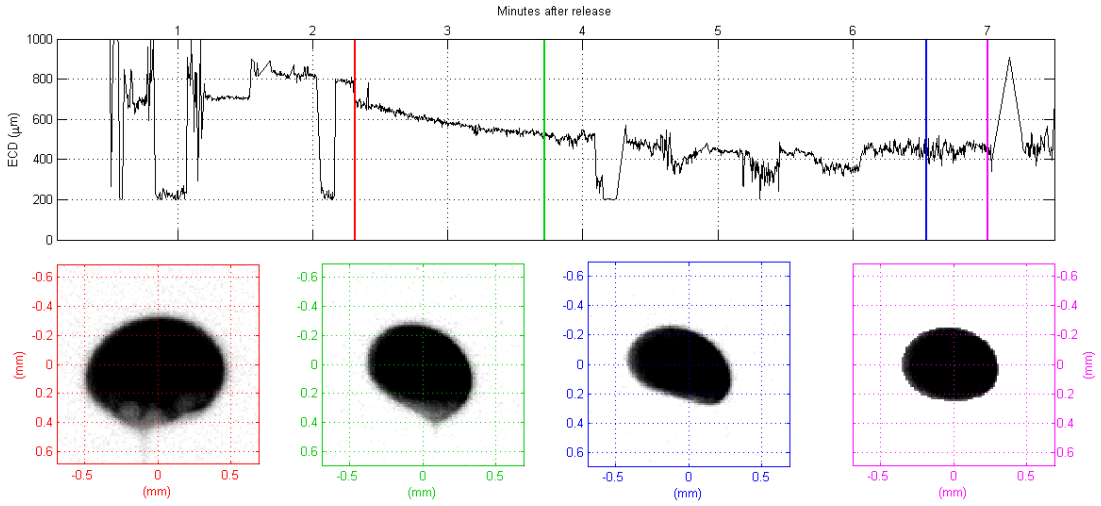

Figure 47: The resulting graph and images of tracking a Kobbe oil droplet that has been treated with Corexit 9500A at a DOR of 1:100 in the Inverted Cone. The graph shows the change in ECD.

This last figure of droplet tracking, figure 48, shows a dispersed droplet with DOR 1:50. Just like the DOR 1:100 figure, this figure clearly shows the tip streaming of the droplet in the beginning followed by a more and more spherical shape without tip streaming. Although the droplet has been tracked for more than 16 minutes, the last part of the graph had to be removed. This has been done because the MATLAB script had lost the droplet and was no longer able to track it.

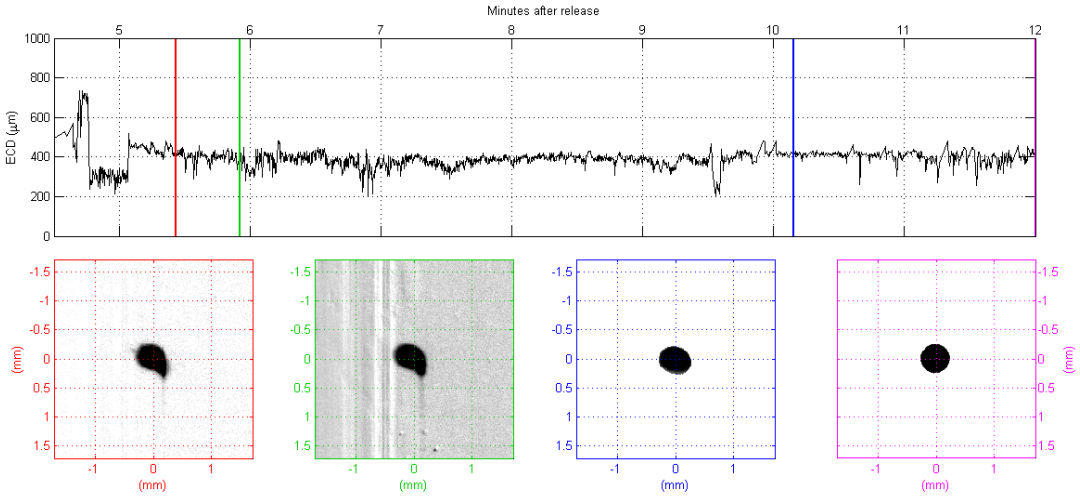

Figure 48: The resulting graph and images of tracking a Kobbe oil droplet that has been treated with Corexit 9500A at a DOR of 1:50 in the Inverted Cone. The graph shows the change in ECD.

The images are not as clear as the other images since the droplet size is much smaller, the camera needs to be zoomed in quite a bit. Nonetheless, the tip-streaming and stabilizing of the droplet is visible.

This method of tracking individual droplets provides good knowledge about the behavior of (dispersed) oil droplet over time and the possibility of tip-streaming. However, the experimental set-up does have some limitations. It is difficult to trap a small droplet in the observation cell, this makes it hard to study a wide range of different droplet sizes in the distribution.

To make it easier and quicker to study several droplets and in different turbulence levels, another method called montages, is an option.

4.2.2 Montages

Tracking a droplet for a longer period of time can be very challenging, especially small droplets dispersed with a high DOR. An easier way of showing the stability over time and in different turbulence levels, is by making montages. This has been explained in chapter 3 and the results are shown here.

During a regular tracking experiment, the water column is relatively stable. When making the montage, the droplets are kept in the first cone for approximately one hour before being released and recorded. This is a simpler method to study the stability of the dispersed droplets and their ECD.

Figure 49 shows the montages for non-treated oil during free flow and after 1 hour of turbulent conditions in the first cone. The droplets are now broken up and spherical, unlike a, where the droplets are unstable and blobby and differ much more in spherical diameter.

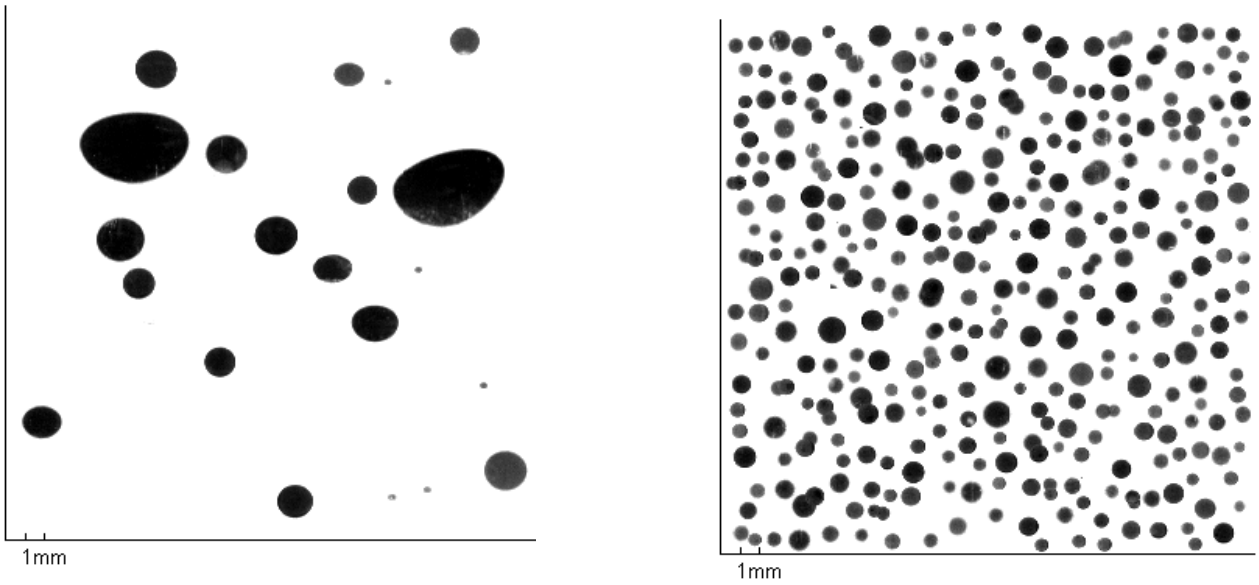

Figure 49: The resulting montages of experiments in the Inverted Cone. The left image shows a montage at t=0 and right for t= 1h for non-treated Kobbe oil.

In figure 50, the same experimental set up is used but instead of non-treated oil, the oil was dispersed with Corexit 9500A at a DOR of 1:100. As can be seen in the montages, tip streaming does not continue and the droplets are completely stable and spherical after one hour in the turbulent conditions. It must be mentioned that some of the oil got stuck to the walls of the cone during the one hour capture. The images do therefor not give an illustration of the volume or concentration of the oil. The script used to make these montages, takes random images from all the images made of the oil droplets during the rising.

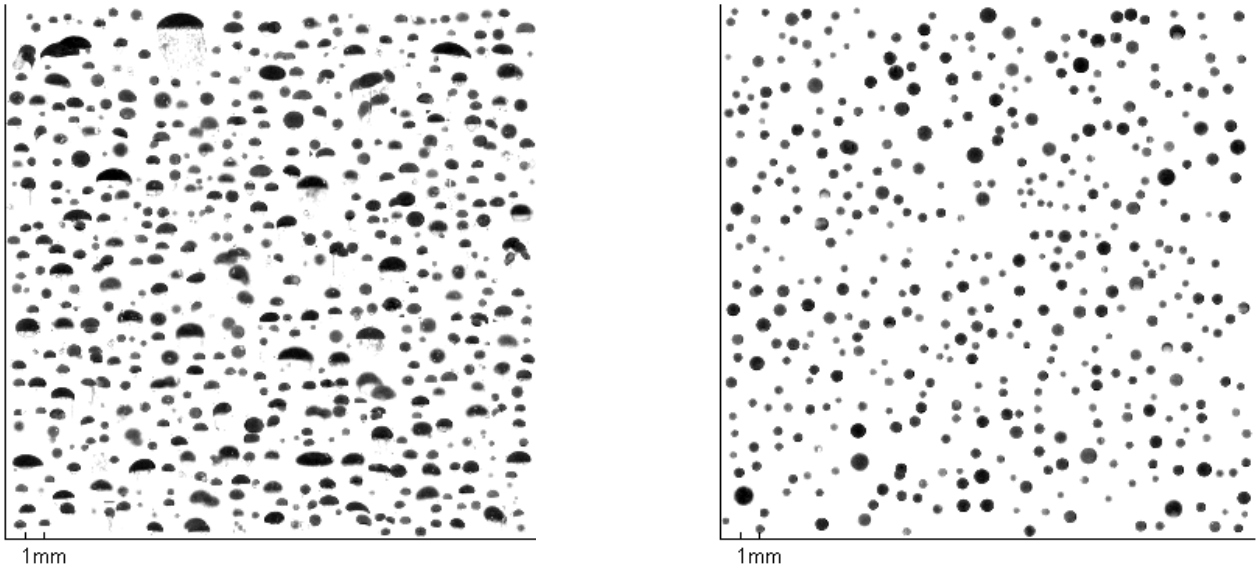

Figure 50: The resulting montages of experiments in the Inverted Cone. The left image shows a montage at t=0 and right for t= 1h for Kobbe oil treated with Corexit 9500A DOR 1:100.

This method is less disturbed by the limitations of the previous method, droplet tracking. However, it is also a much rougher method which does not provide much detail.

The results in these Inverted Cone studies show that the tip-streaming stops quite short after release and although not a large range of droplet sizes has been studied, it shows that the droplets stabilize and contain a spherical shape.

4.3 OSCAR

In this thesis, the initial droplet formation and secondary breakup of treated and non-treated crude oil have been studied. The third part of this study was to perform a modelling study towards subsurface blowouts in the Barents sea. The experimental details for this study can be found in chapter 3.8. This chapter presents the results of this study.

4.3.1 Vertical profile study

The first simulations were performed to study the vertical profile of the oil plume in the water column. The following four figures show the vertical profiles and mass balance for a 1500 m^3/day of oil without response (figure 51) and with subsurface injection of dispersant (figure 52) 3 hours after the start of the release.

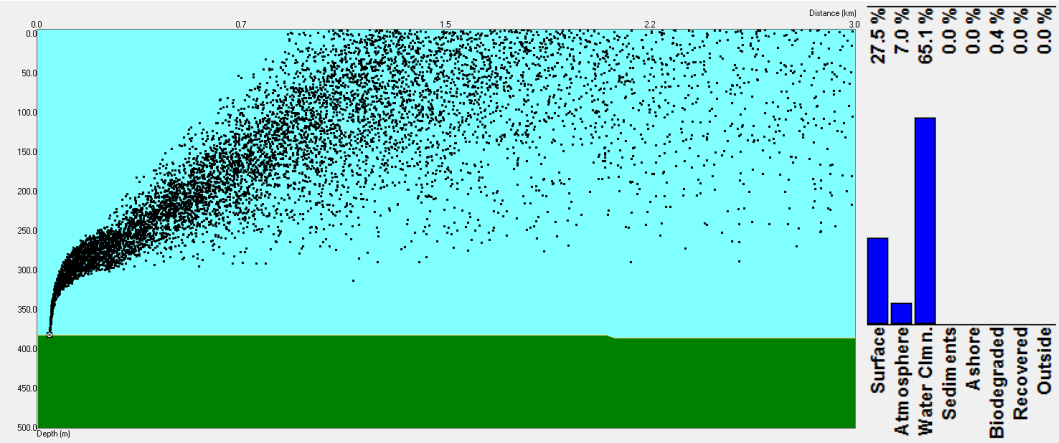

Figure 51: Vertical profile and mass balance for a 1500 m^3/day release after 3 hours without subsurface injection of dispersants.

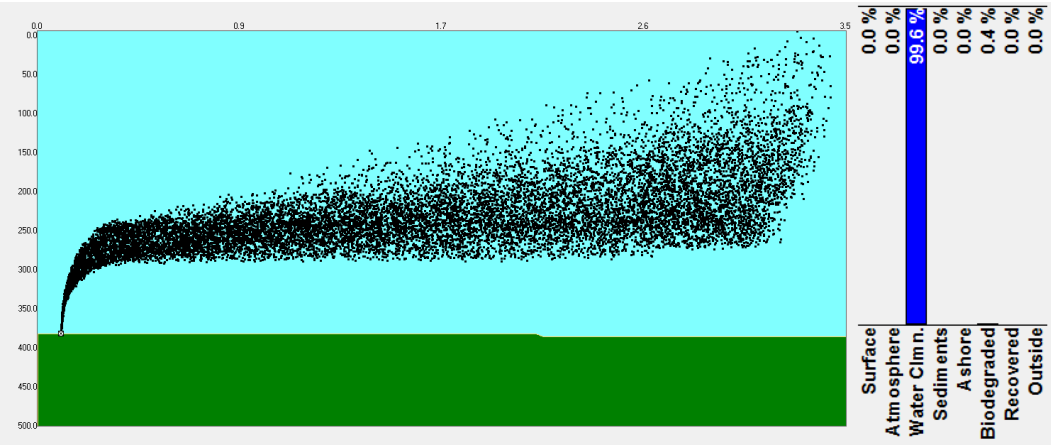

Figure 52: Vertical profile and mass balance for a 1500 m^3/day release after 3 hours with subsurface injection of dispersants.

Comparison of the two figures above, the vertical profiles of 1500 m^3/day release without and with subsurface dispersant injection, shows that the plume becomes trapped for a longer time and distance. For the treated release, the plume stretches out to more than 3 km before surfacing and from the image can be seen that droplets escape the plume and rise vertically on their own. The mass balance supports this as the differences in percentage of oil in water column, 65.1 % and 99.6 % differ greatly, just like the percentage of oil on the surface after 3 hours: 27.5 % for non-treated oil and 0.0% for the oil which has been treated subsurface with dispersants.

Figures 54 shows the surface spreading at the same time, 3 hours after the start of the release. The left image shows the spreading for non-treated oil and the right figure for oil with subsurface injection of dispersant.

The green and red particles represent oil dispersed in the water column, where red represents droplets > 5 mm and the green from light to dark 0 - 5 mm droplets, as shown in figure 53. The purple and white particles represent the surface oil. The darker the purple particles, the thicker the slick, as can be seen in figure 53.

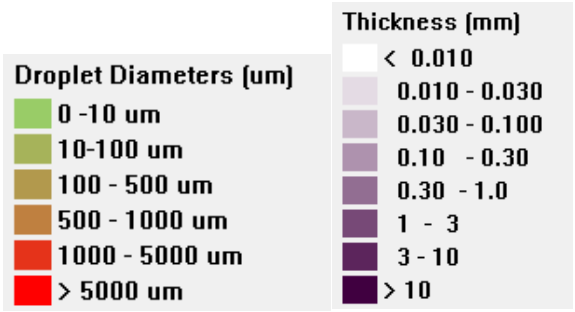

Figure 53: Explanation for the oil particles in the water column. Green represents very small droplets whereas red represents droplets >5 mm. The right image explains the surface particles. White particles represent a thin slick, dark purple represents >10 mm.

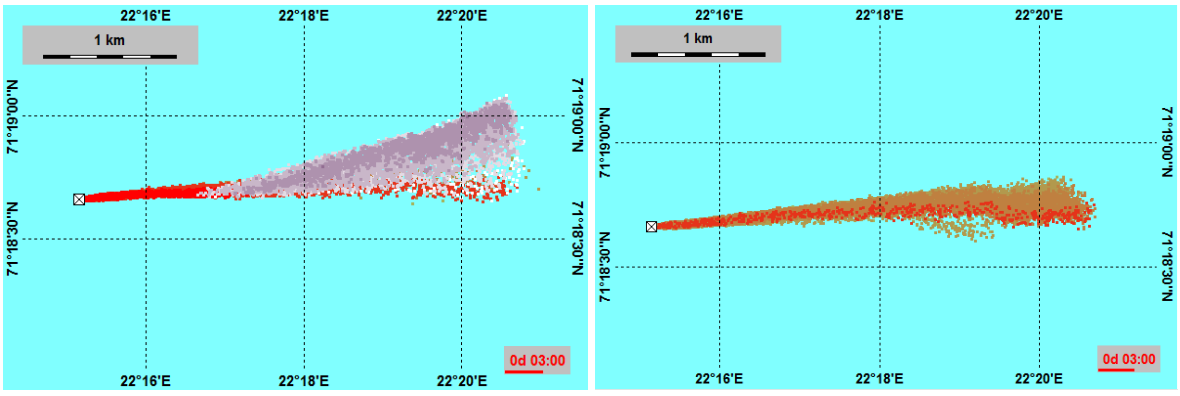

Figure 54: Surface images of the 3 hour 1500 m^3/day releases. The left image is without treatment and the right image shows the resulting image with subsurface dispersant.

The next figures show the same but for a release of 4500 m^3/day. Figure 55 shows the vertical profile and mass balance for a release without response and figure 56 for a release with subsurface injection of dispersant.

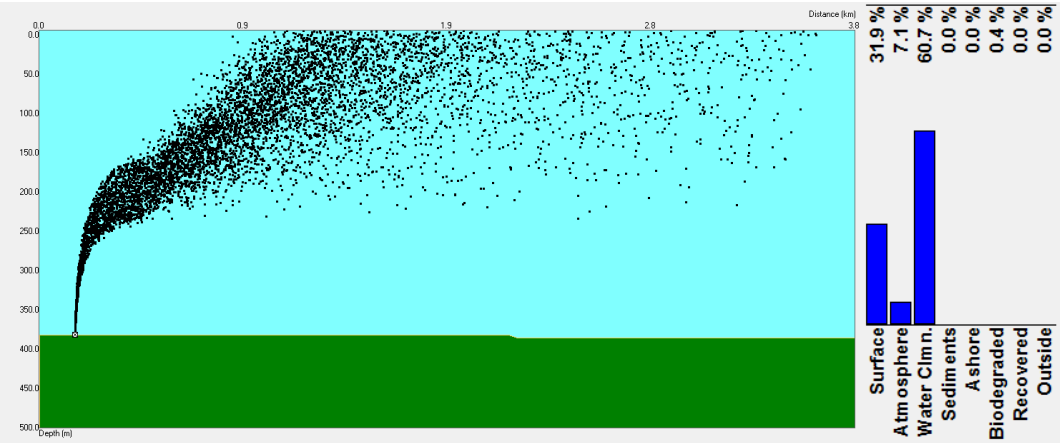

Figure 55: Vertical profile and mass balance for a 4500 m^3/day release after 3 hours without subsurface injection of dispersants.

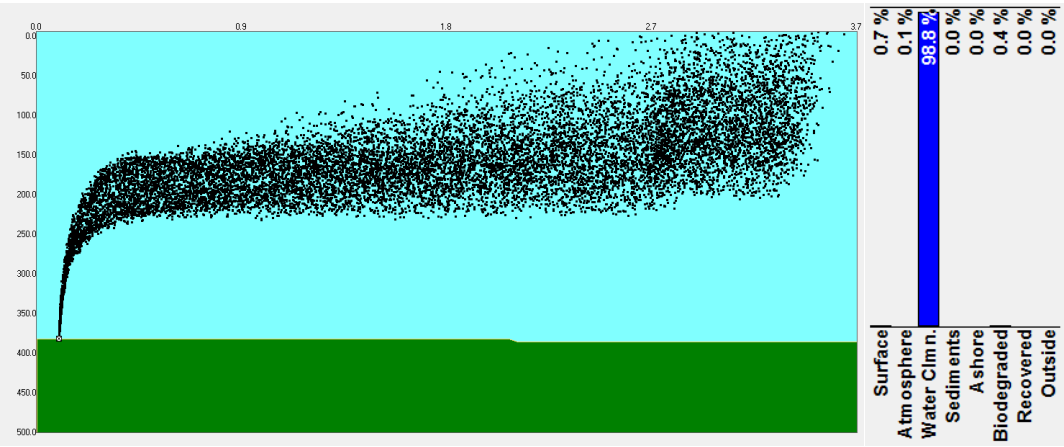

Figure 56: Vertical profile and mass balance for a 4500 m^3/day release after 3 hours with subsurface injection of dispersants.

Just as for the 1500 m^3/day release, during the treated 4500 m^3/day release, the plume becomes trapped. However, this time the plume remains higher up in the water column. Where the 1500 m^3/day plume stays between 250 and 300 m depth, the 4500 m^3/day plume is trapped between 150 and 250 m depth. The mass balance shows a clear difference between the two releases with respectively 60.7 % and 98.8 % for the oil in the water column for non-treated and treated, and 31.9 % and 0.0% for the oil at the surface after 3 hours. This can also be seen in the next two figures: these two show the surfacing and

spreading of the oil at the same time. The left figure shows the non-treated oil and the right image the oil treated with subsurface injection of dispersants.

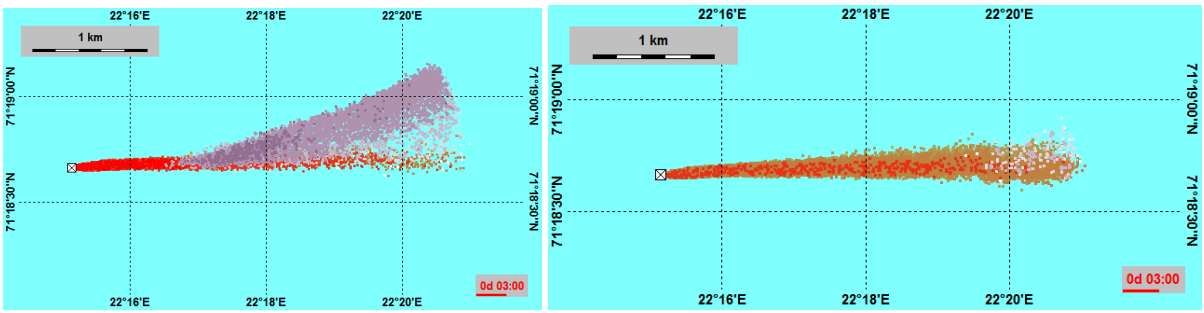

Figure 57: Surface images of the 3 hour 4500 m^3/day releases. The left image is without treatment and the right image shows the resulting image with subsurface dispersant.

In the table below, 6, the most important parts of the mass balances are summarized to clarify the differences between the two different releases and between the treatments.

Table 6: Summary of the massbalances for the different releases after 3 hours.

Release	Surface in %	Atmosphere in %	Water column in %	Biodegraded in %
1500 m^3/day	25.7	7.0	65.1	0.4
1500 m^3/day with subsurface dispersant	0.0	0.0	99.6	0.4
4500 m^3/day	31.9	7.1	60.7	0.4
4500 m^3/day with subsurface dispersant	0.7	0.1	98.8	0.4

Table 7 shows the Plume3d results. The d95 is the droplet size in the 95th percentile of the distribution and the d50 is calculated using equation 34.

$$d_{50} = \frac{d_{95}}{\left(\frac{\log(1-\left(\frac{95}{100}\right)}{\log\left(\frac{50}{100}\right)}\right)^{\frac{1}{1.8}}}$$

Equation 34

Table 7: The d_{95} and the d_{50} for the four different releases that have been studied.

Release	d_{95} in µm	d_{50} in µm
1500 m^3/day	8830	3916
1500 m^3/day with subsurface dispersant	1230	545
4500 m^3/day	7600	3370
4500 m^3/day with subsurface dispersant	1230	545

A decrease in d_{50} is observed for both 1500 and 4500 m^3/day releases when treated with dispersant subsurface.

4.3.2 Ten day releases

The next simulations were 10 day releases under the same conditions. The results for 1500 m^3/day are shown in figures 58, 59 and 60.

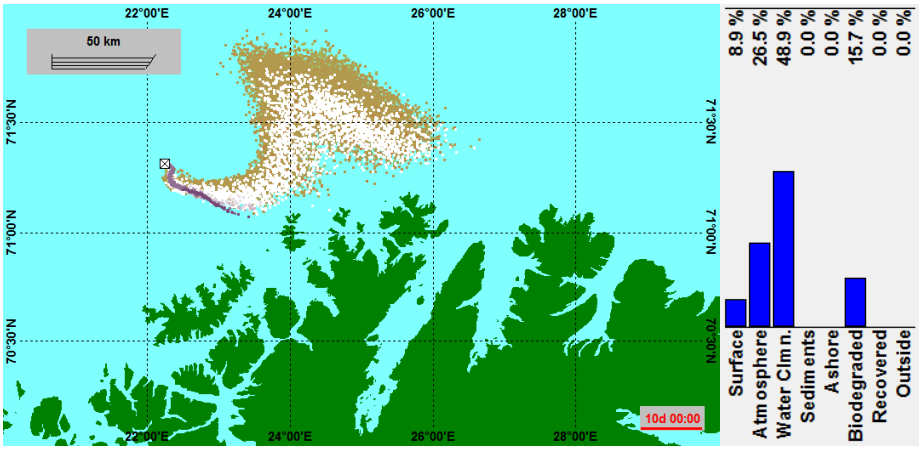

Figure 58: Surface profile and mass balance after 10 days for a 1500 m^3/day release without treatment.

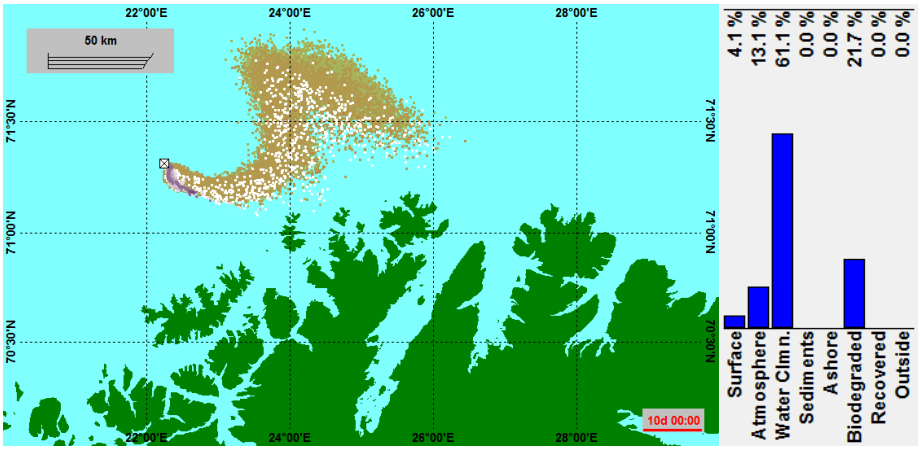

Figure 59: Surface profile and mass balance after 10 days for a 1500 m^3/day release with subsurface dispersant injection.

From the image itself it can be seen that there is less oil on the surface for the treated plume (figure 59) than for the non-treated (figure 58). However, when looking at the mass balance, one can see that although there is a more than 50 % reduction in percentage surface oil, 8.9 % and 4.1 % respectively, both do not have big amounts of surface oil. When comparing the percentage of oil in the water column a difference of 12 % can be observed between the two simulations with 48.9 % for the non-treated oil and 61.1 % for the blowout with subsurface injection of dispersants.

A third simulation was performed with the same release conditions but instead of subsurface dispersant injection as an oil spill response, here surface dispersant application was simulated. Less oil has surfaced after 10 days (0.5% for surface spraying compared to 4.1% for subsurface injection) but the percentage of biodegraded oil is much lower (13.9% for surface spraying compared to 21.7% for subsurface injection).

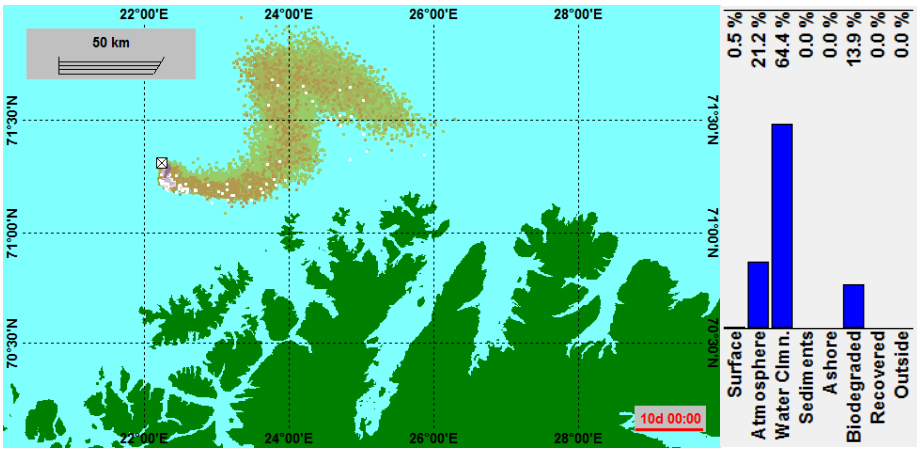

Figure 60: Surface profile and mass balance after 10 days for a 1500 m^3/day release with surface application of dispersant.

The same simulations have been performed for a 4500 m^3/day release.

Figure 61 shows the surface profile and mass balance of the release when no oil spill response has been carried out.

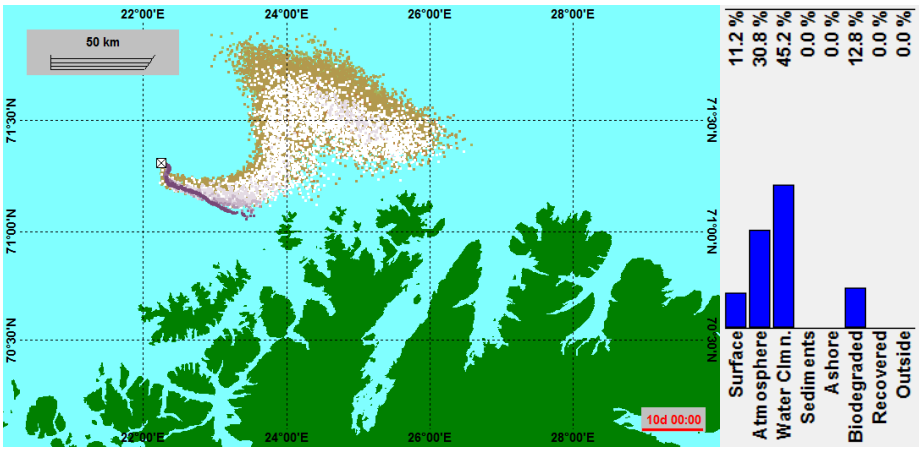

Figure 61: Surface profile and mass balance after 10 days for a 4500 m^3/day release without any treatment.

Figure 62 shows the surface profile and mass balance of an oil release with subsurface dispersant injection. A comparison between the two mass balances shows that the percentages of oil on the surface to not differ much, 11.2 % for non-treated and 9.5 % for the treated oil. A greater difference is observed between the percentage evaporated and oil in the water column (19.0% and 52.9% for treated and 30.8% and 45.2% for non-treated oil).

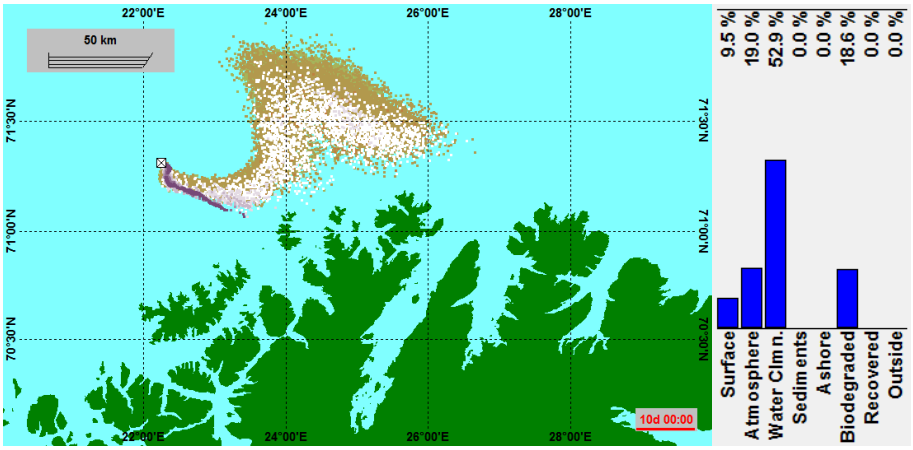

Figure 62: Surface profile and mass balance after 10 days for a 4500 m^3/day release with subsurface injection of dispersant.

As a last comparison, just as for the 1500 m^3/day release, a simulation was performed with surface application of dispersant. The results can be seen in figure 63.

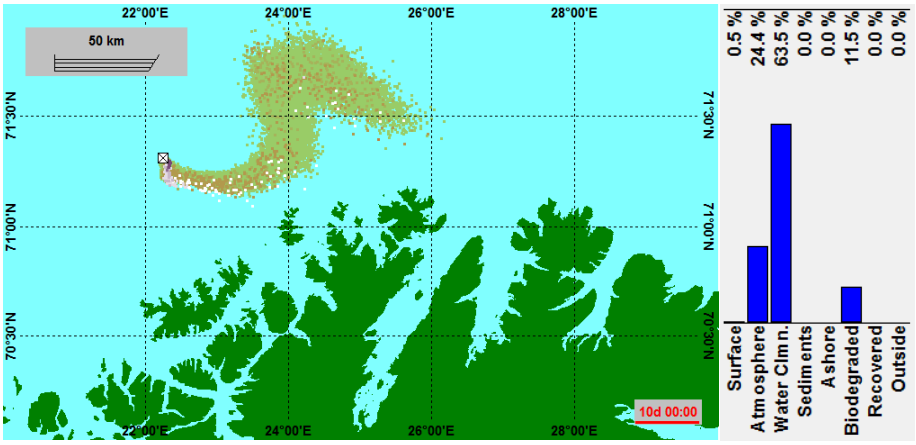

Figure 63: Surface profile and mass balance after 10 days for a 4500 m^3/day release with surface application of dispersant.

With only 0.5% of oil left on the surface and 63.5% in the water column, this seems to be the most effective dispersant treatment for this release. However, when looking at the percentage of oil that is biodegraded, it is observed that only 11.5 % has degraded after 10 days where as for the subsurface treated oil that is 18.6%.

4.3.3 Ten day releases in calm weather conditions

To show what happens to released oil in very calm weather conditions, a release without wind has been simulated. Because there is no wind, there are also almost no breaking waves, causing a thick slick to form and very little of the oil to be in the water column as can be seen in figure 64 for 1500 m^3/day releases without any treatment.

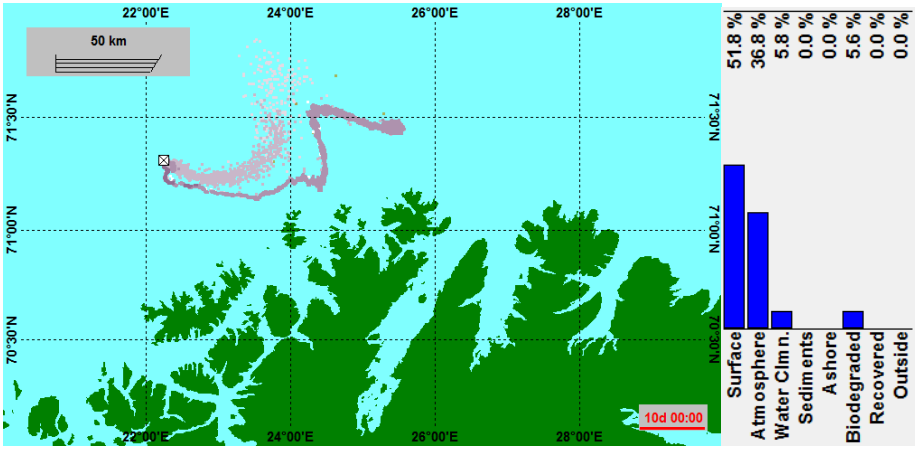

Figure 64: Surface profile and mass balance after 10 days for a 1500 m^3/day release without any treatment and in very calm weather conditions.

Figures 65 shows the surface profile and mass balance for the same simulation but with subsurface dispersant injection. A difference between the two simulations is observed when comparing the surface profiles, but even more when comparing the mass balances. The non-treated release has 5.8% oil in the water column compared to 51.8% of oil on the surface after ten days. The subsurface treated release on the other hand, has 19.5% of the oil in the water column and 45.3% on the surface. A larger difference can be seen when comparing the biodegraded oil: after ten days, only 5.6% of the non-treated oil has degraded, compared to 18.1% for the oil injected with dispersant subsurface.

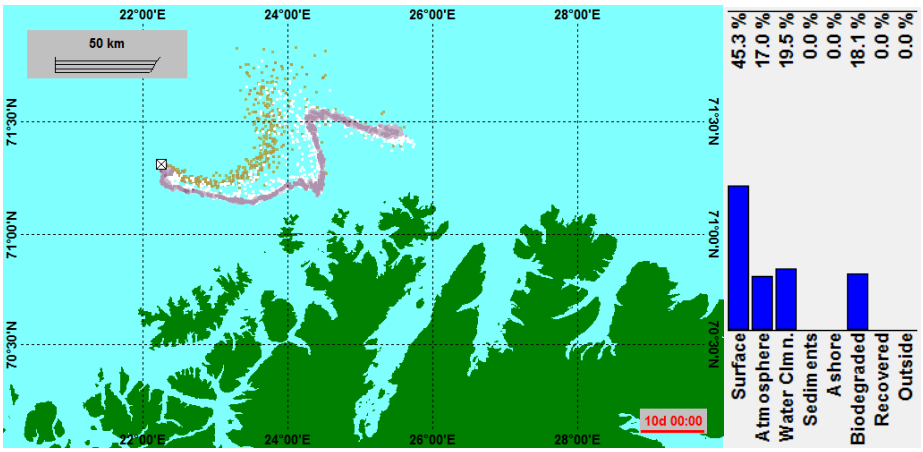

Figure 65: Surface profile and mass balance after 10 days for a 1500 m^3/day release with subsurface injection of dispersant and in very calm weather conditions.

In order to be effective, dispersants that have been applied on the surface oil slick, need breaking waves to cause the oil to disperse into the water column. When there is no wind, there are almost no breaking waves and as can be seen in figure 66 this results in very little oil in the water column (4.4%) and only 0.01% difference in surface oil compared to non-treated releases (51.7% for surface treated and 51.8% for non-treated).

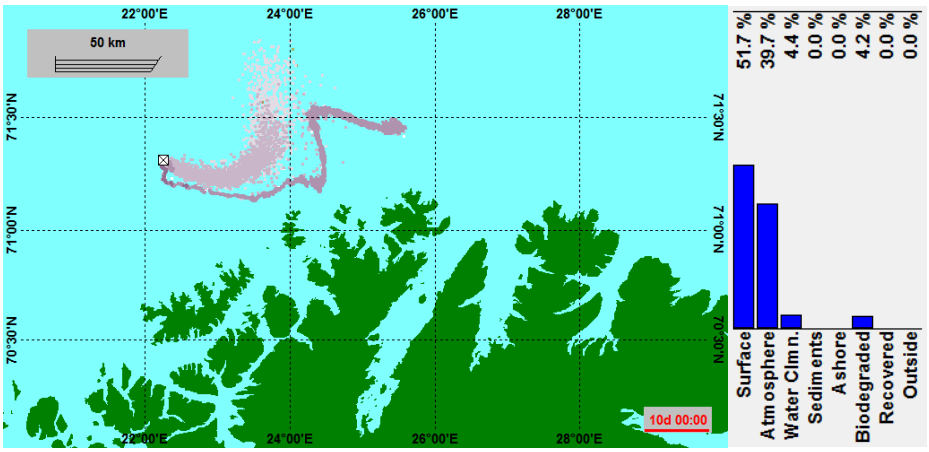

Figure 66: Surface profile and mass balance after 10 days for a 1500 m^3/day release with surface application of dispersant and in very calm weather conditions.

This shows the importance of breaking waves and the advantage of subsurface injection of dispersants.

The last three figures show the results of the same simulations under calm conditions but for a 4500 m^3/day release for non-treated, subsurface treated and surface treated oil releases.

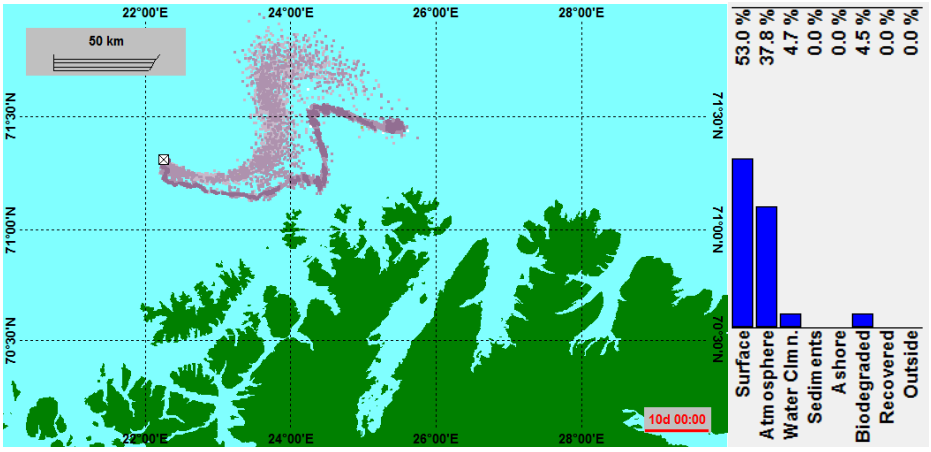

Figure 67: Surface profile and mass balance after 10 days for a 4500 m^3/day release without any treatment and in very calm weather conditions.

Although the difference in surface oil is only 2.5 % between non-treated and oil injected with dispersant, the difference of oil in the water column is 8.5% and the difference in biodegraded oil is 9.5% (see figure 67 for non-treated and figure 68 for subsurface treated oil releases).

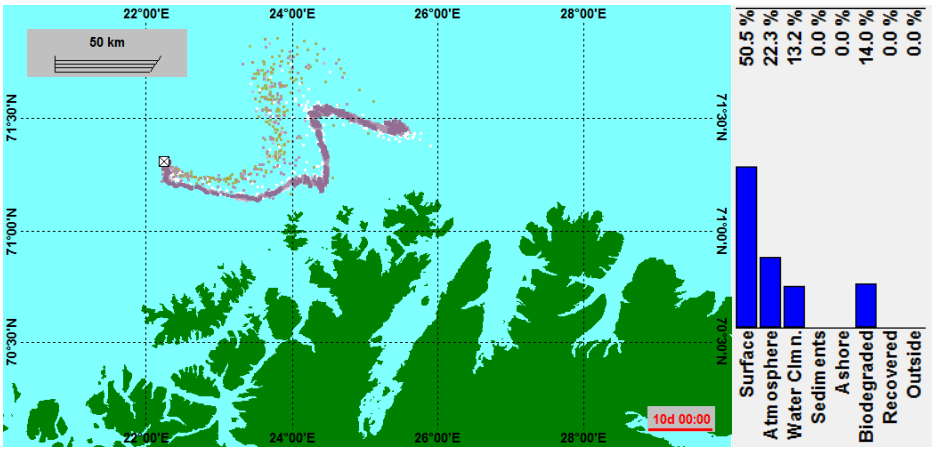

Figure 68: Surface profile and mass balance after 10 days for a 4500 m^3/day release with subsurface injection of dispersant and in very calm weather conditions.

The simulation of the release treated by spraying dispersant on the surface slick shows very little improvement compared to non-treated oil when the weather conditions are very calm as can be seen in figure 69.

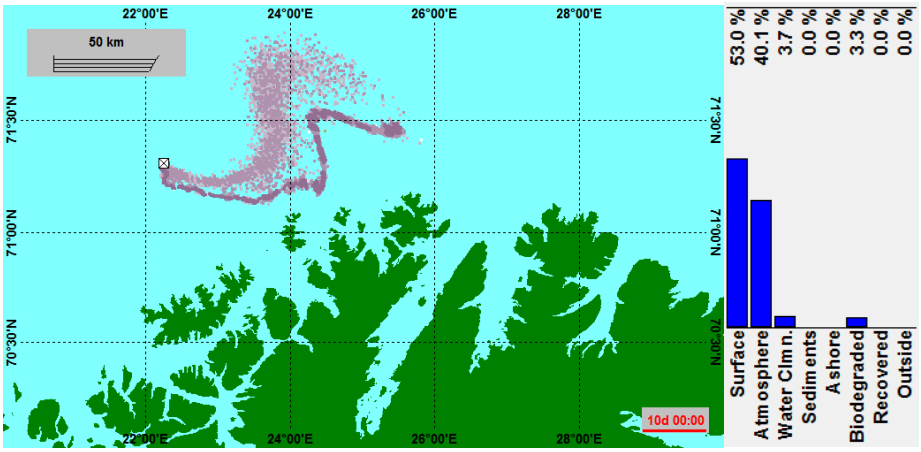

Figure 69: Surface profile and mass balance after 10 days for a 4500 m^3/day release with surface application of dispersant and in very calm weather conditions.

Conclusion

The objectives of this thesis were to perform experimental laboratory and simulation studies towards subsurface oil releases and the effects of surfactant combinations and commercially available dispersants.

Studying the influence of oil release temperature is important since the real oil temperature can be significantly higher than usually used during laboratory testing. Experiments show that when the temperature of Troll B oil increases, the effectivity of several surfactant combinations, including Corexit 9500A, increases. This is opposed to what has been previously observed. Where in previous studies the decrease in effectivity seemed to be an effect of surfactant chemistry, it is also a possibility that it is an oil chemistry effect, as Kobbe oil showed decreased effectivity at higher temperatures. However, more experiments are needed to draw a conclusion.

Several models are available for predicting initial droplet formation, but little have been done on secondary breakup of droplets. The study presented in this thesis has shown that the secondary break-up of Kobbe oil treated with Corexit 9500A involves tip-streaming, as that was observed both at dispersant-to-oil ratios of 1:100 and of 1:50. However, tip-streaming of the treated oil is finished within 10 minutes and the droplets remain stable and spherical from then on. Testing in more turbulent conditions showed that after 1 hour in those conditions, the droplets have broken up in small, spherical and stable droplets.

To illustrate how several processes regarding subsurface releases of oil and subsurface injection of dispersant can be described by a model system like OSCAR, a detailed simulation study of oil releases in the Barents Sea was performed . The results show that when dispersant is injected in the plume subsurface, the d_{50} of the oil is much smaller compared to a non-treated release, and the plume stretches out over a longer distance before surfacing. Simulations of oil releases under very calm weather conditions show the advantage of subsurface injection of dispersants when there are no breaking waves to support spraying of dispersant on the surface oil slick.

References

Aamo, O. M., Reed, M., Daling, P. and Johansen, Ø. 1993. A laboratory-based weathering model: PC version for coupling to transport models. Proceedings of the 1993 Arctic and Marine Oil Spill Program (AMOP). 617-626.

Almeda, R., Hyatt, C. and Buskey, E. J., 2014. Toxicity of dispersant Corexit 9500A and crude oil to marine microzooplankton. Ecotoxicology and Environmental Safety 106: 76-85.

Andreassen, I. and Sørheim, K. R., 2013. Fram crude oil-properties and behavior at sea. SINTEF Materials and Chemistry. Marine Environmental Technology. Trondheim, Norway.

Anna, S. L. and Mayer, H. C., 2006. Microscale tipstreaming in a microfluidic flow focusing device. Physics of Fluids (1994-present) 18: 121512.

Bergh Lindersen, P. J., 2013. Modelling of subsurface releases of oil and gas. Master thesis, Norwegian University of Science and Technology, NTNU, Trondheim, Norway.

Box, G. E. P. and Wilson, K. B., 1951. On the experimental attainment of optimum conditions. Journal of the Royal Statistical Society. Series B (Methodological) 13: 1-45.

Box, G. E. P., Hunter, W. G. and Hunter, J. S. 1978. Statistics for experimenters. USA. John Wiley & Sons.

Brandvik, P. J., 1998. Statistical simulation as an effective tool to evaluate and illustrate the advantage of experimental designs and response surface methods. Chemometrics and Intelligent Laboratory Systems 42: 51-61.

Brandvik, P. J. and Daling, P. S., 1998a. Optimisation of oil spill dispersant composition by mixture design and response surface methods. Chemometrics and Intelligent Laboratory Systems 42: 63-72.

Brandvik, P. J. and Daling, P. S., 1998b. Optimising oil spill dispersants as a function of oil type and weathering degree: a multivariate approach using partial least squares (PLS). Chemometrics and Intelligent Laboratory Systems 42: 73-91.

Brandvik, P. J., Johansen, Ø., Leirvik, F., Farooq, U. and Daling, P. S., 2013. Droplet breakup in subsurface oil releases–Part 1: Experimental study of droplet breakup and effectiveness of dispersant injection. Marine Pollution Bulletin 73: 319-326.

Brandvik, P. J., Johansen, Ø., Farooq, U., Angell, G. and Leirvik, F., 2014. Subsurface oil releases-experimental study of droplet distributions and different dispersant injection techniques - version 2. SINTEF Materials and Chemistry. Environmental Technology. Trondheim, Norway.

Campo, P., Venosa, A. D. and Suidan, M. T., 2013. Biodegradability of Corexit 9500 and dispersed South Louisiana crude oil at 5° and 25° C. Environmental Science & Technology 47: 1960-1967.

Chen, F. and Yapa, P. D., 2003. A model for simulating deep water oil and gas blowouts-Part II: Comparison of numerical simulations with “Deepspill” field experiments. Journal of Hydraulic Research 41: 353-365.

Collins, R. T., Jones, J. J., Harris, M. T. and Basaran, O. A., 2008. Electrohydrodynamic tip streaming and emission of charged drops from liquid cones. Nature Physics 4: 149-154.

Cornell, J. A. 1990. Experiments with mixtures: designs, models, and the analysis of mixture data, second edition. Vol 895. USA. John Wiley & Sons.

Daling, P. S., Brandvik, P. J., Mackay, D. and Johansen, O., 1990. Characterization of crude oils for environmental purposes. Oil and Chemical Pollution 7: 199-224.

Daling, P. S. and Brandvik, P. J., 1991. Characterization and prediction of the weathering properties of oils at sea-a manual for the oils investigated in the DIWO project. DIWO-Report no. 16. IKU Petroleum Research.

Davies, E. J., Nimmo-Smith, W. A. M., Agrawal, Y. C. and Souza, A. J., 2012. LISST-100 response to large particles. Marine Geology 307: 117-122.

Davies, E. J., Brandvik, P. J., Johansen, Ø., Nagamine, I., Dunnebier, D., Masutani, S. and Leirvik, F., unpublished. Fate of subsea dispersed oil droplets: An experimental study combining the SINTEF MiniTower (oil droplets created by a turbulent jet) and the concept of Univ. of Hawaii's inverted cone system.

De Bruijn, R., 1993. Tipstreaming of drops in simple shear flows. Chemical Engineering Science 48: 277-284.

Durst, F. 2008. Fluid mechanics: an introduction to the theory of fluid flows. Germany. Springer Science & Business Media.

Eggleton, C. D., Tsai, T.-M. and Stebe, K. J., 2001. Tip streaming from a drop in the presence of surfactants. Physical Review Letters 87: 048302, 1-4.

EMSA, European Maritime Safety Agency, 2014. Inventory of national policies regarding the use of oil spill dispersants in the EU member states.

Fanneløp, T. K. and Sjøen, K., 1980. Hydrodynamics of underwater blowouts. Technical report, The Ship Research Insitute of Norway.

Fisher, R. A., 1926. The arrangement of field experiments. Journal of the Ministry of Agriculture of Great Britain 33: 503-513.

Fuller, C., Bonner, J., Page, C., Ernest, A., McDonald, T. and McDonald, S., 2004. Comparative toxicity of oil, dispersant, and oil plus dispersant to several marine species. Environmental Toxicology and Chemistry 23: 2941-2949.

Gardiner, W.W., Word, J.Q., Word, J.D., Perkins, R.A., McFarlin, K.M., Hester, B.W., Word, L.S. and Ray, C.M., 2013. The actute toxicity of chemically and physially dispersed crude oil to key arctic species under arctic conditions during the open water season. Environmental Toxicology and Chemistry 32, 10: 2284-2300.

Gopalan, B. and Katz, J., 2010. Turbulent shearing of crude oil mixed with dispersants generates long microthreads and microdroplets. Physical Review Letters 104: 054501.

Hinze, J. 1955. Fundamentals of the hydrodynamic mechanism of splitting in dispersion processes. A.I.CHe.E. Journal 1: 289-295.

Holand, P. 1998. Offshore blowouts: causes and control. the Netherlands. Gulf Professional Publishing.

Johansen, Ø., 1997. Hydratdannelse og dråpestørrelse ved dypvannsutblåsninger. SINTEF report STF66 F97082, SINTEF Applied Chemistry, Trondheim, Norway.

Johansen, Ø., 2000. DeepBlow–a Lagrangian plume model for deep water blowouts. Spill Science & Technology Bulletin 6: 103-111.

Johansen, Ø., 2003. Development and verification of deep-water blowout models. Marine Pollution Bulletin 47: 360-368.

Johansen, Ø., Rye, H. and Cooper, C., 2003. DeepSpill—field study of a simulated oil and gas blowout in deep water. Spill Science & Technology Bulletin 8: 433-443.

Johansen, Ø. And Durgut, I., 2006. Implementation of the near-field module in the ERMS project. ERMS report. Trondheim, Norway.

Johansen, Ø., Brandvik, P. J. and Farooq, U., 2013. Droplet breakup in subsea oil releases–Part 2: Predictions of droplet size distributions with and without injection of chemical dispersants. Marine Pollution Bulletin 73: 327-335.

Juhasz, A. 2011. Black tide: the devastating impact of the Gulf oil spill. USA. John Wiley & Sons.

Karabelas, A., 1978. Droplet size spectra generated in turbulent pipe flow of dilute liquid/liquid dispersions. AIChE Journal 24: 170-180.

Khuri, A. I. and Cornell, J. A. 1987. Response surfaces: designs and analyses. Vol 152. USA. CRC press.

Leardi, R., 2009. Experimental design in chemistry: a tutorial. Analytica Chimica Acta 652: 161-172.

Lefebvre, A. H., 1989. Atomization and Sprays. Taylor and Francis.

Lessard, R. R. and DeMarco, G., 2000. The significance of oil spill dispersants. Spill Science & Technology Bulletin 6: 59-68.

Martines-Bazán, C., Montañés, J. L., 2002. Statistical description of the bubble cloud resulting from the injection of air into a turbulent water jet. International Journal of Multiphase Flow 28: 597-615.

Masutani, S. M. and Adam, E., 2000. Experimental study of multi-phase plumes with application to deep ocean oil spills. Massachusetts Institute of Technology. Final Report to the MMS. USA.

Myers, D. 2005. Surfactant science and technology. USA. John Wiley & Sons.

Reed, M., French, D., Rines, H. and Rye, H. 1995a. A three-dimensional oil and chemical spill model for environmental impact assessment. International Oil Spill Conference. 1995. American Petroleum Institute61-66.

Reed, M., Aamo, O. M. and Daling, P. S., 1995b. Quantitative analysis of alternate oil spill response strategies using OSCAR. Spill Science & Technology Bulletin 2: 67-74.

Reed, M., Johansen, Ø., Brandvik, P. J., Daling, P., Lewis, A., Fiocco, R., Mackay, D. and Prentki, R., 1999. Oil spill modeling towards the close of the 20th century: overview of the state of the art. Spill Science & Technology Bulletin 5: 3-16.

Rosen, M. J. and Kunjappu, J. T. 2012. Surfactants and interfacial phenomena. USA. John Wiley & Sons.

Rønningsen, H. P., 2012. Rheology of petroleum fluids. Annual Transactions of the Nordic Rheology Society 20.

Salager, J.-L., Marquez, N., Graciaa, A. and Lachaise, J., 2000. Partitioning of ethoxylated octylphenol surfactants in microemulsion-oil-water systems: influence of temperature and relation between partitioning coefficient and physicochemical formulation. Langmuir 16: 5534-5539.

Scheffe, H., 1958. Experiments with mixtures. Journal of the Royal Statistical Society. Series B (Methodological): 344-360.

Scheffe, H., 1963. The simplex-centroid design for experiments with mixtures. Journal of the Royal Statistical Society. Series B (Methodological): 235-263.

Schobert, H. 2013. Chemistry of Fossil Fuels and Biofuels. USA. Cambridge University Press.

Sequoia Scientific Inc. 2012. LISST-100X particle size analyzer user's manual. In: Inc SS, editor, USA, pp.

SINTEF Marine Modelling Group, 2014. SINTEF MEMW Users Manual version 6.6.1. In: Group SMM, editor. SINTEF Materials and Chemistry, Trondheim, Norway, pp.

Suryo, R. and Basaran, O. A., 2006. Tip streaming from a liquid drop forming from a tube in a co-flowing outer fluid. Physics of Fluids (1994-present) 18: 082102.

Sørheim, K. R. and Moldestad, M. Ø., 2008. Weathering properties of the Goliat Kobbe and two Goliat Blend of Kobbe and Realgrunnen crude oils. SINTEF Materials and Chemistry. Trondheim, Norway.

Tissot, B. P. and Welte, D. H., 1984. Petroleum Formation and Occurrence, 2nd edition. Springer-Verlag, New York.

Topham, D. R., 1984. The modelling of hydrocarbon bubble plumes to include gas hydrate formation. Chemical Engineering Science 39: 1613-1622.

USGS, 2008. Circum-Arctic resource appraisal: Estimates of undiscovered oil and gas north of the Arctic Circle. Fact sheet United States Geological Survey.

Wang, Z. and Stout, S. 2010. Oil spill environmental forensics: fingerprinting and source identification. USA. Academic Press.

www.gulfresearchinitiative.org. 2015. Gulf of Mexico, Research Initiative. Investigating the effect of oil spills on the environment and public health. Michael Carron and Kevin Shaw. Last visited: May 15th, 2015.

www.nalcoesllc.com. 2015. www.nalcoesllc.com/nes/1602.htm, Nalco, Environmental Solutions. Last visited: May 15th, 2015.

www.NASA.org. 2015. Explaining rapid climate change: tales from the ice. http://earthobservatory.nasa.gov/Features/Paleoclimatology_Evidence/paleoclimatology_evidence_2.php. Riebeek, H. Last visited: May 15th, 2015.

www.petroleumskartet.no. 2015. Norsk Oljemuseum. Last visited: May 15th, 2015.

Yapa, P. D. and Zheng, L., 1997. Simulation of oil spills from underwater accidents I: Model development. Journal of Hydraulic Research 35: 673-688.

Yapa, P. D. and Zheng, L., 1997. Modelling oil and gas releases from deep water: A review. Spill Science & Technology Bulletin 4: 189-198.

Yapa, P. D., Zheng, L. and Nakata, K., 1999. Modeling underwater oil/gas jets and plumes. Journal of Hydraulic Engineering 125: 481-491.

Yapa, P. D., Zheng, L. and Chen, F., 2001. A model for deepwater oil/gas blowouts. Marine Pollution Bulletin 43: 234-241.

Zhao, L., Boufadel, M. C., Socolofsky, S. A., Adams, E., King, T. and Lee, K., 2014a. Evolution of droplets in subsea oil and gas blowouts: Development and validation of the numerical model VDROP-J. Marine Pollution Bulletin 83: 58-69.

Zhao, L., Torlapati, J., Boufadel, M. C., King, T., Robinson, B. and Lee, K., 2014b. VDROP: A comprehensive model for droplet formation of oils and gases in liquids-Incorporation of the interfacial tension and droplet viscosity. Chemical Engineering Journal 253: 93-106.

Zheng, L. and Yapa, P. D., 1998. Simulation of oil spills from underwater accidents II: model verification. Journal of Hydraulic Research 36: 117-134.

Zheng, L., Yapa, P. D. and Chen, F., 2003. A model for simulating deepwater oil and gas blowouts-Part I: Theory and model formulation. Journal of Hydraulic Research 41: 339-351.

Appendix A

In this appendix A, the combined graphs from the initial MiniTower study are presented. The graphs show the droplet diameter versus the relative volume distribution for the three experimental triangles for DOR 1:500 (figures 70, 71 and 72) and for DOR 1:250 (figures 73, 74 and 75). The graphs for DOR 0 and DOR 1:100 are presented in the main part of the thesis and can be found in chapter 4.1.1.

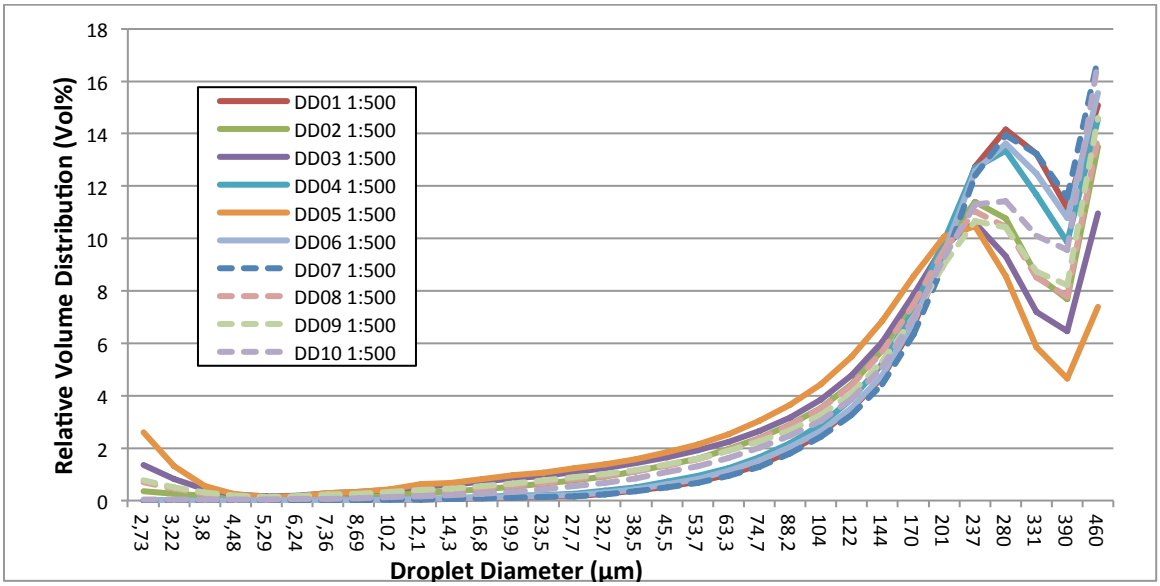

Figure 70: Relative volume distribution vs droplet diameter for Troll oil treated with DOR 1:500 surfactant mixtures of the first experimental triangle.

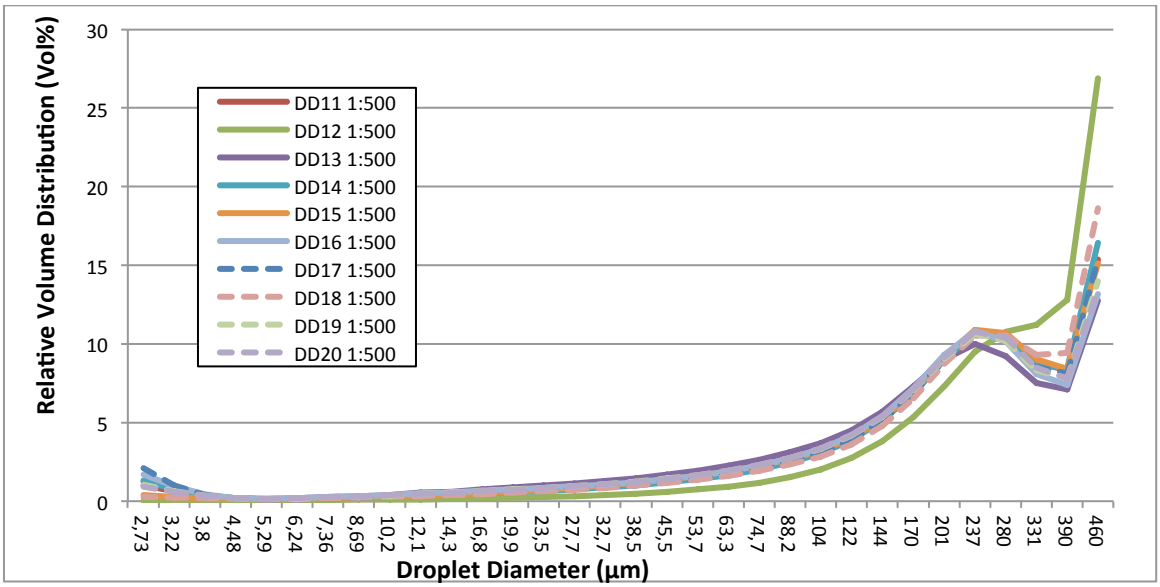

Figure 71: Relative volume distribution vs droplet diameter for Troll oil treated with DOR 1:500 surfactant mixtures of the second experimental triangle.

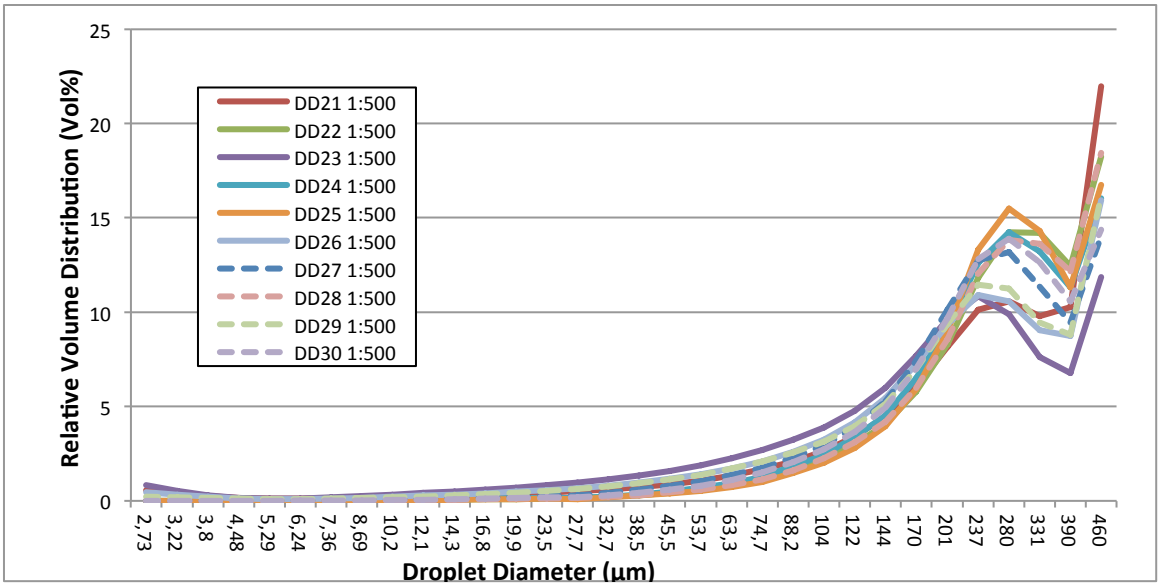

Figure 72: Relative volume distribution vs droplet diameter for Troll oil treated with DOR 1:500 surfactant mixtures of the third experimental triangle.

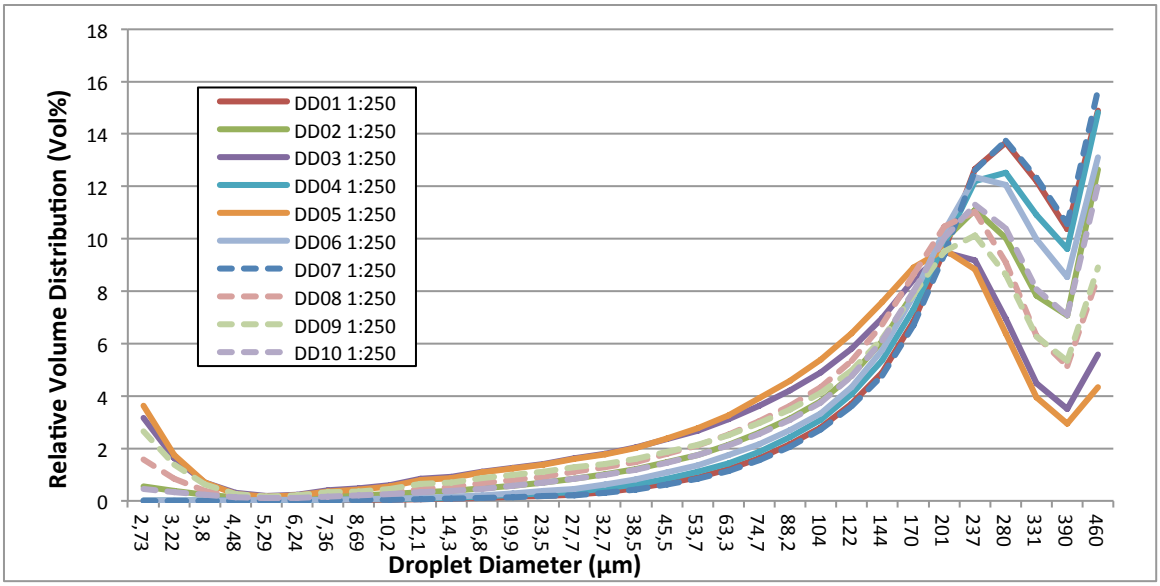

Figure 73: Relative volume distribution vs droplet diameter for Troll oil treated with DOR 1:250 surfactant mixtures of the first experimental triangle.

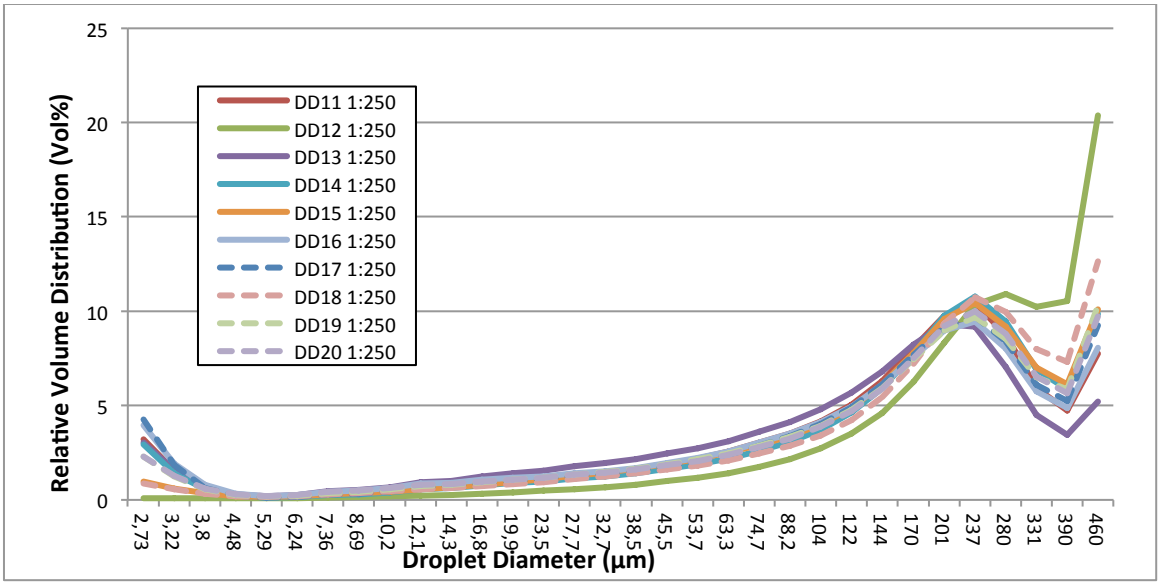

Figure 74: Relative volume distribution vs droplet diameter for Troll oil treated with DOR 1:250 surfactant mixtures of the second experimental triangle.

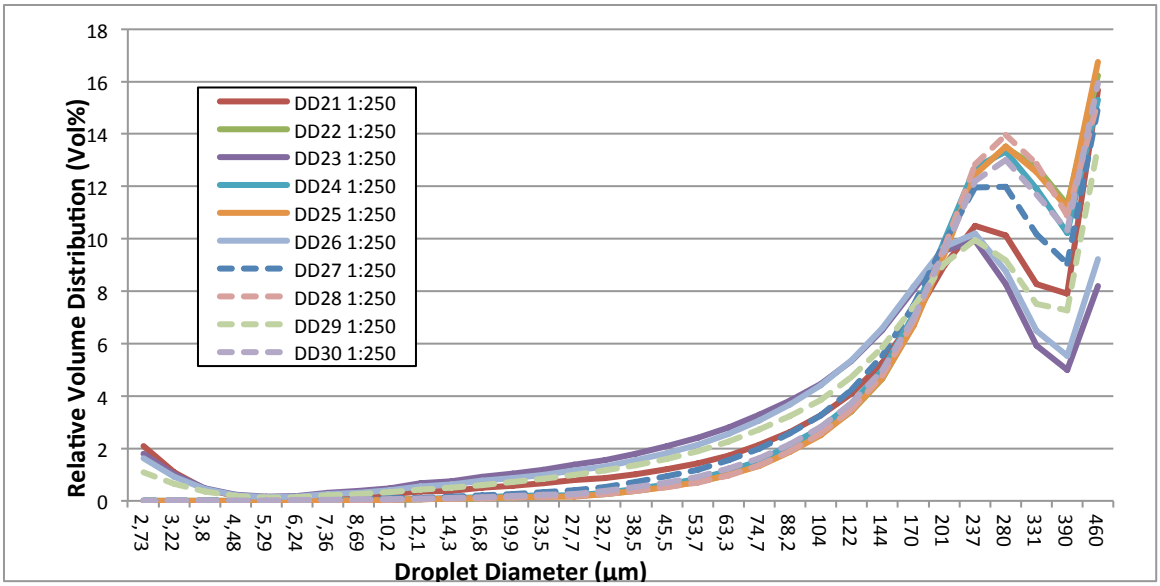

Figure 75: Relative volume distribution vs droplet diameter for Troll oil treated with DOR 1:250 surfactant mixtures of the third experimental triangle.